ADVANCED AND INNOVATIVE WIND ENERGY CONCEPT DEVELOPMENT: DYNAMIC INDUCER SYSTEM

RESEARCH REPORT

AUGUST 1981

P. B. S. LISSAMAN
A. D. ZALAY
B. H. HIBBS

AeroVironment, Inc.
Pasadena, California

FOREWORD

The work summarized in this report was supported by SERI under the Wind Energy Innovative Systems Program. The technical project manager was Dr. Irwin E. Vas, assisted by Mr. Richard Mitchell. The subcontract administrator was Ms. Lori Miranda.

This research report summarizes the results to-date of the development of a novel wind turbine system, the dynamic inducer. This report discusses the results of analytic investigations, and wind-tunnel and field-testing of a dynamic inducer system. The program demonstrated that a significant improvement in performance of the rotor is achievable with the dynamic inducer system. The results suggest that additional testing of the concept can lead to further performance improvements and demonstrate substantial cost/benefit advantages over conventional rotors.

PREFACE AND LIST OF CONTRIBUTORS

ABSTRACT

The performance benefits of the dynamic inducer tip vane system have been experimentally demonstrated for the first time. Tow-tests conducted on a three-bladed, 3.6-meter diameter rotor have shown that a dynamic inducer can achieve a power coefficient (based upon power blade swept area) of 0.5, which exceeds that of a plain rotor by about 35%. Wind tunnel tests conducted on a one-third scale model of the dynamic inducer achieved a power coefficient of 0.62 which exceeded that of a plain rotor by about 70%. The dynamic inducer substantially improves the performance of conventional rotors and indications are that higher power coefficients can be achieved through additional aerodynamic optimization. It is noted that the wind turbine system used as a baseline unit is the Kedco 1200, a conventional propeller-type wind turbine with power blades designed for optimum performance without tip vane augmentation. In addition, the tip vane utilized a standard conventional NACA airfoil selected on conservative grounds to guarantee acceptable performance. More advanced high lift-to-drag airfoil sections are expected to improve the tip vane effectiveness.

The analytical and experimental development efforts summarized in this report suggest that the dynamic inducer can play a major role in future turbine technology. A new method for calculating wind tunnel corrections for augmented wind turbines is developed. This shows that corrections are very significant. For example, with a blockage of 16%, the corrected power coefficient is about 20% lower than that actually measured.

LIST OF FIGURES

LIST OF FIGURES (continued)

LIST OF TABLES

TABLE OF CONTENTS

TABLE OF CONTENTS (continued)

NOMENCLATURE LIST

a	axial interference factor at plane of rotor
A_v	area of tip vane normalized by actuator area
A	area of actuator disk normalized to cross-sectional area of wind tunnel
A_w	area of rotor wake normalized to cross-sectional area of wind tunnel
AR	aspect ratio
b	span of tip vane
b'	augmentation factor at zero power level of actuator
B	span of tip vane normalized by rotor radius (b/R)
$\bar{c}$	mean geometric chord (b/A)
C	normalized chord ($\bar{c}/R$)
C_D	drag coefficient
$C_{D_{free}}$	drag coefficient of tip vane in freestream in absence of interference from power blade or other tip vanes
C_{D_i}	induced drag coefficient of tip vane
C_{D_o}	profile drag coefficient of tip vane
C_H	pressure loss coefficient
C_ℓ	section lift coefficient

C_L lift coefficient

$C_{L_{max}}$ maximum lift coefficient

C_M mass flow coefficient

C_p thrust coefficient

$C_{p_{Betz}}$ thrust coefficient for ideal rotor

C_{PL} power loss coefficient due to drag of tipvanes

C_T thrust coefficient (positive in drag sense)

C_{T_a} axial thrust coefficient on actuator

C_{T_D} thrust coefficient of dynamic inducer alone based on actuator area and freestream velocity

C_{T_D} axial thrust coefficient on augmentor

E efficiency of rotor for a specific tip speed ratio

E_B baseline efficiency of rotor alone

H pressure loss in slipstream

I induction factor

$I*$ induction factor ($I \, X/X_s$)

L/D lift-to-drag ratio of tip vane

M_a mass flow through system

M_o mass flow outside wake

M_w mass flow through wake at downstream station where pressure is constant across wake

N   number of tip vanes

P_o pressure upstream of actuator disk

P_w pressure in wind tunnel at downstream station where pressure is constant across wake

r   tunnel speed correction factor (1/V')

R   radius of rotor

Re   Reynolds number

s   tip to tip separation of successive tip vane passages

S   surface area of tip vane (R^2BC)

T_1 spanwise thrust component of downwind tip of tip vane

T_2 spanwise thrust component of upwind tip of tip vane

u_{at} axial flow velocity induced by tip vane

U_∞ wind velocity

V   normalized freestream velocity

V_a velocity through actuator disk

V_o	velocity of outer flow at downstream station where pressure is constant across wake
V_w	velocity in wake at downstream station where pressure is constant across wake
X	tip speed ratio $(\Omega R/U_\infty)$
X_D	design tip speed ratio
X_s	synchronous tip speed ratio
θ	wind angle
β	feather angle
Ω	rotational velocity of rotor
γ	tilt angle of tip vane (angle positive when upwind tip is tilted below horizontal)
Γ	bound circulation strength
ρ	air density
Λ	sweep angle of tip vane (angle positive when upwind tip lags downwind tip)
α	angle of attack
λ	constant
$\Delta\theta$	wind angle induced by the tip vane

Subscripts

prime (')	denotes performance parameters for dynamic inducer in unbounded flow
Δ	denotes change in parameter
2dim	denotes parameter for two-dimensional lifting surface
3dim	denotes parameter for three-dimensional lifting surface

SECTION 1.0

INTRODUCTION

Innovative concepts are being sought to improve the technical and economic performance of wind energy conversion systems (WECS). One promising technique for improving the cost-effectiveness of WECS is the use of tip vanes. Tip vanes are small airfoils attached approximately at right angles to the rotor tips with their span oriented approximately parallel to the local freestream (Figure 1-1). The tip vanes serve to increase the capture area and power output of the rotor, and have the potential of high power increases without significant penalties in terms of the size, complexity or cost of the system.

The WEC system has the capability of achieving about the same augmentation as a static duct, which also augments the mass flow through the actuator. In the present case, the aerodynamic forces on the moving tip vanes induce flow through the rotor and achieve augmentation. Thus, it is referred to as a dynamic inducer. Since it requires considerably less structure, the dynamic inducer has the potential for surpassing the overall efficiency and economic performance of conventional static augmentors.

The cost/benefit advantages of the dynamic inducer include:

- significant power increases,

- simple and compact structure,

- adaptability to conventional rotors, and

- feathering control via tip vanes possible.

The concept of using tip vanes to increase the power extraction of a wind turbine was first introduced in The Netherlands (van Holten, 1974, 1976). van Holten calculated the increased power extraction by relating the increased mass flow to the radial forces on the tip vanes. For a cylindrical vortex, the induced drag was calculated from the energy in the far wake. The results of the calculations indicated that, for a given frontal area, the power output of a WECS can be doubled by installing tip vanes.

The basic concept of flow induction was discussed in more general terms in the United States (Lissaman, 1976a, b). It was shown that, for a given tip vane rotor geometry, the augmentation varies like X^2, while the drag of the tip vane is proportional to X^3, where X is the tip speed ratio of the rotor.

A more detailed analysis of the dynamic inducer concept was carried out earlier (Lissaman and Walker, 1978). A staggered array vortex model was developed to compute the induced drag and flow augmentation of dynamic inducer systems. For a commercially available 3.6-m diameter WECS, the results of the calculations showed that power augmentation increases of 50% may be attainable at optimal conditions.

Performance calculations for tip vanes were carried out recently (de Vries, 1979). The calculations were based upon momentum arguments and neglected induced drag. They showed that augmentation ratios in excess of 5 may be achievable for high tip speed ratio rotors equipped with optimum tip vanes.

1
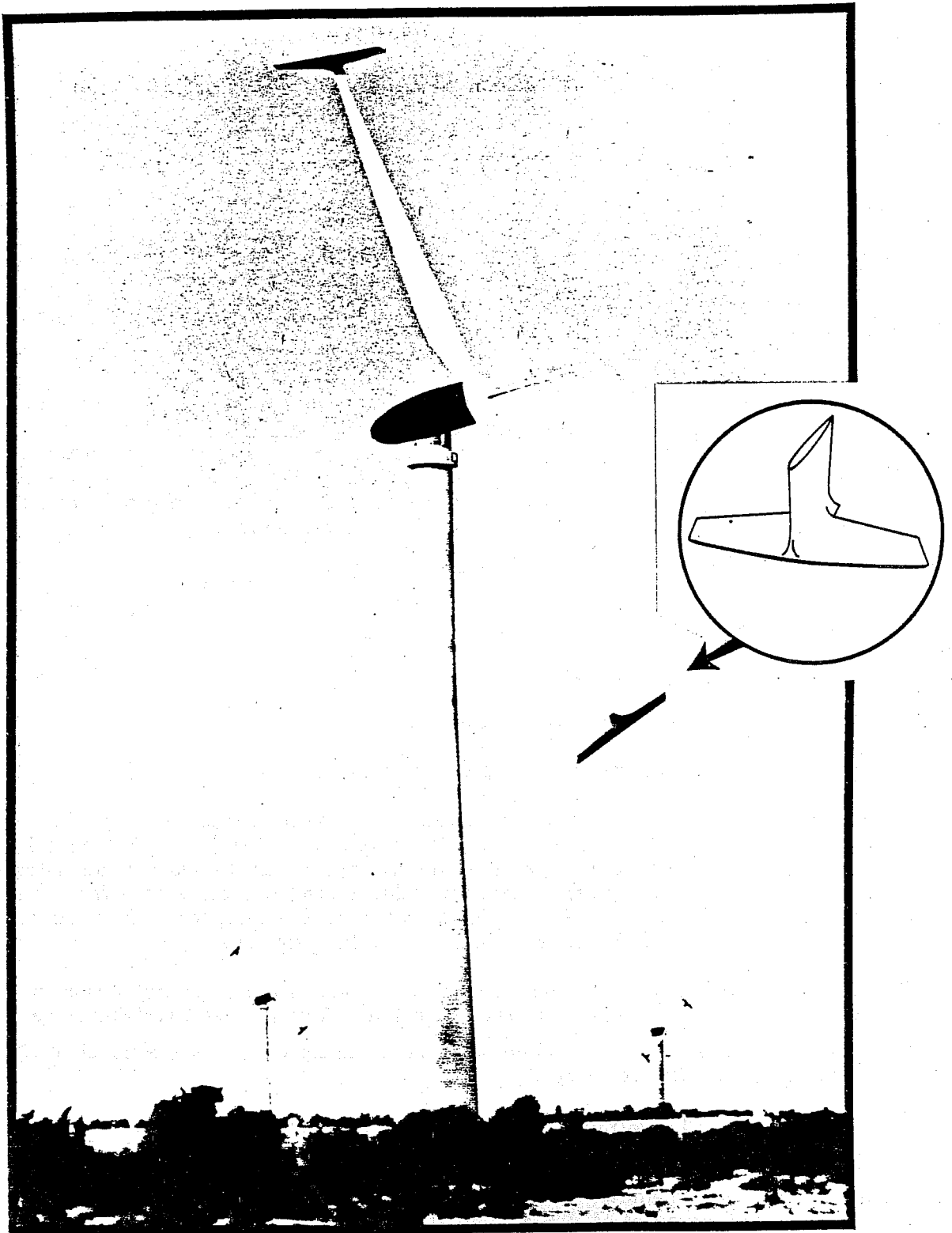
Figure 1-1.   CLUSTER OF DYNAMIC INDUCERS (ADAPTED FROM POSTER SHOWING
               CONVENTIONAL WECS PUBLISHED BY NATIONAL SWEDISH BOARD
               OF ENERGY SOURCE DEVELOPMENT)

In summary, the available theoretical models suggest an excellent performance potential for tip vanes. However, they neglect three-dimensional flows and separation effects, which can be important factors in the overall system performance.

The high augmentations predicted for the dynamic inducer system have not been observed experimentally prior to the present study. Experimental measurements of the flow augmentation and drag of tip vanes were conducted in The Netherlands (van Holten, 1978). Mass augmentation ratios of 4 to 5 have been calculated on a model tip vane system without power blades. The calculations were based upon expansion of the streamtube observed using a smoke tracer for flow visualization. Corresponding torque measurements indicated relatively high total drag for the tip vanes, $C_D \sim 0.03$, attributable primarily to viscous drag. The tip vanes were operated at a synchronous tip speed ratio designed for vortex cancellation. At the synchronous tip speed, the trailing vortex from the upwind tip is aligned with the trailing vortex from the downwind tip of the following tip vane. Analysis of the torque measurements suggested low values of induced drag -- consistent with theory. The drag coefficient of the tip vanes approached the drag coefficient of a two-dimensional airfoil.

Performance measurements on a commercially available 3.6-m diameter WECS fitted with tip vanes were conducted in the United States (Lissaman and Walker, 1978). The observed power output of the dynamic inducer was less than that of the basic rotor at higher tip speed ratios. It is believed that the flow in the tip vane rotor junction was separated, so that the incremental drag due to separation cancelled the anticipated 40% increase in power due to augmentation.

The above experimental results show that the dynamic inducer concept requires careful consideration of separation and drag effects. While theoretical analysis and limited experimental tests have shown the potential for mass flow augmentation, the demonstration of satisfactory performance of the system has been hampered by drag and separation problems. Significantly, no previous results have been published from the complete dynamic inducer system tested under controlled conditions.

For the past three years, AeroVironment Inc. (AV) has been active with the analytical and experimental investigation of the dynamic inducer. This work was originally funded by the U.S. Department of Energy (DOE) and later supported by SERI under Contract No. XH-9-8085-1. The goal of this program was to experimentally substantiate the improved power output of a dynamic inducer system. The specific elements of the program include:

- Task 1 - Analysis. An analytical model was developed with the capability of predicting tip vane performance in viscous rotating flow and for non-synchronous operation. The model was utilized for the development of designs for tip vanes and power blades for wind tunnel tests and field tests.

- Task 2 - Wind Tunnel Test. A scale model of the dynamic inducer was designed, fabricated, and tested in a wind tunnel facility.

- Task 3 - Field Test. A full-scale dynamic inducer system was designed, fabricated, and tested on a conventional three-bladed, 3.6-m diameter WECS.

The following sections describe the accomplishments for each of the above tasks.

3

SECTION 2.0

ANALYTICAL PROGRAM

2.1   DESIGN CRITERIA

To determine the performance characteristics of the dynamic inducer and to select a suitable design based upon these calculations, an analytical investigation was conducted. To evaluate candidate rotor and tip vane designs, the following criteria were used:

- potential for high augmentation,

- compatibility with available three-bladed, 3.6-m, 1200-watt commercial (Kedco) WECS, and

- ease of fabrication.

An available, non-optimum three-bladed rotor was selected as the baseline system (Figure 2-1). While it was recognized that higher augmentations are possible with more advanced configurations, such as a two-bladed, low-solidity, high tip speed rotor, it was felt that further optimization of the WECS design could be achieved once the basic operation of the dynamic inducer was demonstrated.

2.2   PERFORMANCE PREDICTION MODELS

2.2.1   Rotor Performance

The basic computer program used for calculating rotor performance is an updated version of PROP code developed by the NASA Lewis Research Center (Wilson and Lissaman, 1976) and described in a recent report (Hibbs and Radkey, 1980). This program computes horizontal axis windmill performance using the Glauert momentum strip theory. As input, the program uses the twist, chord, and the lift-drag characteristics of the airfoils at several stations along the blade. The specification of the airfoil characteristics at each station allows the inclusion of the Reynolds number effects along the blade's length. As the blade rotates, each element sweeps out an annular strip.

The Glauert strip theory determines the windmill performance by equating the blade forces, both axial and circumferential, determined by a two-dimensional airfoil theory, with the change in momentum of the air going through the annular strip. Once the change in the momentum is known, the axial and circumferential interference factors are computed. This allows computation of the flow velocity and angle of attack at the blade element, closing the problem. Typically, the equations describing the above process are solved in an iterative manner.

Figure 2-2 gives the predicted power coefficient of the baseline rotor system as a function of tip speed ratio and blade feather angle. The calculations show that, at a nominal blade feather angle of 12 degrees, the maximum power coefficient of the rotor is $C_p = 0.415$ at a tip speed ratio X = 3.2. Appendix A gives a tabulation of the detailed performance characteristics of the rotor, including the thrust, torque, and power coefficients.

One-Third Scale Model of Kedco 1200-watt Turbine

Design Tip Speed Ratio	4.5
Solidity	13%
Profile	Wortman FX60-126 (root), FX61-184 (tip)
Twist	9-1/2°

$\overline{c} = 0.36$

3.6

1.2

(dimensions in meters)
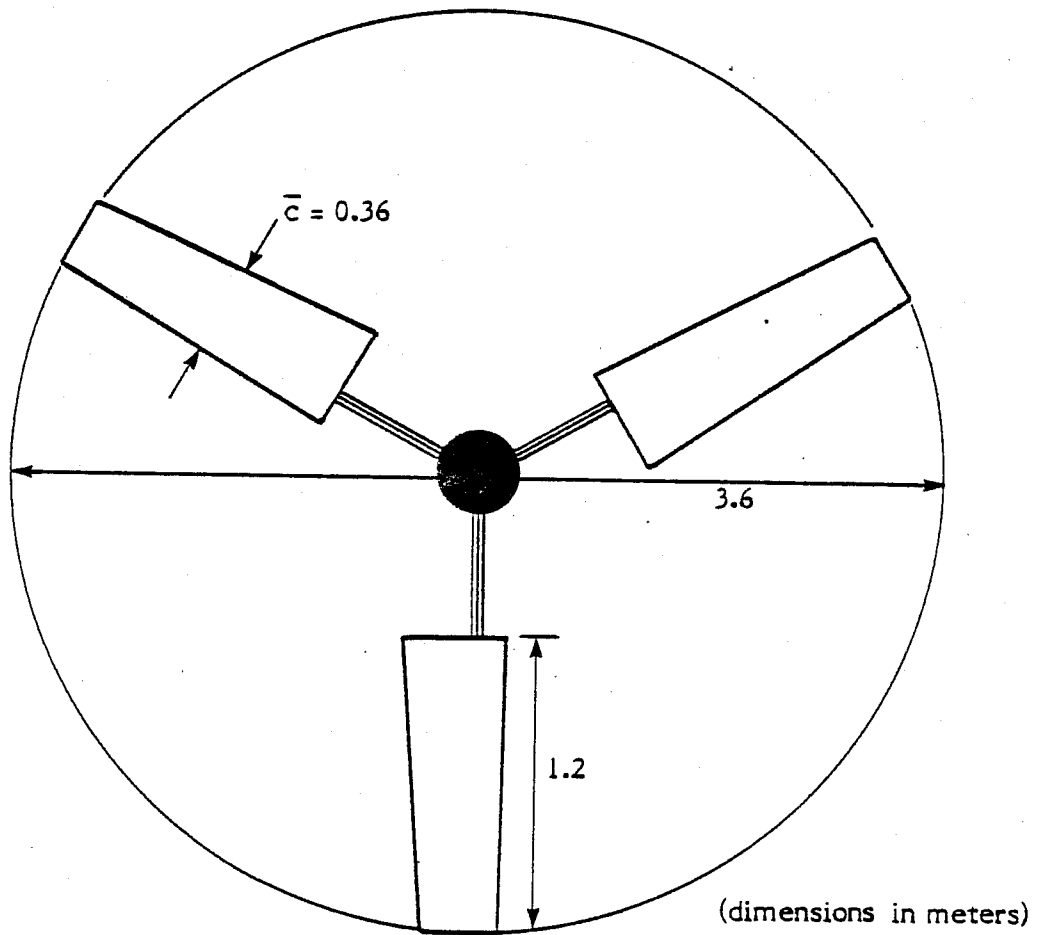
Figure 2-1.   BASELINE ROTOR SYSTEM SELECTED FOR PROGRAM

5

Blade Feather Angle
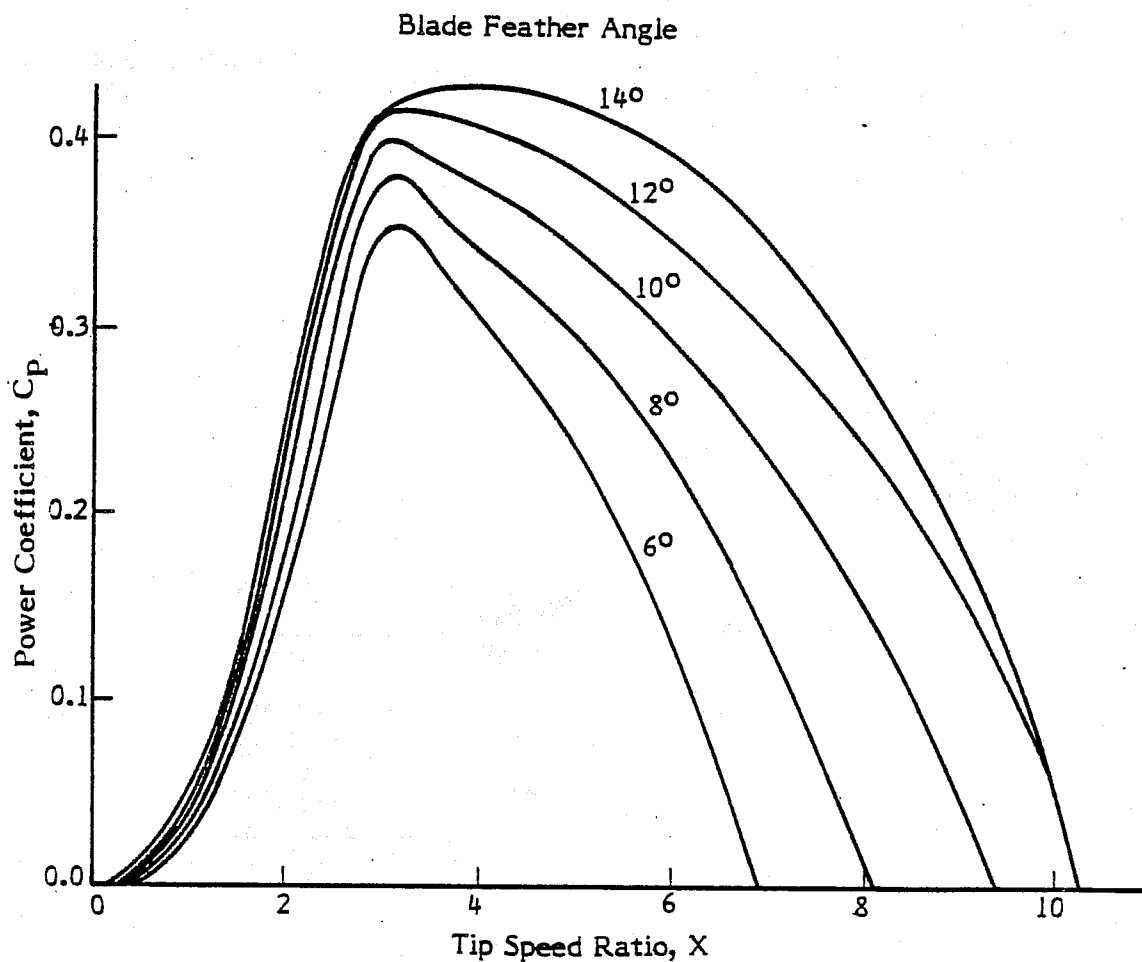
FIGURE 2-2. PREDICTED POWER COEFFICIENT VERSUS TIP SPEED RATIO FOR BASELINE ROTOR

6

2.2.2 Dynamic Inducer Performance

The performance of the dynamic inducer system can be modeled on the basis of momentum theory. The power coefficient for the dynamic inducer is given by:

$$C_P = E C_H C_M - C_{PL} \quad , \tag{2-1}$$

where the efficiency of the rotor for a specific tip speed ratio is found from

$$E = E_B \left[1 - (1 - X/X_D)^2 \right], \tag{2-2}$$

where

X_D = rotor design tip speed ratio

E_B = rotor base efficiency (normally set to 80%)

C_H = pressure loss coefficient

C_M = mass flow coefficient

C_{PL} = power loss coefficient due to the drag of the tip vanes

The pressure loss coefficient is equal to the normalized axial momentum through the rotor,

$$C_H = 4a(1-a) \quad , \tag{2-3}$$

where

a = axial interference factor at the plane of the rotor

The mass flow coefficient of the system is given by:

$$C_M = \Delta C_M + 1 - a \quad , \tag{2-4}$$

where the incremental mass flow generated by the tip vanes, ΔC_M, is given by

$$\Delta C_M = \frac{X C C_L I^*}{4\pi} \quad . \tag{2-5}$$

The chord of the tip vane is normalized by the rotor radius is $C = \bar{c}/R$, and the lift coefficient of the tip vane is C_L.

The induction factor, I^*, consists of the induction factor at the synchronous tip speed ratio, I, scaled by the ratio of actual to synchronous tip speed ratio,

$$I^* = \frac{I X}{X_S} \quad . \tag{2-6}$$

Figure 2-3 gives the axial induction factor taken from an earlier work (Lissaman and Walker, 1978).

7
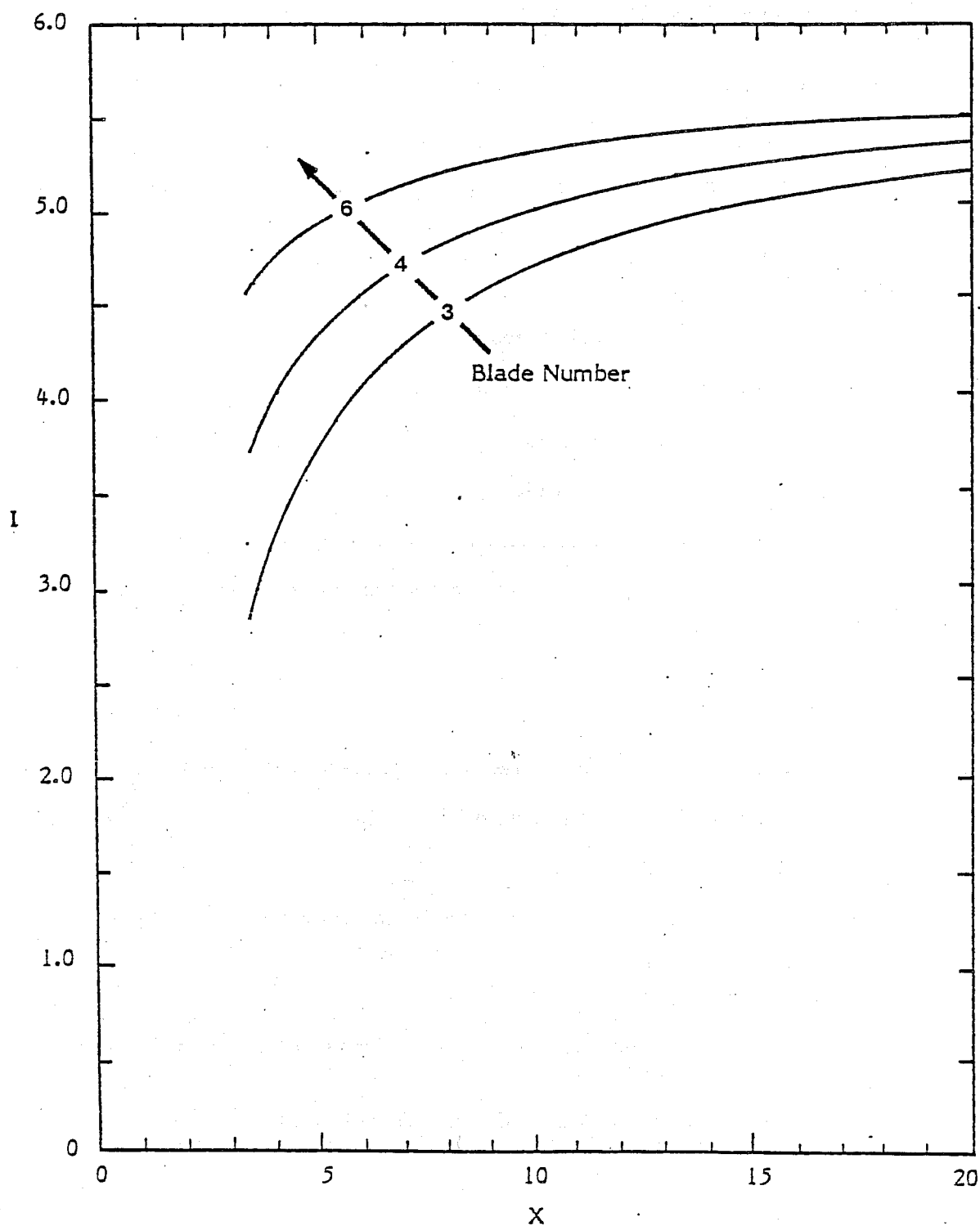
Figure 2-3. AXIAL INDUCTION FACTOR FOR DIFFERENT RATIOS OF TIP SPEED RATIO AND BLADE NUMBER

The power coefficient loss due to tip vane drag is given by

$$C_{PL} = \frac{X^3 A_v N (C_{D_o} + C_{D_i})}{\pi} \,,$$ (2-7)

where

A   =   area of a tip vane normalized by the actuator area

N   =   number of tip vanes

C_{D_o} =   profile drag coefficient of the tip vane

C_{D_i} =   induced drag coefficient of the tip vane

The induced drag coefficient of the tip vane, C_{D_i}, was calculated from a planar staggered array program developed at AV. The planar staggered array program calculated the downwash field and induced drag coefficient for an array of 20 tip vanes represented by 200 horseshoe vortices and 220 trailing vortices. Figure 2-4 shows a sketch of the planar wake geometry.

The AeroVironment dynamic inducer performance model, DYPERF, uses the above formulation to optimize C_P for the best value of the axial interference factor, $\underline{a}$. The input parameters include:

- the span, parasite drag coefficient (drag coefficient excluding induced drag), angle of attack for each of 10 tip vane sections

- the chord and twist distribution of the tip vane,

- the design tip speed ratio, rotor efficiency, and number of blades for the power blade, and

- the loading (CC_L) of the power blade.

Figure 2-5 shows a sample output from a staggered array wing. The plot shows a tip vane lift coefficient normalized by the two-dimensional lift coefficient, and a tip vane-induced drag coefficient normalized by the three-dimensional lift coefficient for high aspect ratio planforms, as a function of the spacing parameter,

$$\frac{b}{b+s} = \frac{N B X}{2\pi} \,,$$ (2-8)

where b is the tip vane span and s is the tip vane separation (Figure 2-5).

At the synchronous condition, b/b+s = 1, the lift coeffient of the tip vane is about 80% of the two-dimensional lift coefficient, while the drag coefficient is about 50% of the three-dimensional drag coefficient for high aspect ratio planforms. At higher tip speed ratios (subsynchronous operation), the lift and drag coefficients of the tip vane approaches that of a three-dimensional low aspect ratio airfoil. The minimum drag for the tip vane is predicted to occur at supersynchronous conditions, X/X_S = b/b+s = 0.8.
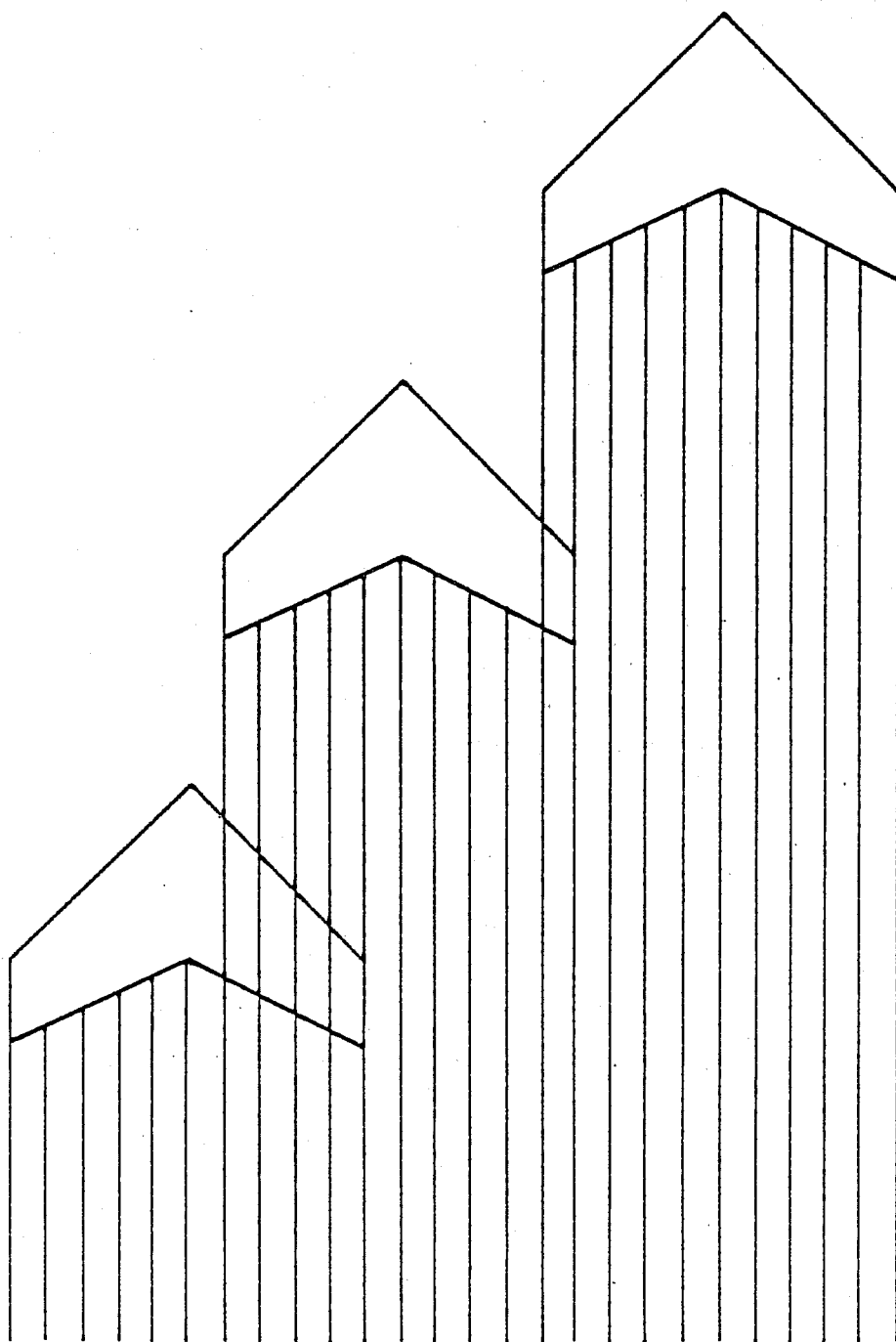
Figure 2-4.   SKETCH OF WAKE GEOMETRY FOR TIP VANE INDUCED DRAG
CALCULATIONS

Relative Induced Drag Performance
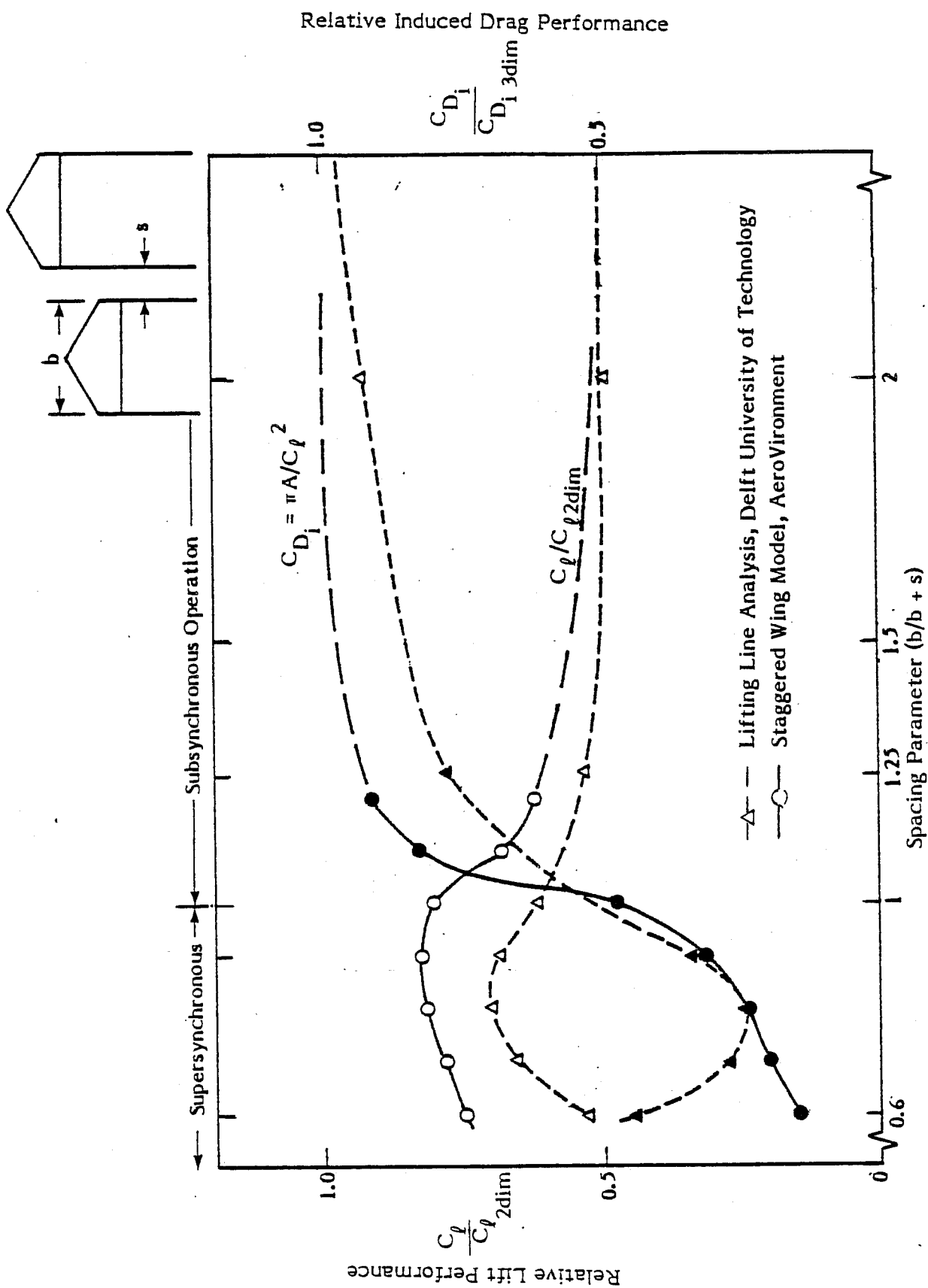
Figure 2-5.   PREDICTED INDUCED DRAG AND LIFT COEFFICIENTS FOR ASPECT RATIO 2 TIPVANES

11
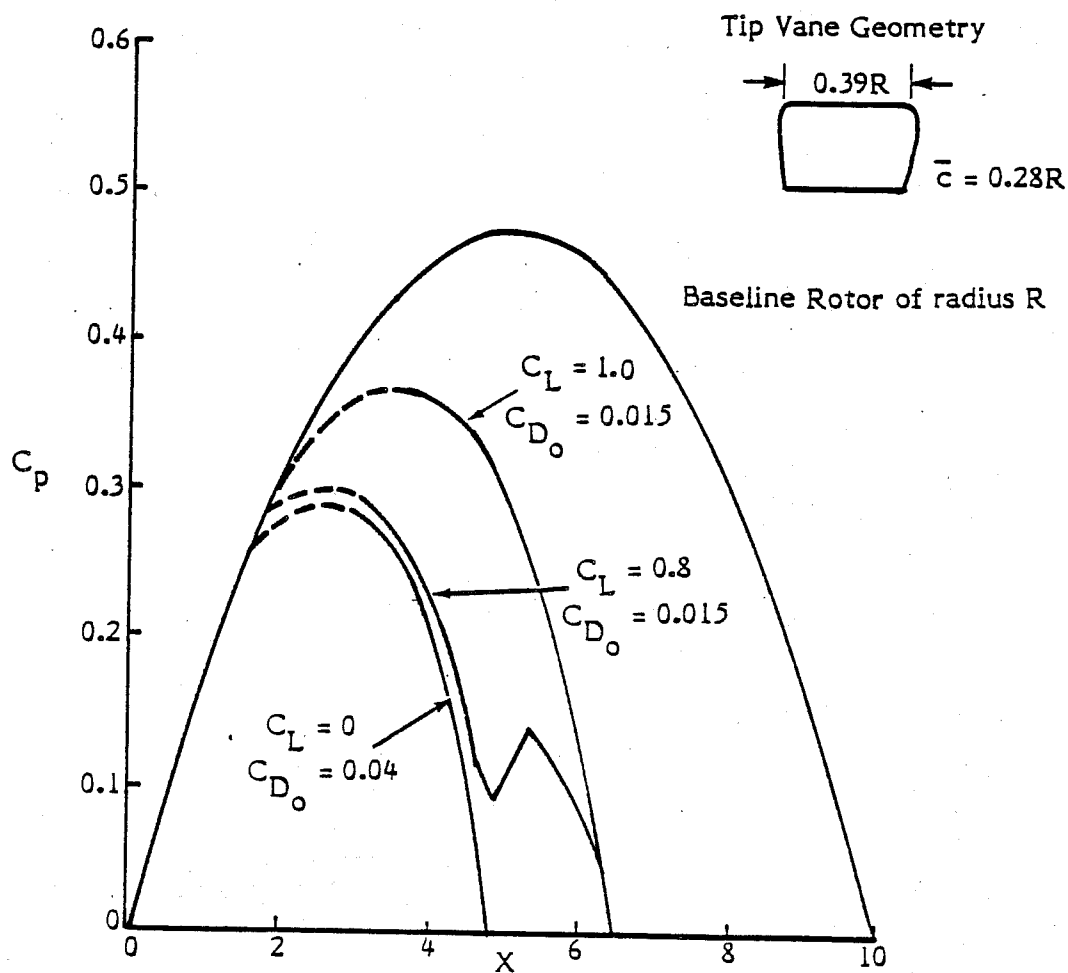
Figure 2-6. PREDICTED POWER COEFFICIENT VERSUS TIP SPEED RATIO FOR BASELINE ROTOR SYSTEM WITH 1.4 ASPECT RATIO TIP VANES

Figure 2-5 gives, for comparison purposes, the lift and induced drag coefficients calculated upon the basis of lifting-line analysis (van Bussel, 1978) for the tip vane. Results from the AV-staggered wing model show the same general trends as the lifting-line analysis. However, the AV program predicts higher induced drag and higher lift coefficients at subsynchronous tip speed ratios, and lower induced drag and lower lift coefficients at supersynchronous tip speed ratios. This result is attributed to differences in the two formulations. The lifting-line analysis assumes that the lift distribution on a tip vane is principally affected by the disturbing downstream flow field of the preceding tip vane. Thus, the analysis considers only the velocity perturbation caused by the wing itself and its follower.

On the other hand, the AV-staggered wing model includes the velocity perturbation caused by the wing itself and up to 19 followers. In this respect, the AV-staggered wing model is believed to be more representative of the actual dynamic inducer configuration. However, the two models are planar so that the full three-dimensional tip vane wake geometry is not adequately represented. For this reason, the predicted tip vane performances shown in Figure 2-5 are approximate.

Based upon the above formulation, performance calculations were carried out for different tip vane configurations. Figures 2-6 through 2-8 give the predicted power coefficients for three candidate tip vane configurations. The power coefficient versus tip speed ratio of the baseline rotor is approximated as a parabola with a maximum $C_p = 0.475$ and is also shown in the figures.

The results of the calculations indicate that the baseline rotor equipped with a set of medium aspect ratio, high lift-to-drag ratio tip vanes can achieve a power coefficient approaching the ideal performance (Betz) limit of 0.593.

2.3   SENSITIVITY OF THE DYNAMIC INDUCER TO DESIGN PARAMETERS

2.3.1   Size of Tip Vane

An expression for the total power augmentation of the dynamic inducer system was given in the previous section. This formulation can be normalized by the performance of an ideal rotor and further simplified by assuming a synchronous tip speed ratio, and by assuming that all the augmentation is recovered by the rotor (E = 1.0), so that

$$\frac{C_p}{C_{p_{Betz}}} = 1 + (\frac{3X}{8\pi}) I C C_L \left[1 - \frac{9\pi X}{(L/D) I}\right] , \qquad (2-9)$$

where L/D is the lift-to-drag ratio of the tip vane.

A second relationship which governs the size of the tip vane is obtained from the condition that the design tip speed ratio of the rotor matches the tip speed ratio of the tip vanes at the minimum drag condition

$$X_D = X_{min\ drag} , \qquad (2-10)$$

where $X_{min\ drag}$ equals f X_S, and f is a function of the aspect ratio of the tip vane, as illustrated in the earlier induced drag calculations.

13
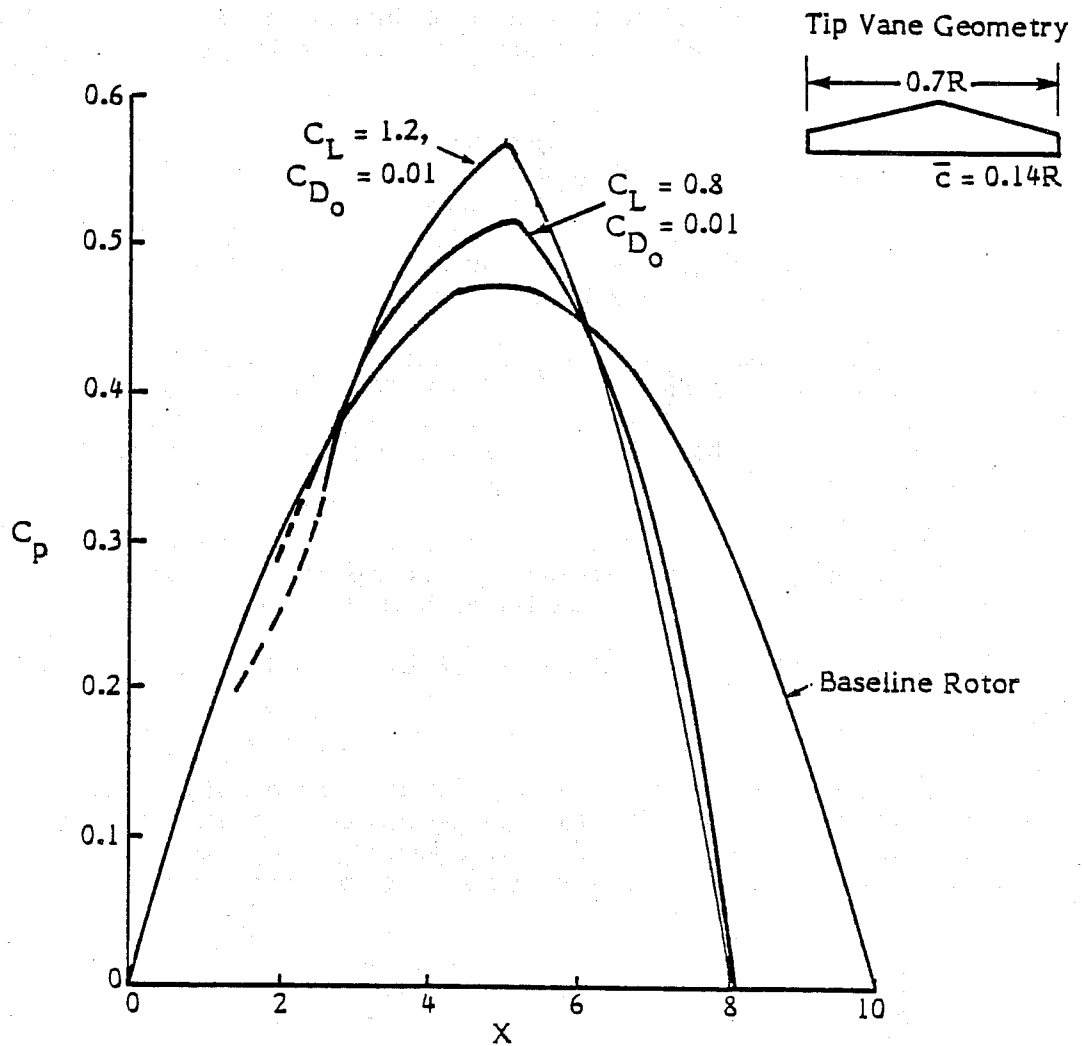
Figure 2-7. PREDICTED POWER COEFFICIENT VERSUS TIP SPEED
RATIO FOR BASELINE ROTOR SYSTEM WITH 5.0 ASPECT
RATIO TIP VANES
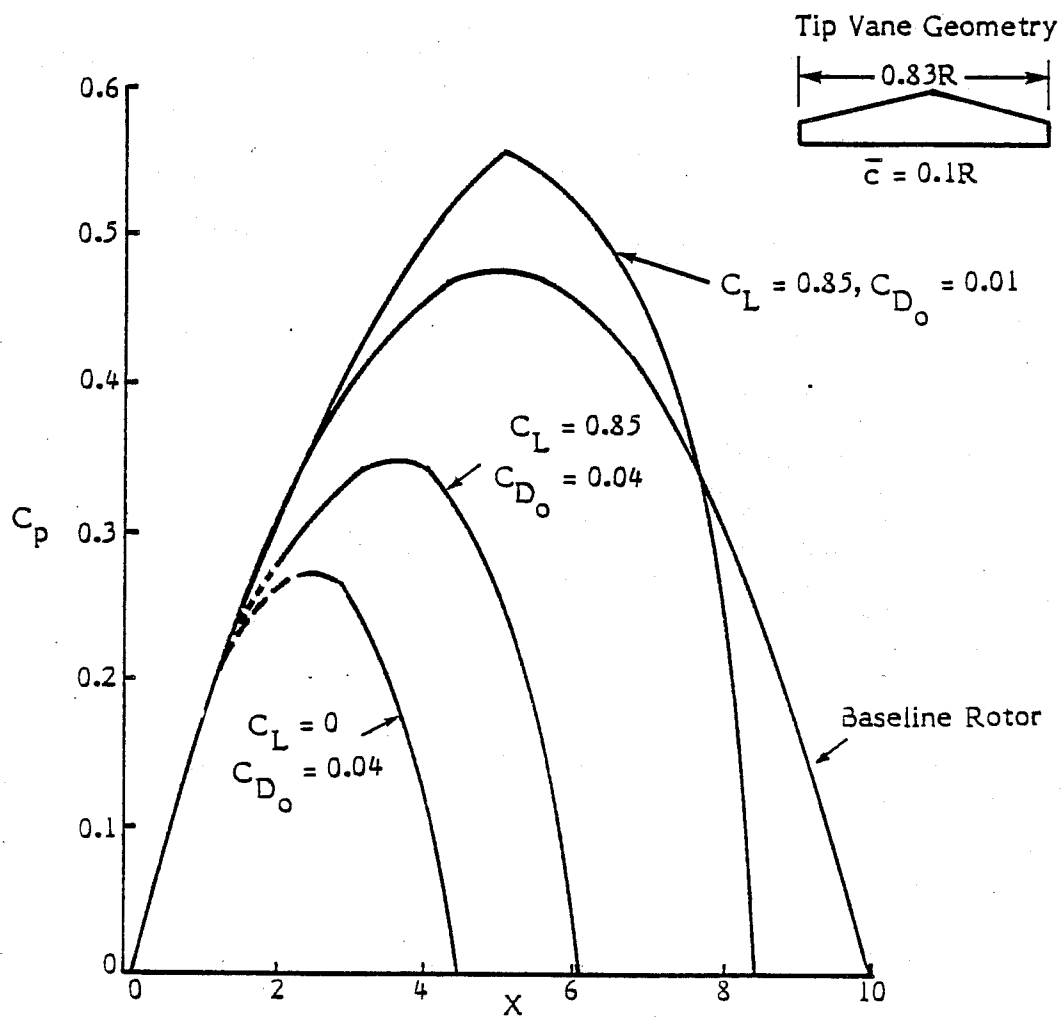
Figure 2-8. PREDICTED POWER COEFFICIENT VERSUS TIP SPEED RATIO FOR BASELINE ROTOR SYSTEM WITH 8.3 ASPECT RATIO TIP VANES

Therefore, it follows that the optimum span of the tip vane normalized by the rotor radius is given by

$$B = \frac{2\pi f}{N X_D} \quad .$$

(2-11)

It is important to note that the span of the tip vane is inversely proportional to the design tip speed ratio of the rotor, so that large tip vanes are necessary for low tip speed ratio turbines. Conversely, small tip vanes are suitable for high tip speed ratio rotors, such as the modern, low solidity, two-bladed WECS.

The above relationship governs the size of the tip vane for a given system. Based upon earlier measurements (Lissaman and Walker, 1978), for example, for the three-bladed baseline rotor, the design tip speed ratio is $X_D = 4.0$, and array calculations suggest that for medium aspect ratio tip vanes the minimum induced drag configurations occurs in the range of $f = 1$ to 1.3. Therefore, the optimum tip vane span is $B = 0.5$ to 0.7. To achieve a power coefficient approaching the Betz limit, the geometric chord of the tip vanes is selected to be $C = 1.2$ to 1.4.

2.3.2 Profile of Tip Vane

The lift-to-drag ratio of the tip vane plays an important role in the power augmentation of the system. A formulation was given in the preceding section for the power coefficient of the dynamic inducer normalized by the power coefficient for an ideal rotor. For the dynamic inducer to achieve a lift coefficient greater than or equal to the Betz limit, $C_p/C_{p_{Betz}} \geq 1$, the lift-to-drag ratio of the tip vane is

$$L/D \geq 9\pi X/I \quad .$$

(2-12)

Figure 2-9 shows the minimum lift-to-drag ratio necessary to equal or surpass the Betz limit for a three-bladed dynamic inducer system. The results show that for the baseline rotor with a design tip speed ratio $X_D = 4$, the tip vane $L/D \geq 34$ for $C_p/C_{p_{Betz}} \geq 1$.

Note that for higher tip speed ratio rotors, higher values of the tip vane L/D are necessary to achieve the same performance. However, as noted earlier, the size of the tip vane will be reduced for higher a tip speed ratio system. Thus, a tradeoff occurs between the tip vane size and L/D. For example, for the selected low tip speed ratio, three-bladed baseline system, the necessary size for the tip vane is relatively large, while the necessary L/D is low. Clearly, it is a conservative design with room for improvement.

An important factor in the overall L/D of the tip vane is the performance of the selected airfoil section. Figure 2-10 is a plot of the lift-to-drag ratio versus Reynolds number, Re, for different airfoils. The calculated Reynolds number for a one-third scale model of the baseline rotor system operating in a wind tunnel is Re = 384,000. At this Reynolds number, the maximum lift-to-drag ratio of 125 is achieved with the NACA 4415 profile. This profile has an lift-to-drag ratio of 150 for the full-scale baseline rotor with Re = 852,000. For this reason, the NACA 4415 section was selected as the tip vane design for this program.

Note that for large WECS with $Re > 10^6$, the maximum lift-to-drag ratio is likely to be higher, particularly with advanced airfoils of the incipient separation type. These results suggest that the design of tip vanes for high tip speed ratio of large WECS is attractive.

16
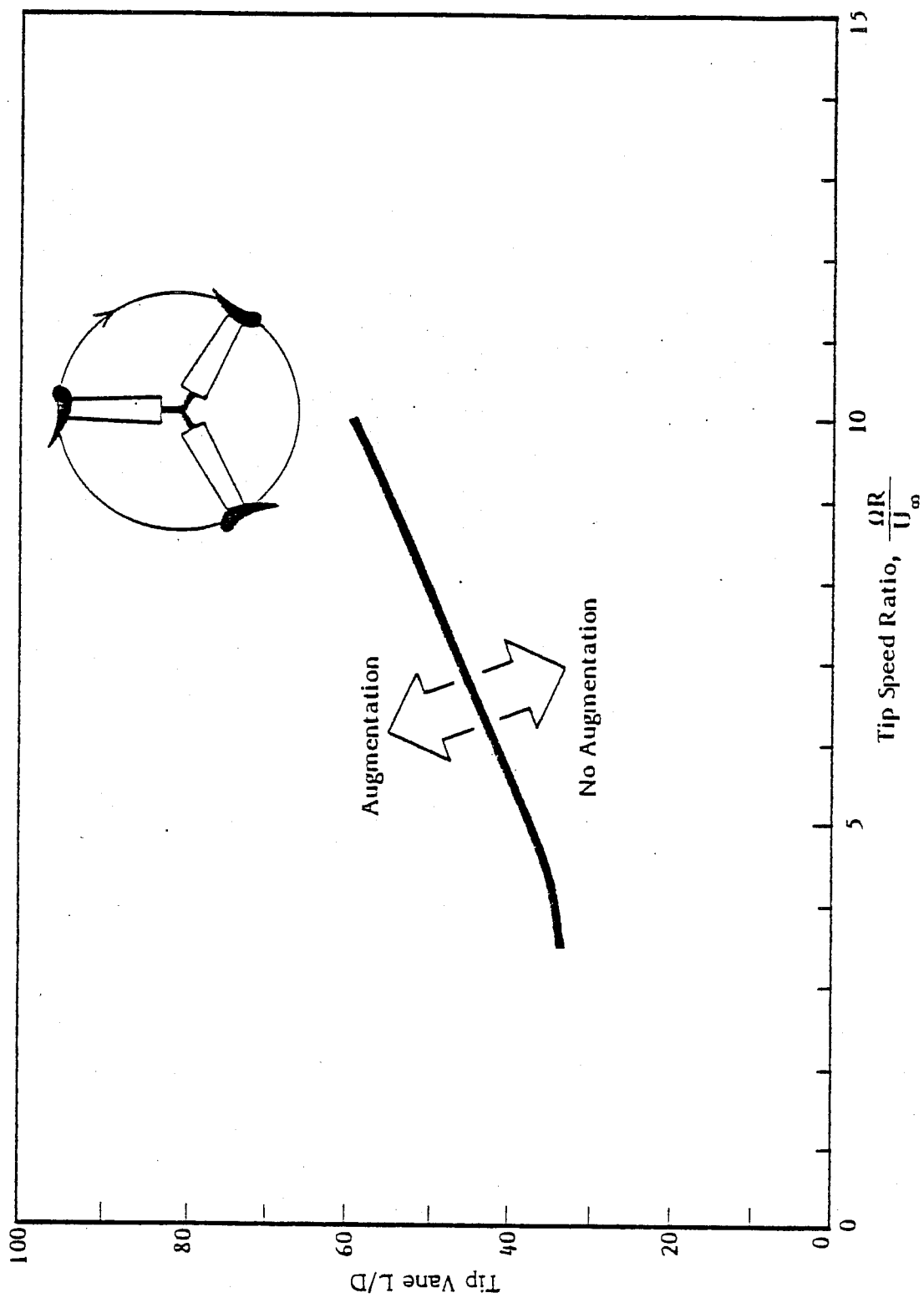
Figure 2-9. MINIMUM TIP VANE LIFT–TO–DRAG RATIO REQUIRED TO EQUAL OR EXCEED THE BETZ LIMIT
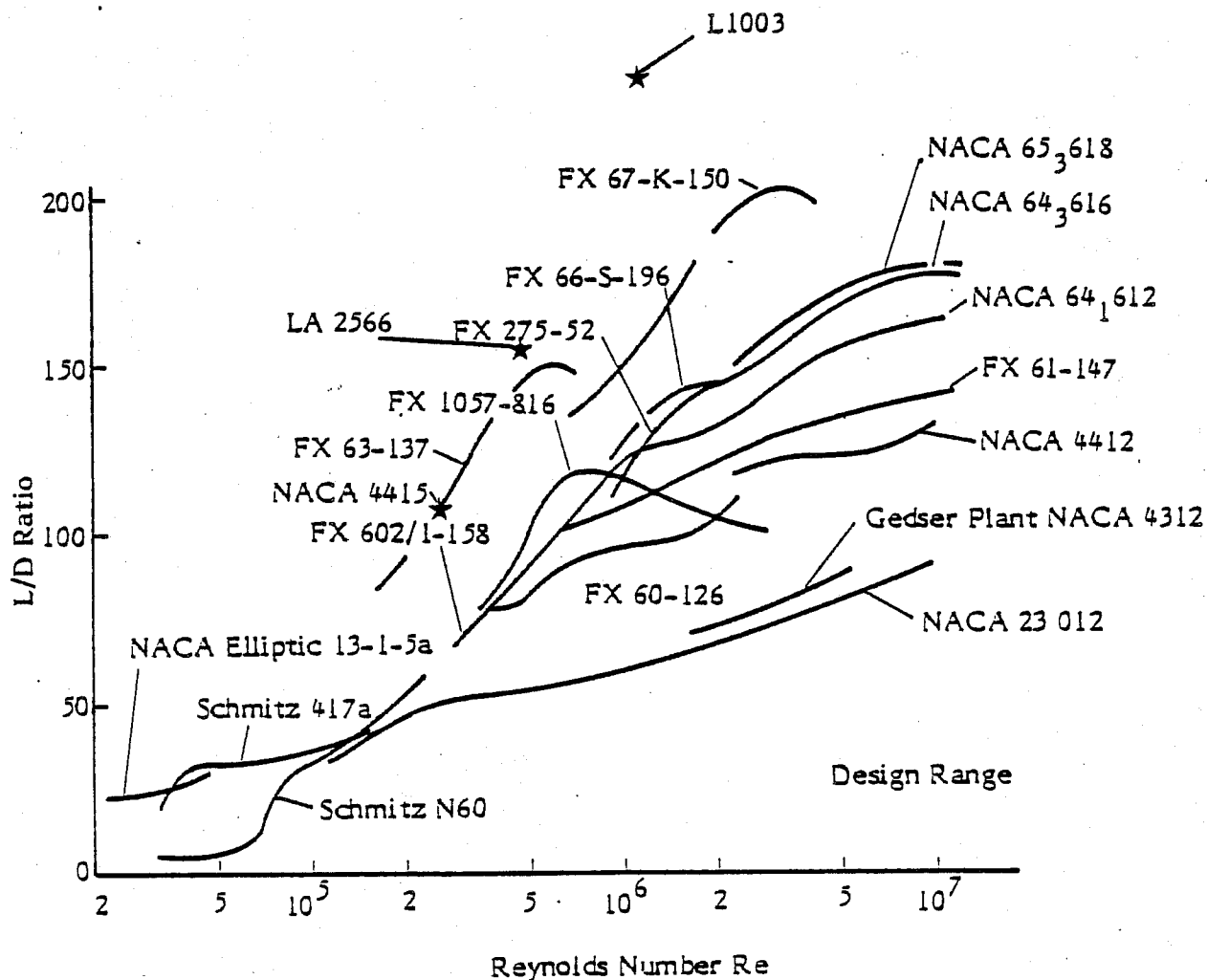
Figure 2-10. LIFT-TO-DRAG RATIO AS A FUNCTION OF REYNOLDS NUMBER FOR VARIOUS AIRFOIL SECTIONS

2.3.3 Geometry of Tip Vanes

To maximize the performance of the dynamic inducer, a tip vane geometry with the highest lift-to-drag ratio is sought. Aspect ratio, taper, and twist can be used to control the spanwise loading of the tip vanes and to maximize the lift-to-drag ratio. With the exception of twist, the effect of these parameters on dynamic inducer performance was investigated in the present study. To minimize the complexity of the tip vanes for design and fabrication purposes, only straight tip vanes without twist were considered.

A tip vane operates in the wake of the preceding tip vane and power blade. Therefore, variations occur in the spanwise loading of the tip vane due to vortex interactions. Figure 2-11 illustrates a two-dimensional tip vane array operating in the synchronous mode. The figure shows that the trailing vortex filament from a tip vane generates a downwash on the upwind portion and an upwash on the downwind portion of the following tip vane. The idealized sketch does not show the trailing vortex shed by the power blade, which also affects the tip vane spanwise loading. Under non-synchronous operating conditions, the spanwise loading distribution is more complicated, since the vortex filament from the upwind tip of a tip vane does not cancel the vortex filament from the downwind tip of the following tip vane.

To maximize the lift-to-drag ratio of the tip vane, it is desirable to obtain a lift coefficient which approaches that of a two-dimensional airfoil. Figure 2-12 shows the spanwise loading distribution computed for a rectangular tip vane. The calculations are based upon the AV staggered-wing model discussed earlier. For comparison, calculations from the Delft model (van Bussel, 1978) are also shown.

In uniform flow, the lift coefficient of the aspect ratio, AR = 2, tip vane is approximately one-half that of a two-dimensional airfoil. For a 40% span wake overlap, s/b = -.4, the lift coefficient of the tip vane begins to approach that of a two-dimensional airfoil. These trends suggest that the lift-to-drag ratio of the tip vane can be maximized through proper selection of aspect ratio and taper.

While the vortex interactions can be used to enhance tip vane performance, the problem of separation is also present. As shown earlier in Figure 2-12, a spike occurs in the spanwise loading distribution at the location of the vortex filament. If the resulting lift coefficient is above that of the maximum lift coefficient of the profile, separation will occur. The incremental lift coefficient of the tip vane, defined as the difference in the maximum lift coefficient between the actual tip vane and a tip vane operating in uniform flow, varies with aspect ratio and is not very sensitive to the taper ratio, as illustrated in Figure 2-13 for candidate tip vane geometries.

Off-design performance is another consideration in the selection of tip vane geometry. Since the tip vane lift-to-drag ratio is influenced by the vortex wake geometry, and since the vortex geometry changes with rotor tip speed ratio, the performance of the dynamic inducer can vary considerably with tip speed. Figure 2-14 illustrates the effect of tip speed ratio on the spanwise lift distribution of the tip vane. The trends indicate that the maximim lift coefficient occurs at slightly supersynchronous tip speeds, $X/X_S \sim 1.4$, for the low aspect ratio design considered.

Considering the effects of tip vane geometry, a medium aspect ratio planform with slight taper was selected for the baseline rotor. The induced drag calculations showed that this design had a sufficiently high lift-to-drag ratio to achieve a performance approaching that
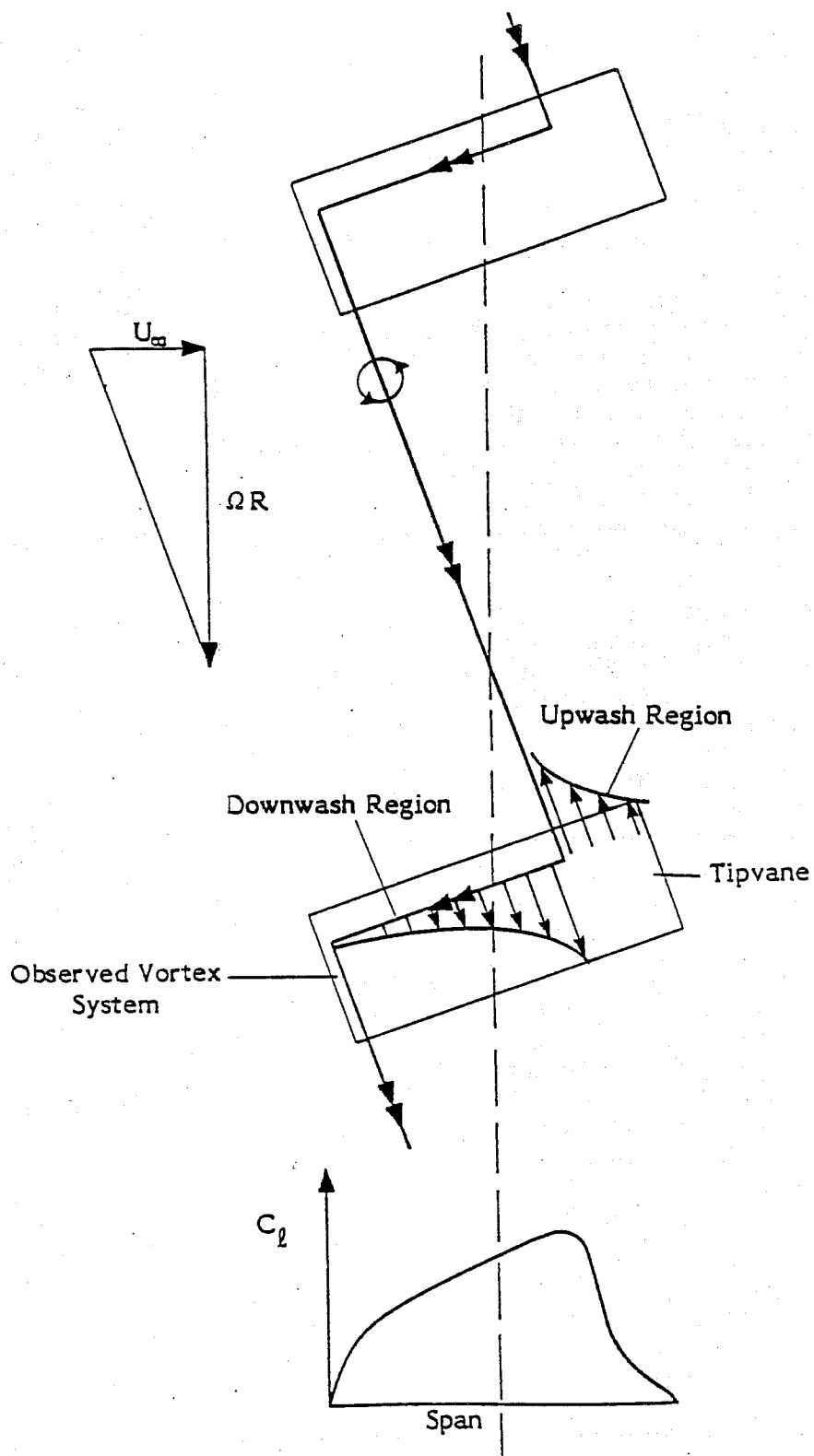
Figure 2-11.   VARIATION IN SPANWISE LOADING OF TIP VANE
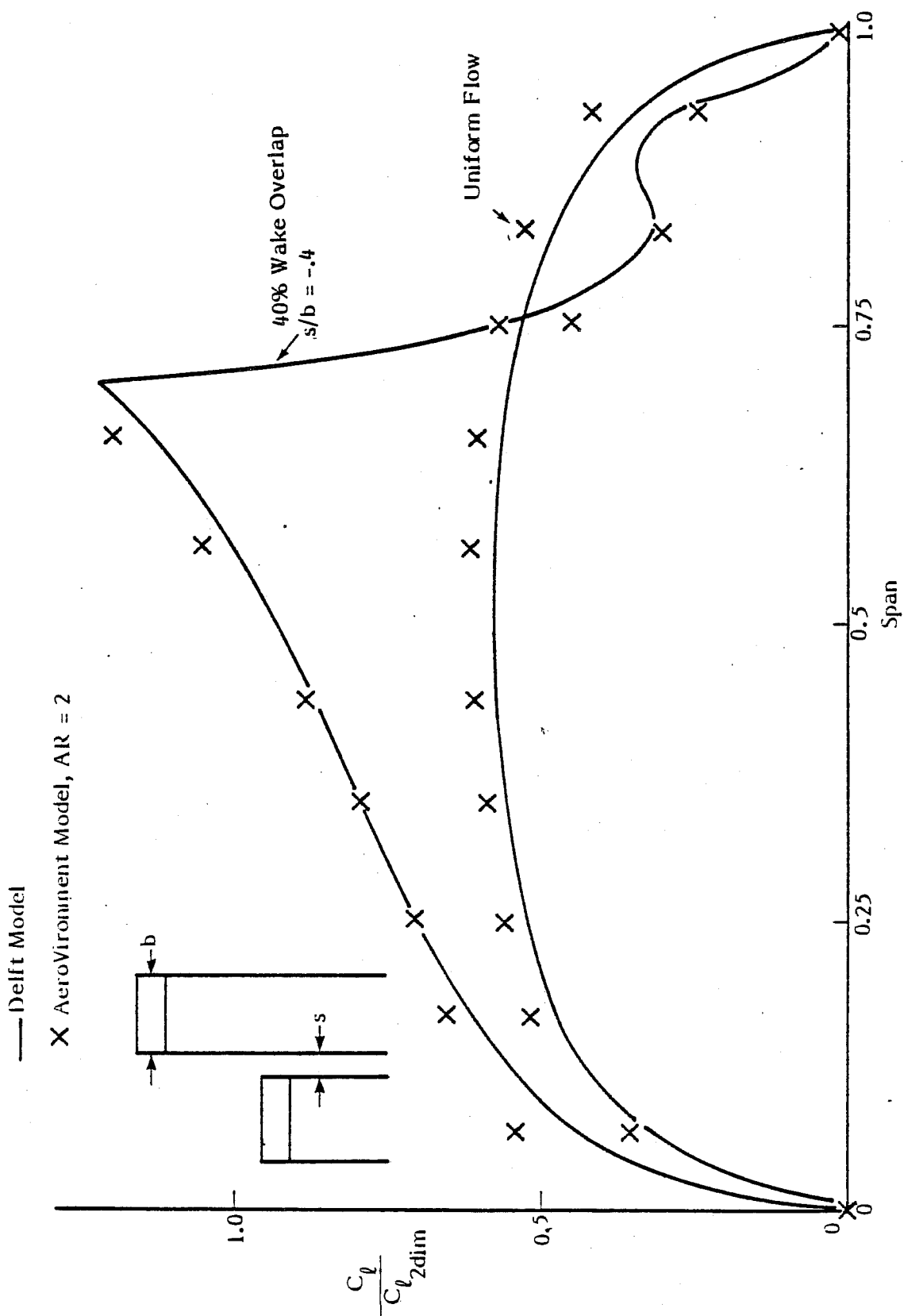
Figure 2-12. SPANWISE LOADING COMPUTED FOR RECTANGULAR TIP VANE

30% Wake Overlap (s/b = -.3, X/X_S = 1.4)

Uniform Flow
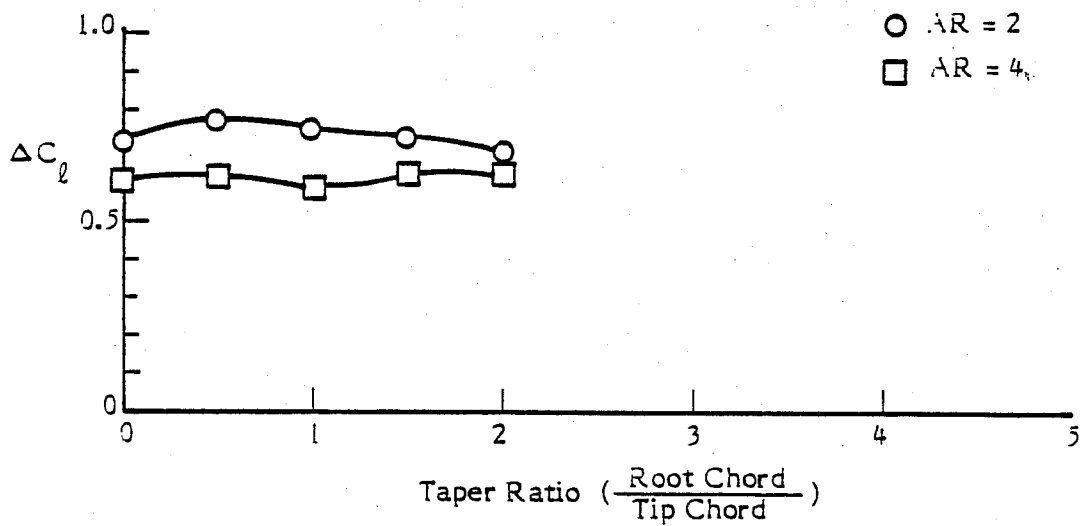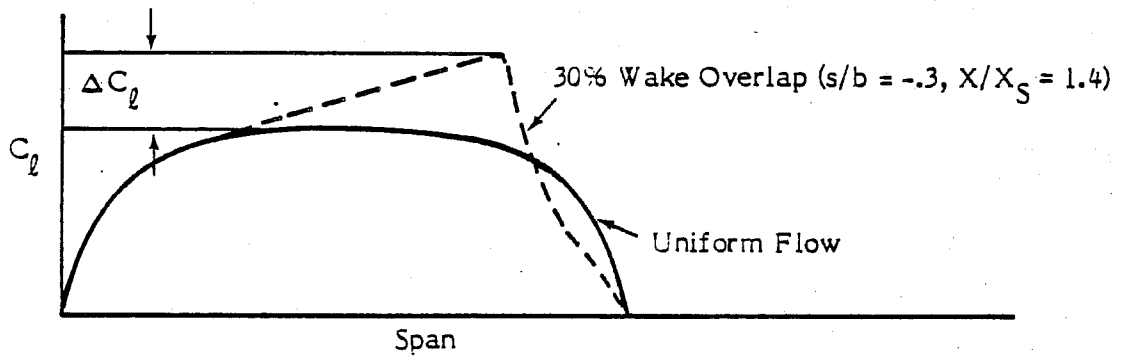
Span

Figure 2-13.   EFFECT OF ASPECT RATIO AND TAPER ON INCREMENTAL LIFT
COEFFICIENT OF TIP VANE
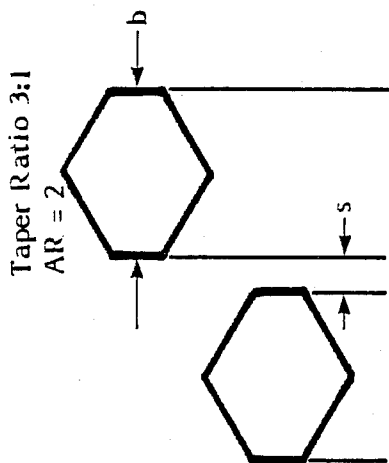
Tip Speed Ratio $(X/X_S = 1/1+s/b)$	Wake Overlap (s/b)
1.0	0
1.4	-.3
1.7	-.4
2.0	-.5

Taper Ratio 3:1
AR = 2

b

s

$\dfrac{C_\ell}{C_{\ell\,2D}}$

Span

s/b = 0 (uniform flow)   0 Wake Overlap
-.3   30%
-.4   40%
-.5   50%
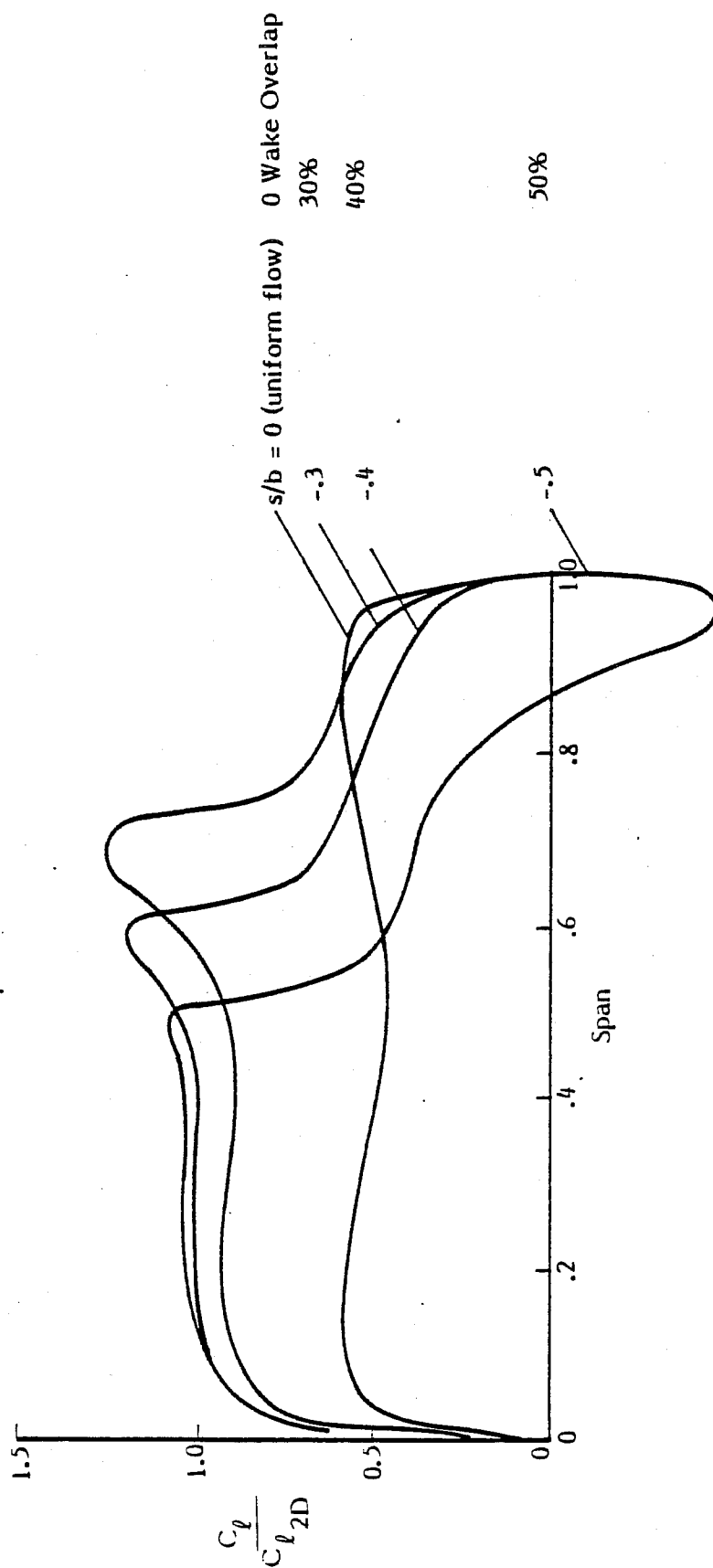
Figure 2-14.   EFFECT OF TIP SPEED RATIO ON SPANWISE LIFT DISTRIBUTION OF TIP VANE

of an ideal WECS rotor. Since the tip vane geometry is optimized for the operating characteristics of the baseline rotor configuration, it is anticipated that different tip vanes will be suitable for different rotors. For example, for a two-bladed, low solidity rotor, rectangular tip vanes may be more advantageous than the above design.

2.3.4   Orientation of Tip Vane

Since a high lift-to-drag ratio is sought for the tip vane, the proper orientation of the tip vanes is critical. Figure 2-15 shows a tip vane orientation. The angular setting of the tip vanes includes an angle of attack, tilt, and sweep.

To achieve the maximum lift-to-drag ratio, an angle of attack corresponding to the $C_{L_{max}}$ of the tip vane profile is sought. Because of vortex interactions, the staggered array calculations indicated maximum section lift coefficients, a factor of 1.6 or so higher than for a two-dimensional airfoil. Therefore, to maintain attached flow, the angle of attack of the tip vane should not exceed the angle of attack for $(1/1.6) C_{L_{max}}$ of the profile. For example, the maximum angle of attack for the tip vane should be approximately 4° for an NACA 4415 profile. Since these calculations neglect the effect of the power blade vortex, they provide only a qualitative setting for the tip vane angle of attack.

The performance of the dynamic inducer is sensitive to tilt. Since the power extraction of the dynamic inducer is proportional to the downwind thrust, and since the downwind thrust is a function of the tip vane tilt, the maximum tilt angle is sought for the tip vanes. However, drag considerations place a limit on the maximum allowable tilt angle. At high tilt angles, vortex cancellation (synchronous operation) is no longer possible, since the vortex filaments do not coincide.

Figure 2-16 shows the effect of tilt-angle on tip vane drag (van Holten, 1978). The drag measurements were obtained by spinning two low aspect ratio tip vanes on struts and measuring the absorbed shaft power. The measurements show that the lowest tip vane drag coefficients occur at tilt angles on the order of 23°. Based upon these empirical measurements, the optimum tilt angle appears to be on the order of 20°. This trend may vary for tip vanes of different geometry.

The sweep angle of the tip vane is determined by the inflow angle at rotor tip. Since it is desirable to maximize the lift-to-drag ratio of the tip vane, the optimum sweep angle is one where the quarter chord line of the tip vane is oriented perpendicular to the local flow so that the spanwise flow is minimized. Thus, the optimum sweep angle of the tip vane is equal to arctangent $(1/X)$, where X is the tip speed ratio of the rotor.

Figure 2-17 shows the effect of sweep angle on tip vane drag (van Holten, 1978). The measurements show that the minimum tip vane drag occurs at about 16° for a pair of low aspect ratio tip vanes mounted on struts. Based upon these observations, a sweep angle of 20° was selected for the dynamic inducer system.

2.3.5   Other Design Considerations

In addition to the geometry and orientation of the tip vanes, other important design considerations involve local flow separation, the effect of the power blade on the loading

ΩR

U_∞

Sweep Angle
Λ

Tilt Angle γ

Tip Vane

Angle of Attack

U_∞

Ω

Ω
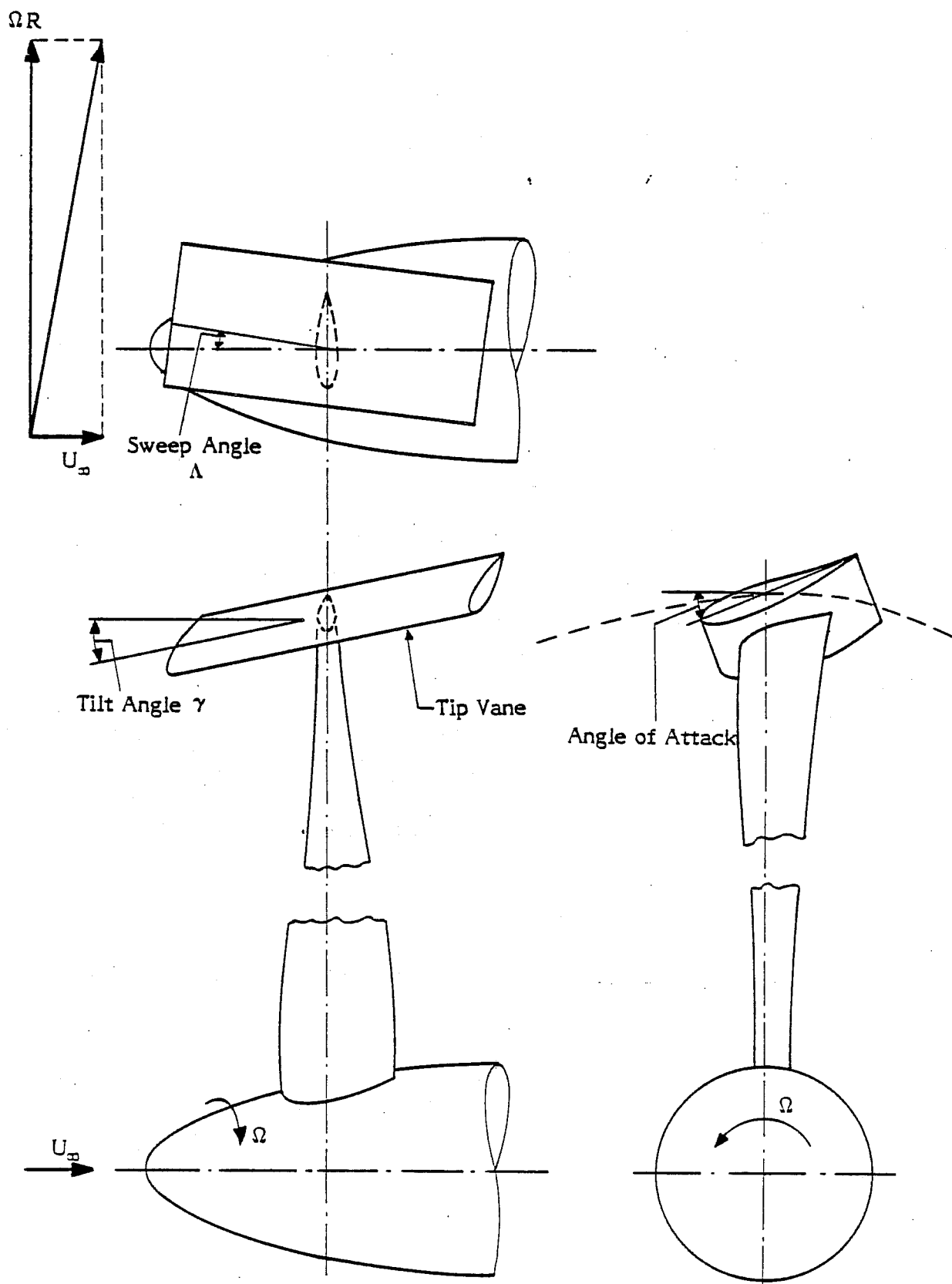
Figure 2-15.   SKETCH OF TIP VANE ORIENTATION

25
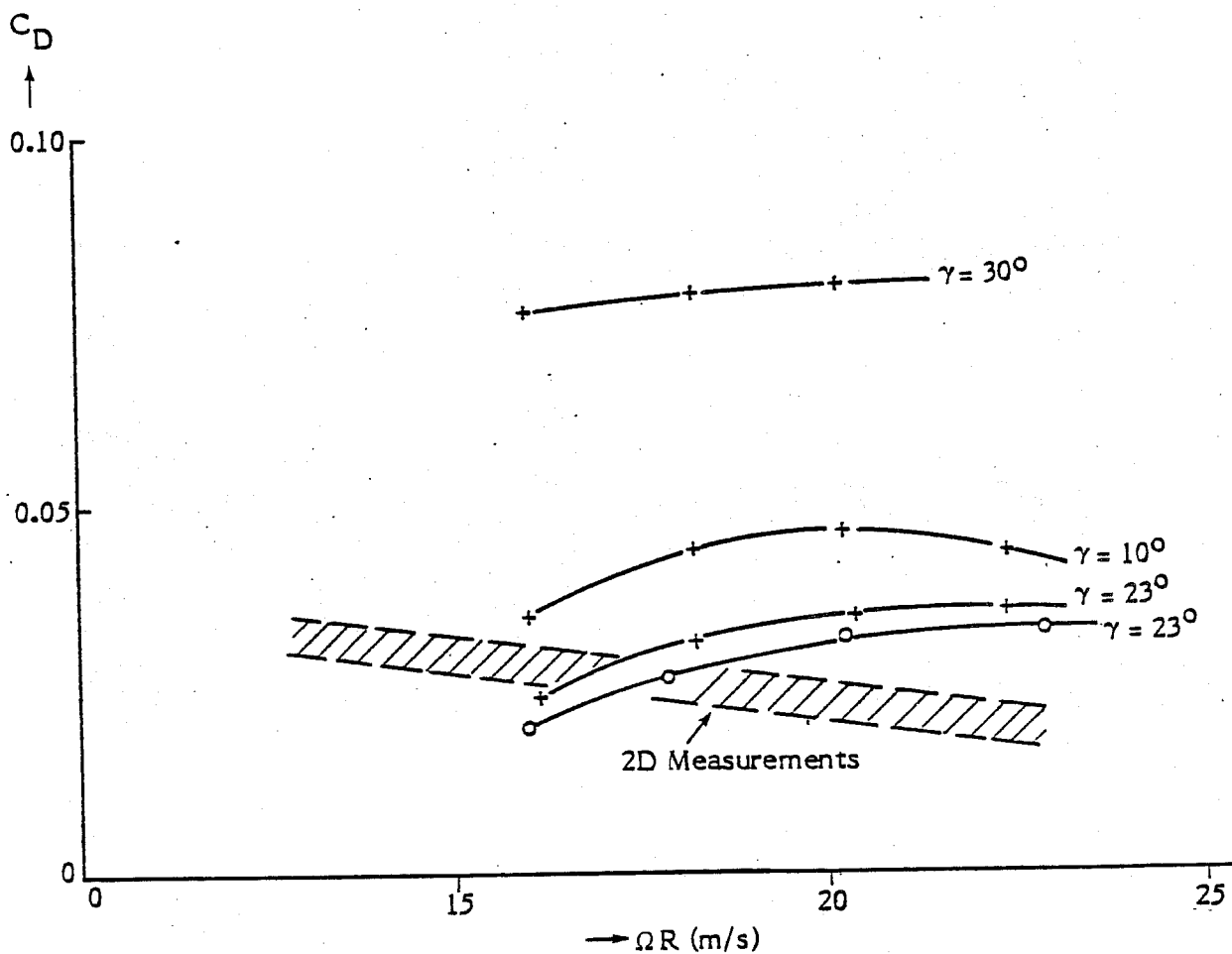
Figure 2-16.   EFFECT OF TILT ANGLE ON TIP VANE DRAG
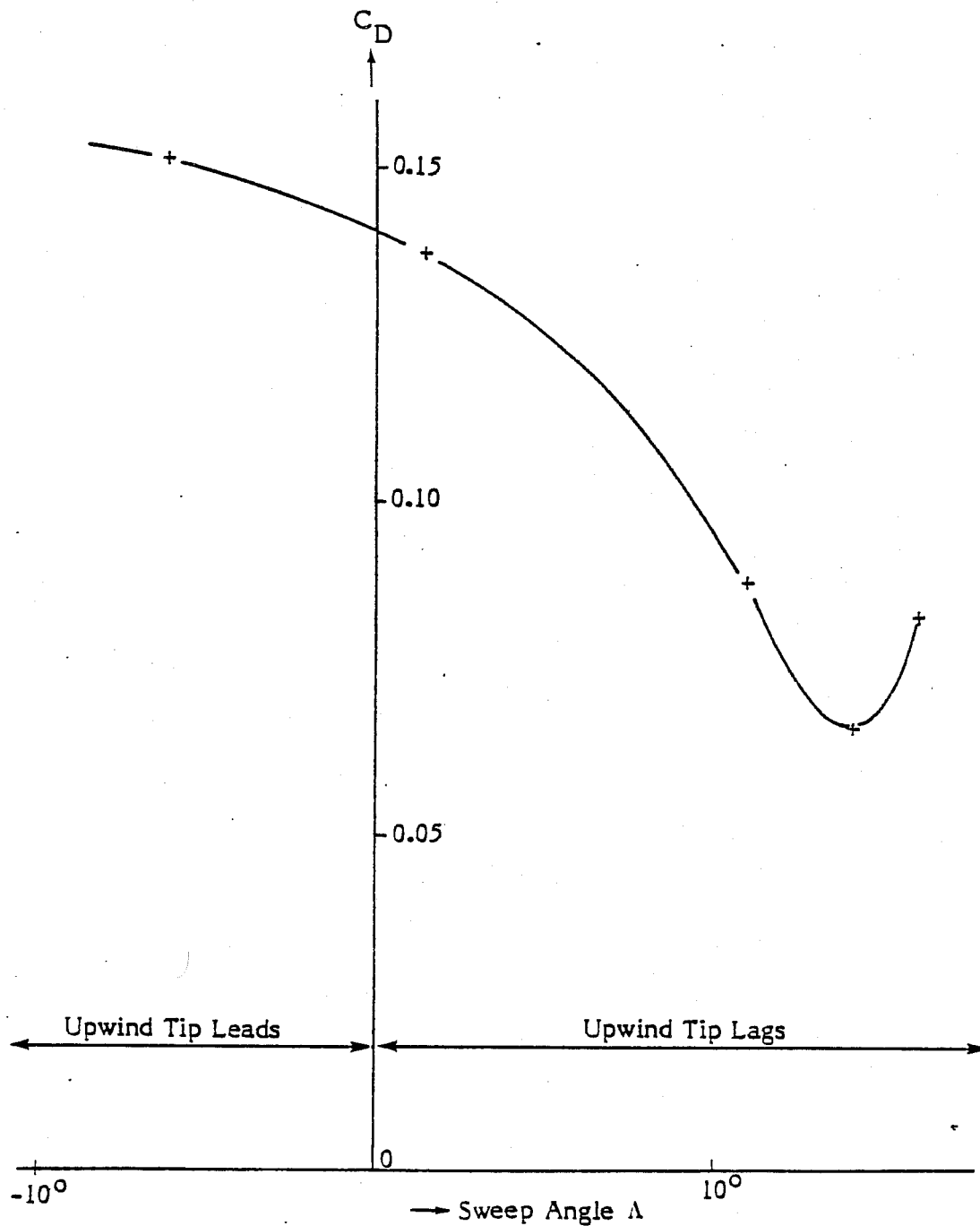
Figure 2-17.   EFFECT OF SWEEP ANGLE ON TIP VANE DRAG

of distribution of the tip vane, the asymmetric thrust on the tip vane, and the effect of the tip vane on the loading distribution of the power blade.

Figure 2-18 shows the tip vane regions where separation is likely to occur based upon earlier experimental tests. Separation can occur at the tip vane power blade junction, on the suction side of the tip vanes, and near the leading edge and tips of the tip vanes on the positive pressure side. Care must be exercised in the design of the tip vane to eliminate separation in these regions.

The presence of the power blade alters the loading distribution of the tip vane. Figure 2-19 shows the flow field induced by the power blade on the tip vane. The trailing vortex from the power blade induces a downwash component on the upwind portion, and an upwash component on the downwind portion of the tip vane. Smaller perturbations occur in the chordwise velocity component.

Figure 2-20 shows the effect of the power blade on the spanwise loading distribution of the tip vane. The calculations were carried out with the staggered wing model discussed earlier, modified to include the trailing vortex from the power blade. The calculations indicate that the power blade increases the loading on the downwind portion and decreases the loading on the upwind portion of the tip vanes, and introduces an additional discontinuity in the loading near the mid-section. Since the upwind portion of the tip vane is more heavily loaded than the downwind portion, and since the power blade unloads the upwind tip and loads the downwind tip, a beneficial effect occurs. A more uniform loading results from the presence of the power blade.

Figure 2-21 illustrates the effect of the power blade on the aerodynamic performance of the tip vane. The calculations were carried out with the staggered array model, including the trailing vortex from the power blade. The calculations show that the presence of the power blade is noticable only at off-design, subsynchronous tip speeds. For the majority of the operating range of the dynamic inducer, the effect of the power blade is not significant.

Since the spanwise loading on the tip vanes is asymmetric, an unequal spanwise thrust occurs at the tips. The resultant tip thrust results in rotor drag. The drag component is given by

$$D = (T_1 - T_2) \cos \gamma \ , \qquad (2\text{-}13)$$

where T_1 and T_2 are the spanwise thrust components at each tip, and γ is the tilt angle. The total tip thrust is given by

$$T_1 - T_2 = \frac{\rho C_T}{64} \left[\frac{d\Gamma^2}{dy}\right]_0^1 \ , \qquad (2\text{-}14)$$

where C_T is the chord of the tip vane at the tip, ρ is the air density, and $\left[d\Gamma/dy\right]_0^1$ is the difference in the gradient of the spanwise loading between the two tips. This formulation suggests that changes in the spanwise loading distribution through modifications in tip shape can reduce the total drag coefficient of the system. As shown in Figure 2-22, raking and rounding of the tip alters the tip vortex trajectory (van Holten, 1979). This can reduce tip suction.

28
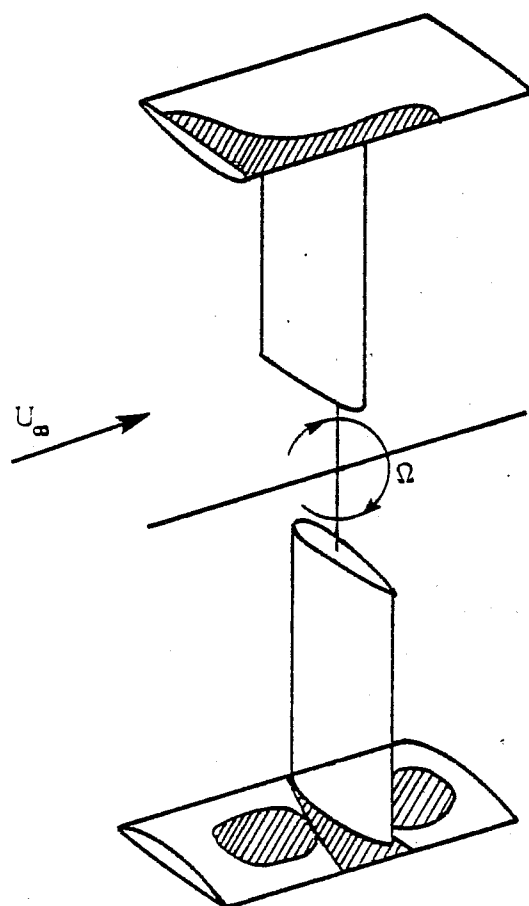
Flow Visualization

- Tufts
- Oil Flow
- Strobe Lamps and
  High Speed Photography

Figure 2-18. SKETCH OF TIP VANE REGIONS WHERE SEPARATION IS LIKELY TO OCCUR

Power Blade Bound Vortex

Downwind Tip

Upwash Component

Chordwise Component

Power Blade Tip Vortex

Chordwise Component

Downwash Component

Upwind Tip
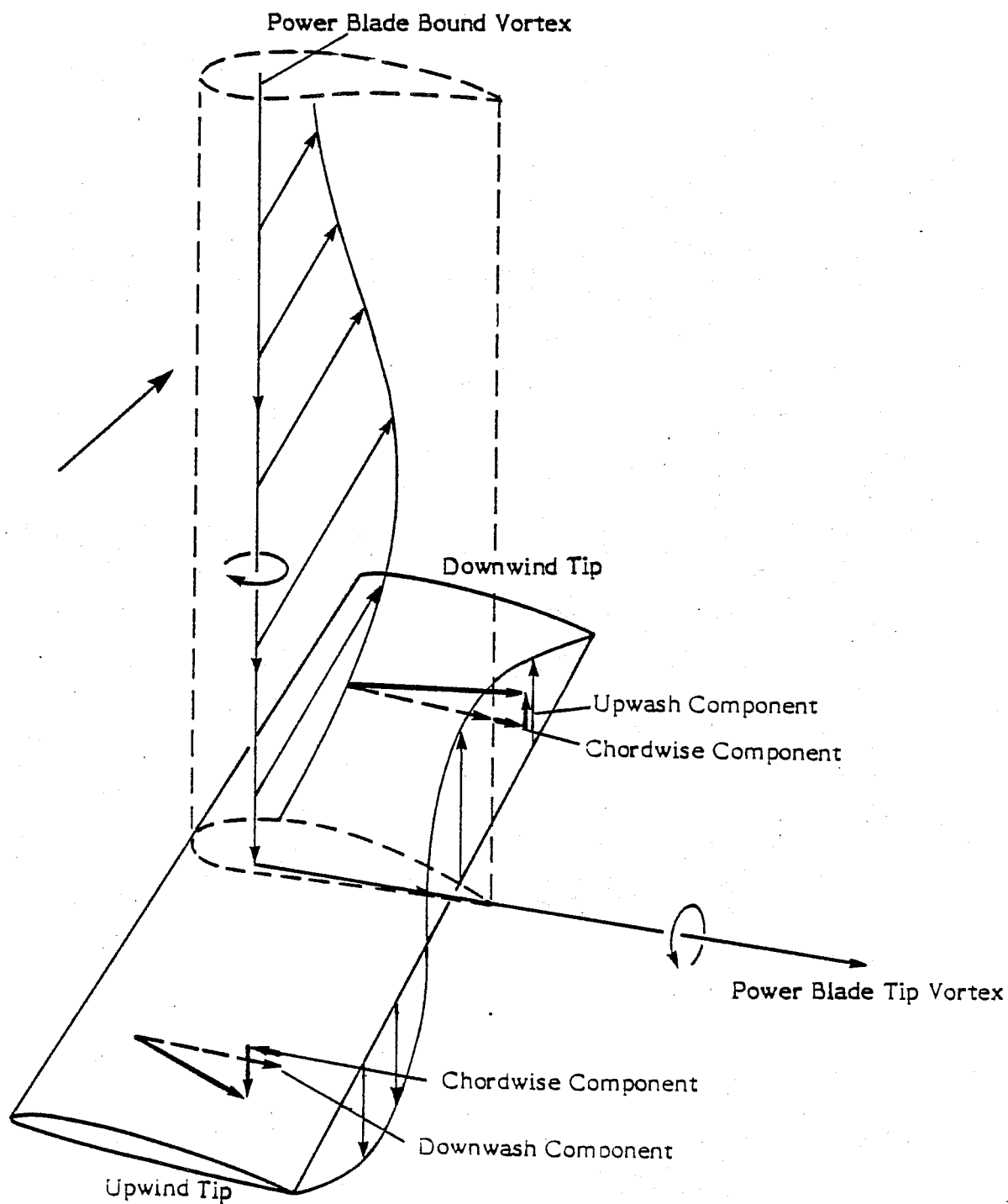
Figure 2-19.   FLOW INDUCED BY ROTOR BLADE AT TIP VANE

30
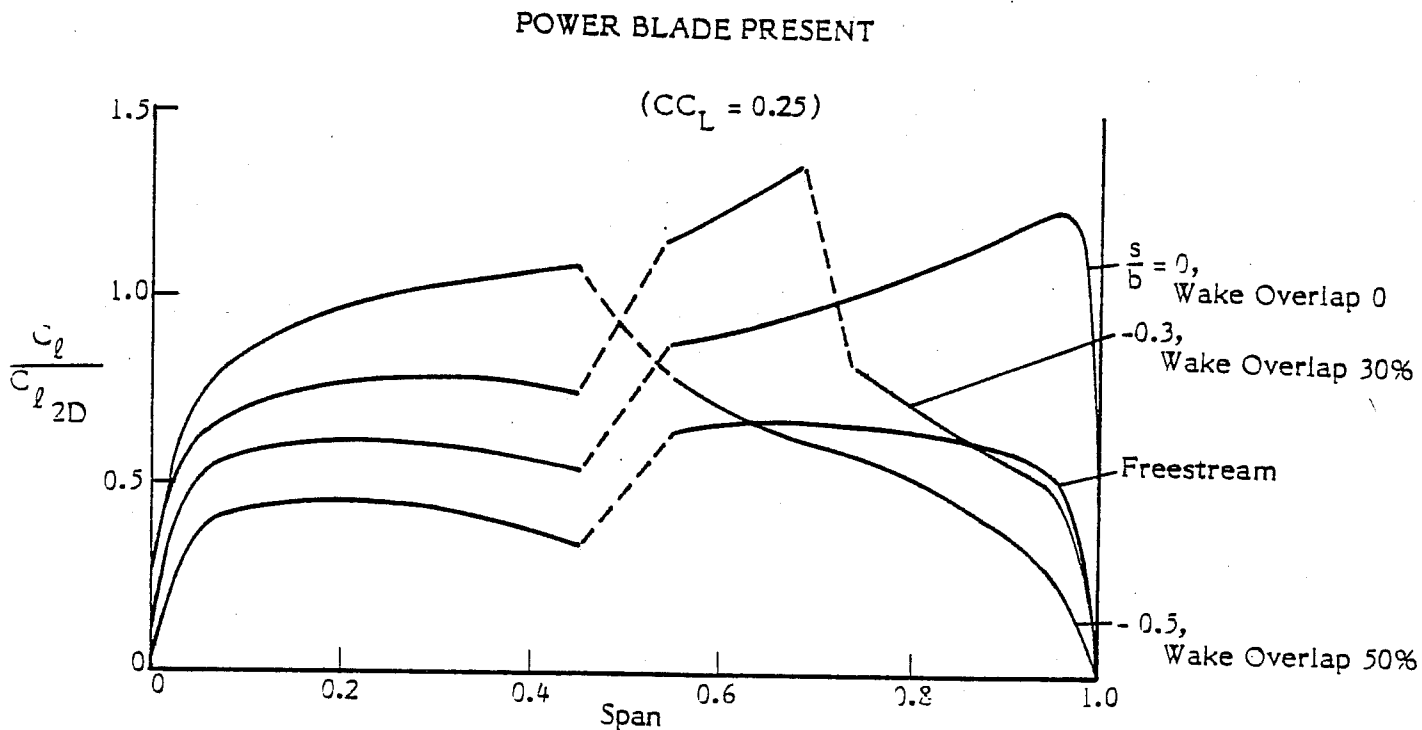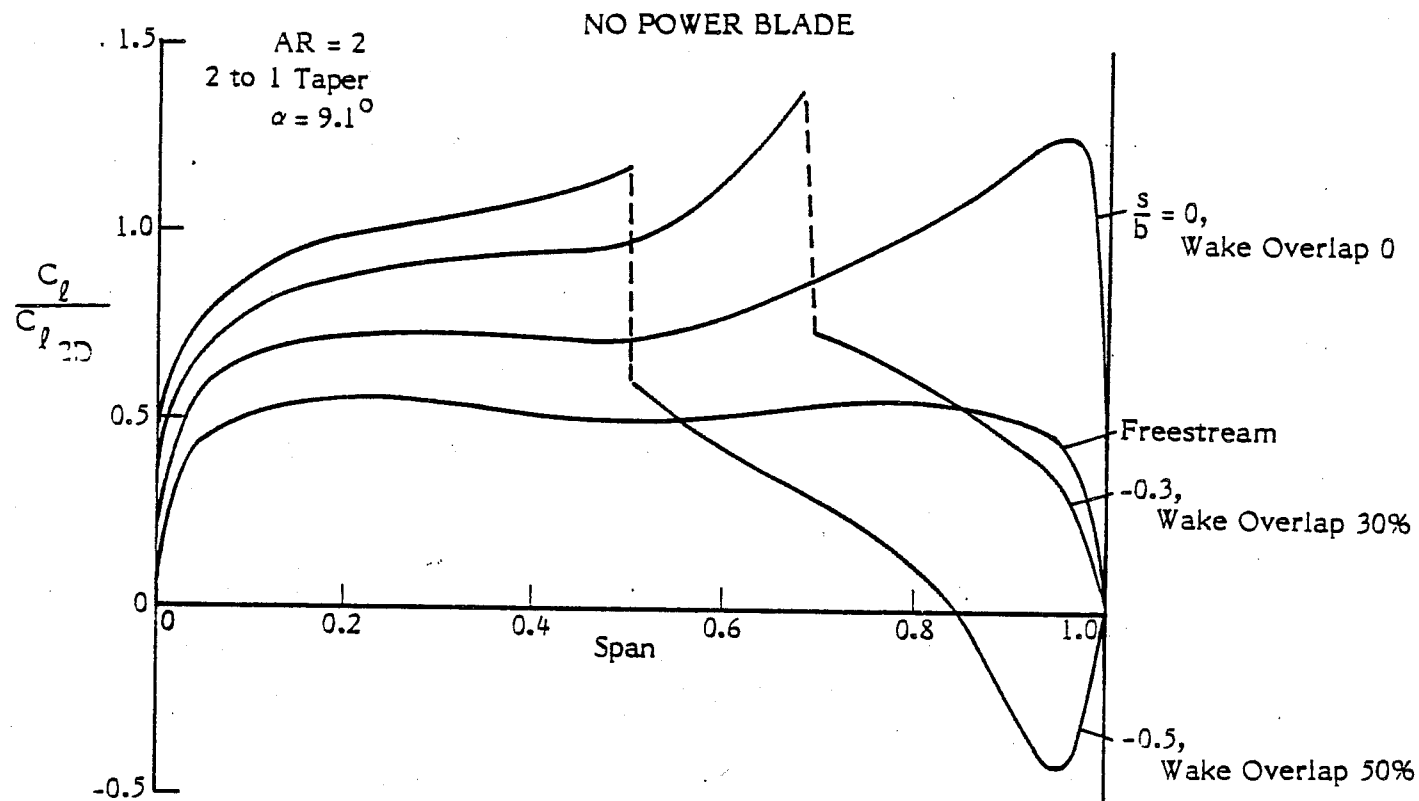
Figure 2-20. EFFECT OF POWER BLADE ON SPANWISE LOADING DISTRIBUTION

31
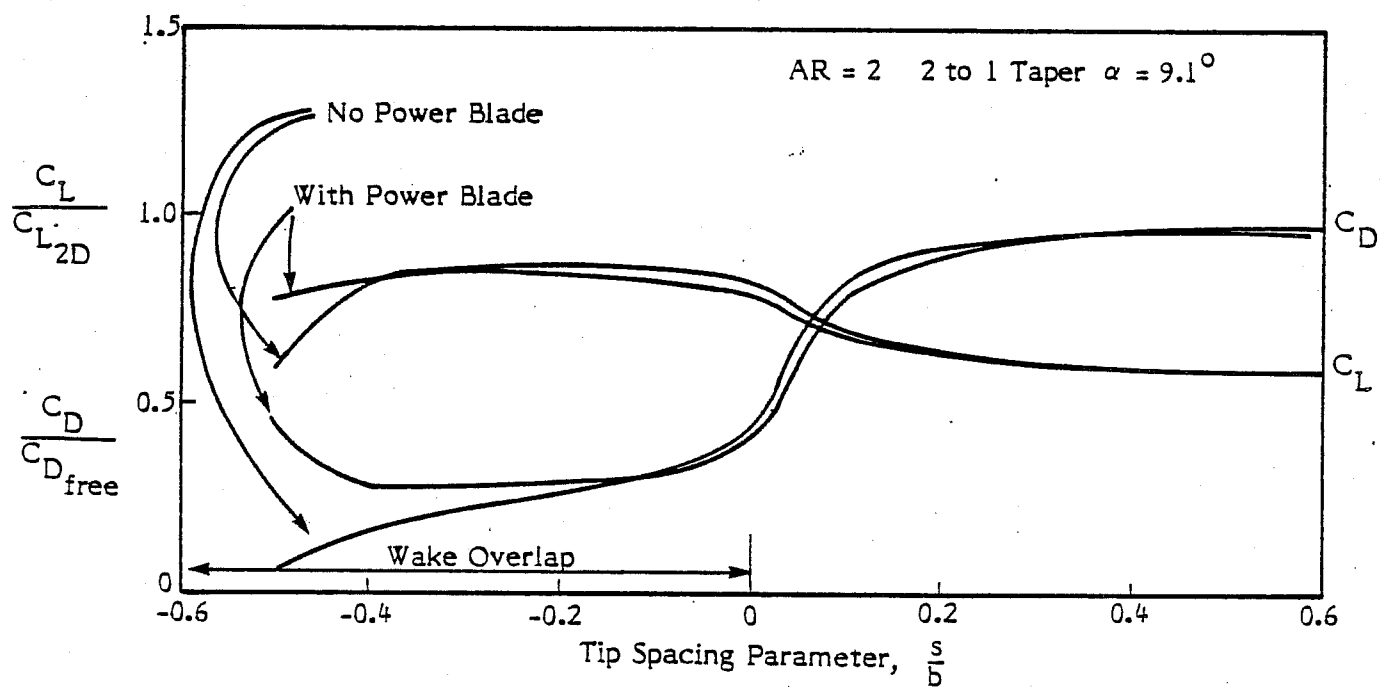
Figure 2-21. EFFECT OF POWER BLADE ON AERODYNAMIC PERFORMANCE OF TIP VANE
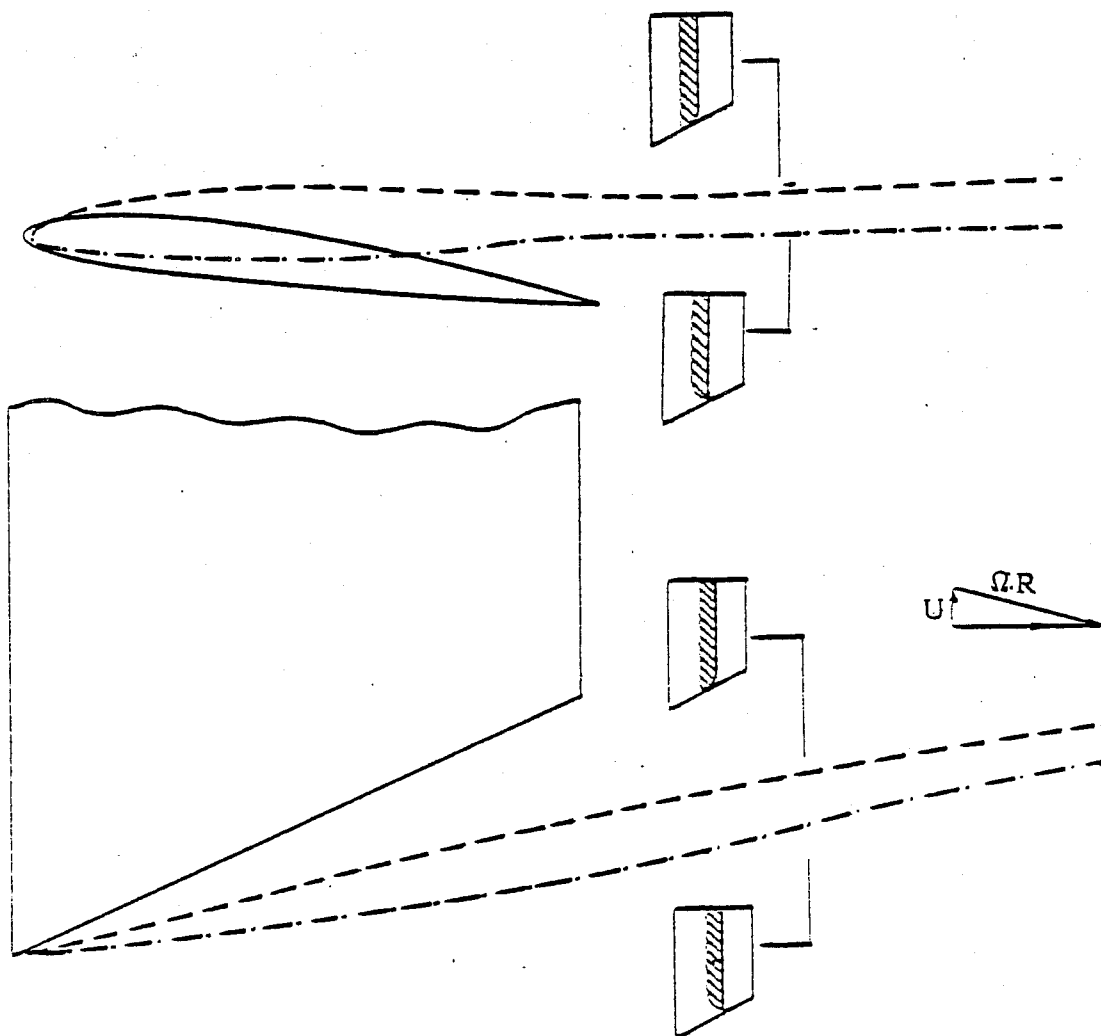
Figure 2-22.   MODIFICATION OF TIP VORTEX TRAJECTORY THROUGH RAKE
AND TIP ROUNDING

Figure 2-23 illustrates the effect of tip shape on the drag coefficient of tip vanes (van Holten, 1979). The results show that by rounding the downwind tip, and by adding a Hoerner tip to the upwind tip, the performance of the dynamic inducer is improved. The tip of the airfoil is tapered gradually to a sharp edge in the Hoerner tip. The sharp edge causes the tip vortex to detach from the tip and tends to reduce the tip suction.

The induction generated by the tip vane affects the angle of attack distribution of the power blade. Figure 2-24 shows a sample induced velocity calculation. The results show that for typical operating conditions, the tip vane induces a positive angle of attack on the power blade, ranging from 1° at the tip to a maximum of 2.5° at 80% blade radius, and diminishing to 1.8° at the blade root. These calculations suggest that for the selected baseline rotor the twisting of the power blades to achieve optimum performance is not necessary. However, for a dynamic inducer with higher augmentation ratio, the power blade twist may have to be altered to achieve optimum performance.

2.3.6   Selected Design Parameters

Based on the above analysis, a dynamic inducer system was designed for the baseline rotor. Table 2-1 summarizes the elements of the design. The performance trends indicated that additional aerodynamic optimization of the system is possible using a lower solidity, higher tip speed ratio baseline rotor.

① Sandpaper strips along nose
② Carborundum grains instead of sandpaper
③ Same as ②, also grains along side-edges
④ Rounded tips
⑤ One vane with Hoerner tip
⑥ Both Hoerner tips, <u>but other configuration:</u>
   attachment knives instead of ball hinges
⑦ Two-dimensional tests with trip-wire

Tilt-angle δ = 20°
incidence θ = -2°
ΩR = 20 m/sec
U = 1.8 m/sec

C_D

0.10

0.05

0.025

0

5°   10°   15°   20°

Yaw angle Λ (degrees)

Figure 2-23.   DRAG COEFFICIENT TIP VANES AS AFFECTED BY TIP SHAPE
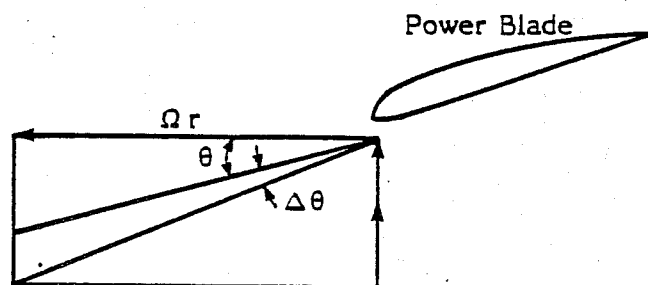
Power Blade

U_∞ = wind velocity

u_{at} = axial flow velocity induced by tip vane

θ = wind angle

$\Delta\theta$ = wind angle induced by tip vane

U_∞ = 12 m/s

CC_L = 0.3

X = 5

R = 0.609 m
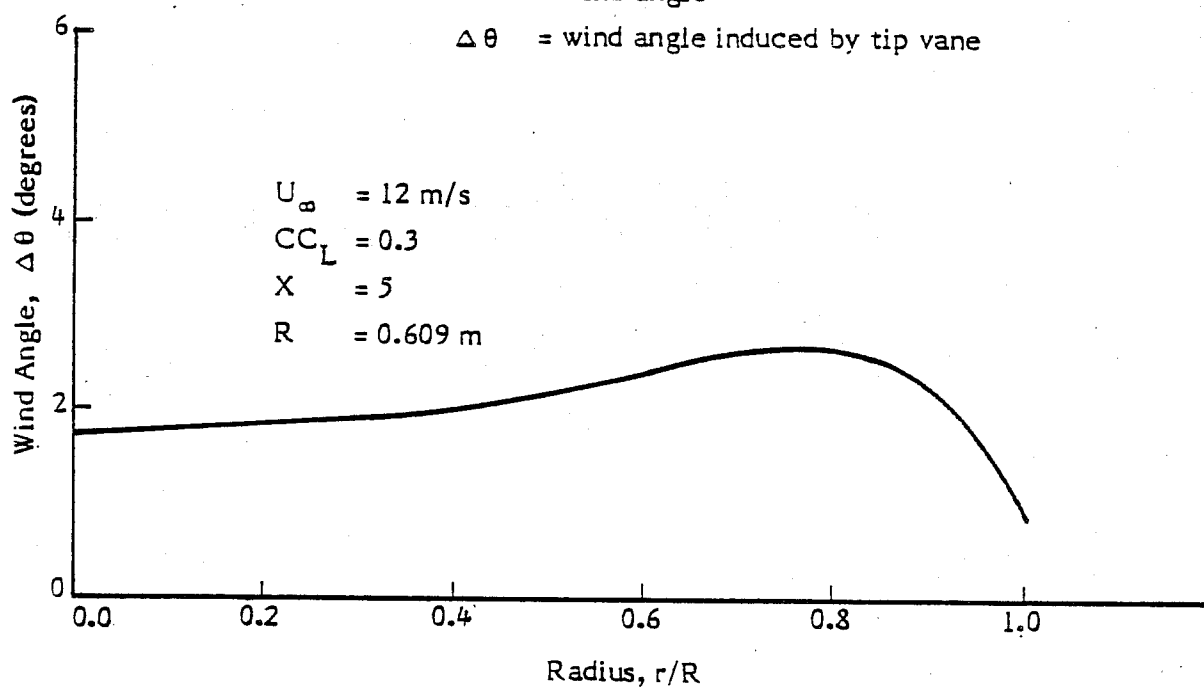
Figure 2-24. EFECT OF TIP VANE ON ANGLE OF ATTACK OF POWER BLADE

Table 2-1. SELECTED DESIGN PARAMETERS FOR DYNAMIC INDUCER

Parameter	Criteria	Result
BASELINE ROTOR		
Design tip speed ratio	Given	X = 4
Solidity	Given	13%
Profile	Given	FX61-126, 184
Twist	Given	9°
Number of blades	Given	3
TIPVANE SYSTEM		
Span	System synchronous at X = 1-3	b/R = .5 to .7
Chord	Desired power augmentation ~ 40%	c̄/R = .12
Profile	High lift-to-drag ratio	NACA 4415
Aspect ratio	Minimize induced drag	4
Taper	Minimize induced drag	3:2
Twist	Simple fabrication	No twist
Power blade/tip vane junction	Minimize parasite drag	Fairing made for junction
Tip modifications	Minimize asymmetric tip suction	Tip of upwind tip raked 30°; Hoerner tip and a rounded tip used on upwind and downwind tips, respectively

SECTION 3.0

WIND TUNNEL TEST PROGRAM

3.1   OBJECTIVES OF TEST

A wind tunnel test program was conducted to determine the performance of a one-third scale model dynamic inducer system. The objectives of the test included:

- obtaining direct measurements of rotor torque, thrust, and rpm, and

- visualizing the flow patterns associated with the dynamic inducer to determine and rectify array anomalies in system performance.

3.2   DESCRIPTION OF MODEL

Figure 3-1 shows the general layout of the dynamic inducer system. A one-third scale model of this system was fabricated for the wind tunnel tests. Consistent with augmented turbines, the power coefficient of the rotor is computed based on the reference disk area of the rotor, $10.2 \ m^2$. The $15°$ tilt of the tip vanes increases the frontal area of the rotor by $15°$.

3.3   DESCRIPTION OF INSTRUMENTATION

As shown in Figure 3-2, the metric system consisted of a three-horsepower D.C. motor, tachometer and in-line shaft-mounted torque, and thrust transducers. The accuracy of the RPM, torque, and thrust monitoring instruments was within 1%, 2%, and 5%, respectively. The D.C. motor was equipped with a regenerative drive and feedback controller enabling it to maintain a specified RPM under an arbitrary positive or negative load. Under negative loads, the motor functioned as a brake (generator), feeding power back into the line. It was expected that the inducer system may require power for spin-up at some settings, but sufficient starting torque was available from the dynamic inducer so that the motor actually operated in the generator mode for all of the test conditions.

3.4   OPERATING PROCEDURE

The thrust and torque coefficients were measured over a range of tip speed ratios from 2 to 8 for a total of 51 different model configurations, including variations in blade feather angle and tip vane geometry. The majority of the tests were conducted at a freestream velocity of 10 m/s, corresponding to a Reynolds number of 640,000 at a nominal tip speed ratio of 4 for the tip chord. The freestream velocity was reduced to 8 m/s at tip speed ratios above 6 to reduce the blade loads. The reference freestream velocity was measured to within 1% by the pitot-static system installed in the wind tunnel.

The tests were conducted in the following manner:

- the tunnel was brought up to speed,

- the rotor RPM was set corresponding to a specified tip speed ratio,

- the tunnel velocity was brought to equilibrium, and
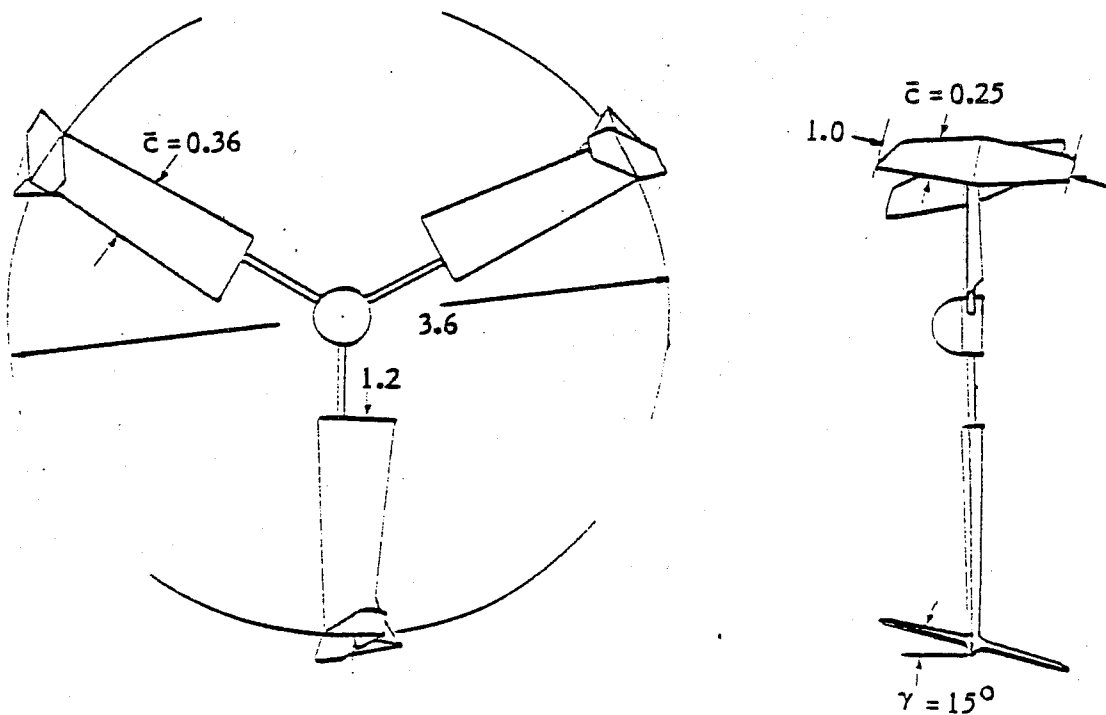
Figure 3-1.   VIEWS OF FULL-SCALE DYNAMIC INDUCER (DIMENSIONS IN METERS)
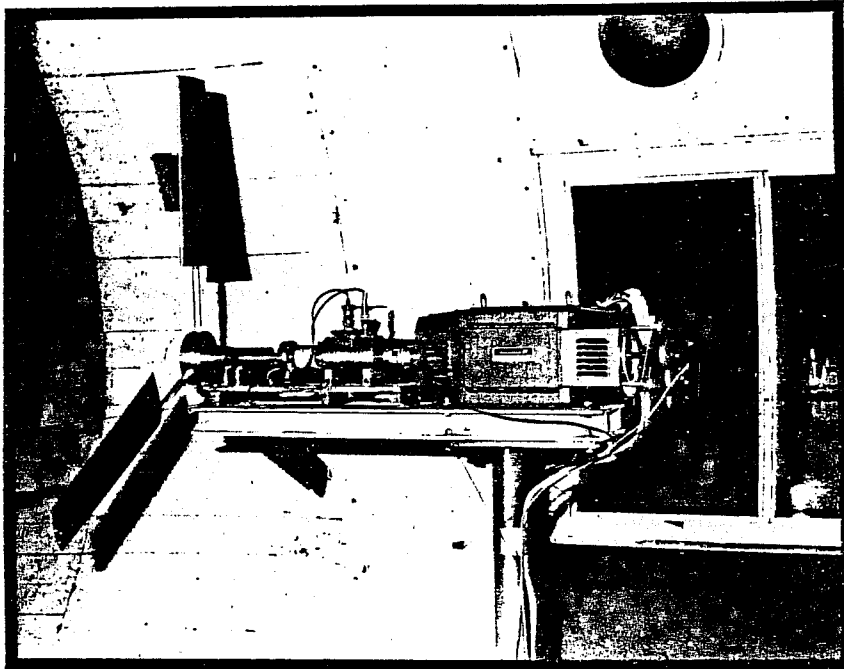
Figure 3-2. ONE-THIRD SCALE WIND TURBINE MODEL INSTALLED IN 10-FOOT DIAMETER WIND TUNNEL

- the RPM, thrust, and torque values were recorded from the digital readouts over a 10-second averaging period. The repeatability of the measurements was within the accuracy of the instruments.

3.5 WIND TUNNEL CORRECTIONS

3.5.1 General Discussion of Corrections for Augmented Systems

It is well known that most wind turbine systems have higher performance coefficients when tested in a wind tunnel than when operating in unbounded flow. The basic reason for this effect is that the wind tunnel wall prevents the major portion of the flow from bypassing the rotor and forces a larger part of the flow through the rotor than would normally happen in the freestream case. The standard method of correction for wind in turbines is well known (Glauert, 1935). The results of this method are shown in earlier work (Wilson et al., 1976) and demonstrate that these tunnel corrections can be quite large.

While wind tunnel correction techniques are available for wind turbines, no techniques have been reported for augmented wind turbines such as the dynamic inducer or ducted turbines. Therefore, a new technique was developed to correct the performance measurements of the dynamic inducer obtained in the wind tunnel. The technique is based on the fundamental relationship between rotor drag and momentum deficit in the wake. It is applied to the wind tunnel measurements obtained with the dynamic inducer model.

3.5.2 Performance of Augmented Turbine in Wind Tunnel

Figure 3-3 is a sketch of the flow field for an augmented wind turbine. For simplicity, the area of the wind tunnel, the fluid density, and the upstream flow velocity is normalized to unity. At a station sufficiently far downstream, the pressure in the wake has returned to a constant value, P_w, the flow in the rotor wake of area, A_w, has a velocity, V_w, while the outer flow has speed, V_o, and pressure is equal to the wake pressure, P_w.

Applying the continuity condition at the downstream station, the flow in the wake, M_w, and outer flow, M_o, are given by

$$1 = M_w + M_o \quad , \tag{3-1}$$

where $M_w = AV_a$, while the areas are related by

$$1 = A_w + A_o \quad . \tag{3-2}$$

Applying the continuity condition to the wake flow, all of the wake flow passes through the actuator so that

$$AV_a = A_w V_w \quad . \tag{3-3}$$

41

Flow in Wind Tunnel

Area = 1

$V = V_o$

$V = V_w$

$V = V_a$

Area = A

Area = A_w

Upstream
Station
$P = P_o$
$V = 1$

Actuator
Station

Downstream
Station
$P = P_w$

Flow in Freestream

$V = V'$

Area = A

$V = V_a'$
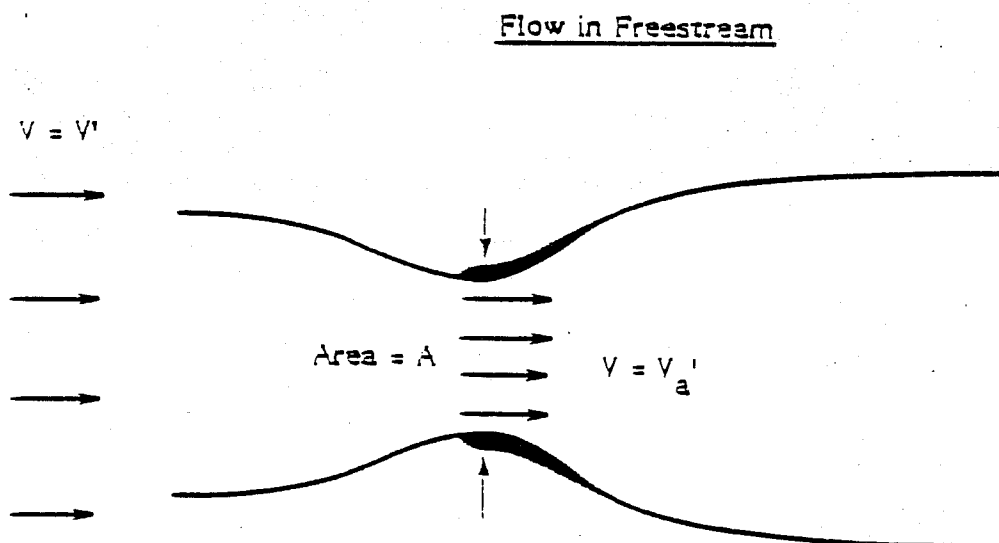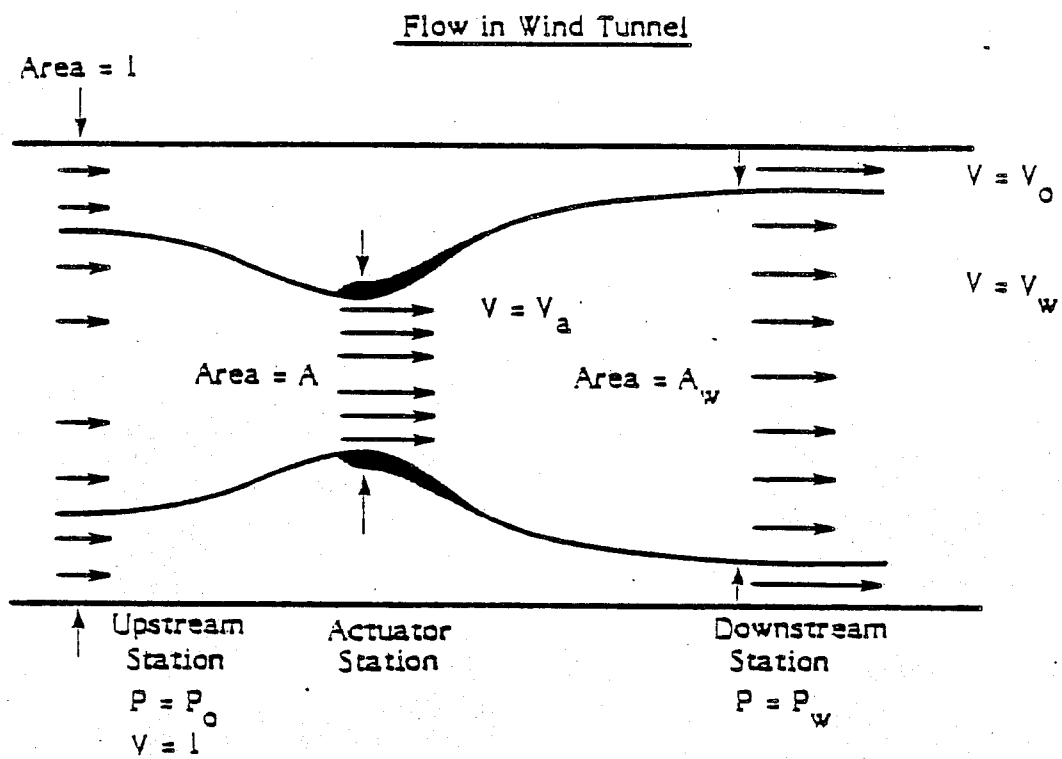
Figure 3-3.   FLOW FIELDS FOR AN AUGMENTED WIND TURBINE

From the above relationships, the flow speed through the actuator is given by

$$V_a = \frac{V_w (V_o - 1)}{(V_o - V_w)A} \quad .$$

(3-4)

The derivation of the above equation is given in Appendix B.

The total change in momentum flux in the downwind direction is given by

$$M_o (1 - V_o) + M_w (1 - V_w) \quad .$$

(3-5)

The axial acceleration is balanced by the thrust on the rotor and the pressure over the ends of the stream tube

$$1/2 \, AC_T = \frac{M_o (1 - V_o) + M_w (1 - V_w) - 1/2 + V_o^2}{2} \quad ,$$

(3-6)

where C_T is the axial force coefficient of the system (positive in the drag sense) and is based on the actuator area, A, and the upstream flow speed. The above equation is combined with Equations (3-1) and (3-2) to yield

$$AC_T = (V_o - 1)(V_o - 1 + 2V_w) \quad .$$

(3-7)

The decrease in total head in the slipstream is obtained by comparing the kinetic energy in the slipstream and wake at the downstream station

$$2 \, H = V_o^2 - V_w^2 \quad .$$

(3-8)

This represents the pressure drop through the actuator so the axial thrust on the actuator is given by

$$2 \, H = C_{Ta} \quad .$$

(3-9)

Now, the total thrust coefficient of the system is given by the thrust coefficient on the actuator and augmentor, $C_T = C_{Ta} + C_{TD}$, where C_{TD} is the thrust coefficient on the augmentor based on the actuator area and upstream velocity. Therefore, the total thrust coefficient of the system is given by

$$C_T = V_o^2 - V_w^2 + C_{TD} \quad .$$

(3-10)

3.5.3   Performance in Unbounded Flow

The tip speed ratio, thrust, and torque coefficients for the augmented turbine operating in the freestream are given by

$$X' = rX \quad ,$$

(3-11)

$$C_T' = r^2 C_T, \; C_{TD}' = r^2 C_{TD} \quad ,$$

(3-12)

43

$$C_p' = r^3 C_p \quad , \tag{3-13}$$

where the unprimed coefficients are the coefficients measured in the tunnel, the primed coefficients represent free air conditions at speed, V', and $r = 1/V'$ is the tunnel speed correction factor for identical performance. Note here that the tunnel speed was normalized to 1.

For an augmented turbine operating in an unbounded flow of velocity, V', and unity density, the mass flow through the system is given by (Lissaman et al., 1980)

$$M_a' = A V_a' V' = A (1 - \lambda a' + b') V' \quad , \tag{3-14}$$

where b' is the no power augmentation (a function of augmentor geometry), and a' is the axial interference factor (a function of actuator head loss).

Assuming that in the far wake the influence of the duct on the wake is negligible, while the axial interference factor has developed to $2a'V'$, the axial force is

$$T' = A 2a' (1 - \lambda a' + b')(V')^2 \quad , \tag{3-15}$$

so that

$$C_T' = 4a' (1 - \lambda a' + b') \quad , \tag{3-16}$$

while

$$C_{TD}' = 4a'b' \quad . \tag{3-17}$$

For propeller systems such as the dynamic inducer, the constant, $\lambda = 1$. However, for ducted systems where the duct is relatively long compared to the actuator scale, it has been shown that $\lambda = 2$ (Lissaman et al., 1978). Thus, the force coefficient for the dynamic inducer is

$$C_T' = 4a' \left(1 - a' + \frac{C_{TD}'}{4a'}\right), \tag{3-18}$$

To simulate the performance of the augmented system in unbounded flow, it is necessary to have the same value of thrust and power in both the unbounded flow and the wind tunnel.

The thrust on the system in the unbounded flow is set equal to the thrust on the system in the wind tunnel,

$$(V')^2 \, 4a' \left(1 - a' + \frac{C_{TD}'}{4a'}\right) = C_T \quad , \tag{3-19}$$

and solving for R,

$$R^2 = 4a' \left(1 - a' + \frac{C_{TD}'}{4a'}\right) C_T \quad . \tag{3-20}$$

For kinematic similarity, the mass flow through the actuator in the unbounded flow is set equal to the mass flow through the actuator in the wind tunnel,

$$\cdot V_a = V_a' V' = V' (1 - a' + \frac{C_{TD}'}{4a'}) \quad , \tag{3-21}$$

so that

$$r = \frac{(1 - a' + \frac{C_{TD}'}{4a'})}{V_a} \quad . \tag{3-22}$$

From the expressions for r^2 and r, r is eliminated to give the expression for the axial interference

$$a' = \frac{(C_T + [C_T{}^2 + (C_T + 4V_a{}^2)(C_{TD}' C_T')]^{1/2})}{2(C_T + 4V_a{}^2)} \quad . \tag{3-23}$$

Given A, C_T, and C_{TD} which, in principle, can be obtained from wind tunnel measurements, Equations (3-4), (3-7), (3-10), (3-12), (3-22), and (3-23) provide means of calculating the wind tunnel speed correction factor.

3.5.4   Wind Tunnel Corrections for Dynamic Inducer

Figure 3-4 shows a plot of C_p'/C_p versus C_T, with C_{TD} as a parameter for the blockage ratio of the model, A = 0.16. Note that A and C_T were measured, but C_{TD} was calculated from the tip vane geometry.

Since it was not convenient to instrument the tip vanes separately, the thrust coefficient of the tip vanes was calculated from the basic aerodynamic loads. For the tip vane geometry shown earlier in Figure 3-1, the total lift and drag forces on N tip vanes are given by

$$L' = 1/2 \, \rho U_\infty^2 C_L' SN \quad , \tag{3-24}$$

$$D' = L' \sin \alpha \quad , \tag{3-25}$$

where the flow velocity and tip vane surface area are $U \sim XV'$ and $S = r^2 BC$, and B and C are the span, and α is the angle of attack of the tip vane. B = b/R, and chord, C = $\bar{c}/R$, of the tip vane normalized to the rotor radius, R. Therefore, the force coefficient based on the actuator area and freestream velocity becomes

$$C_{TD}' = \frac{C_L' \sin \alpha \, BCN(X')^2}{\pi} \quad . \tag{3-26}$$

At typical operating conditions, $C_L' = 1.2$, $X' = 4$, so that $C_{TD}' = 0.3$. At the highest power coefficient setting, the total thrust coefficient of the system was $C_T \sim 1.2$. Thus, the power coefficient of the dynamic inducer was approximately 20% higher in the wind tunnel than in the freestream, according to the results shown in Figure 3-4. Similarly, about a 20% correction is predicted for the rotor alone configuration (C_{TD} = 0) at the highest power coefficient setting.

45
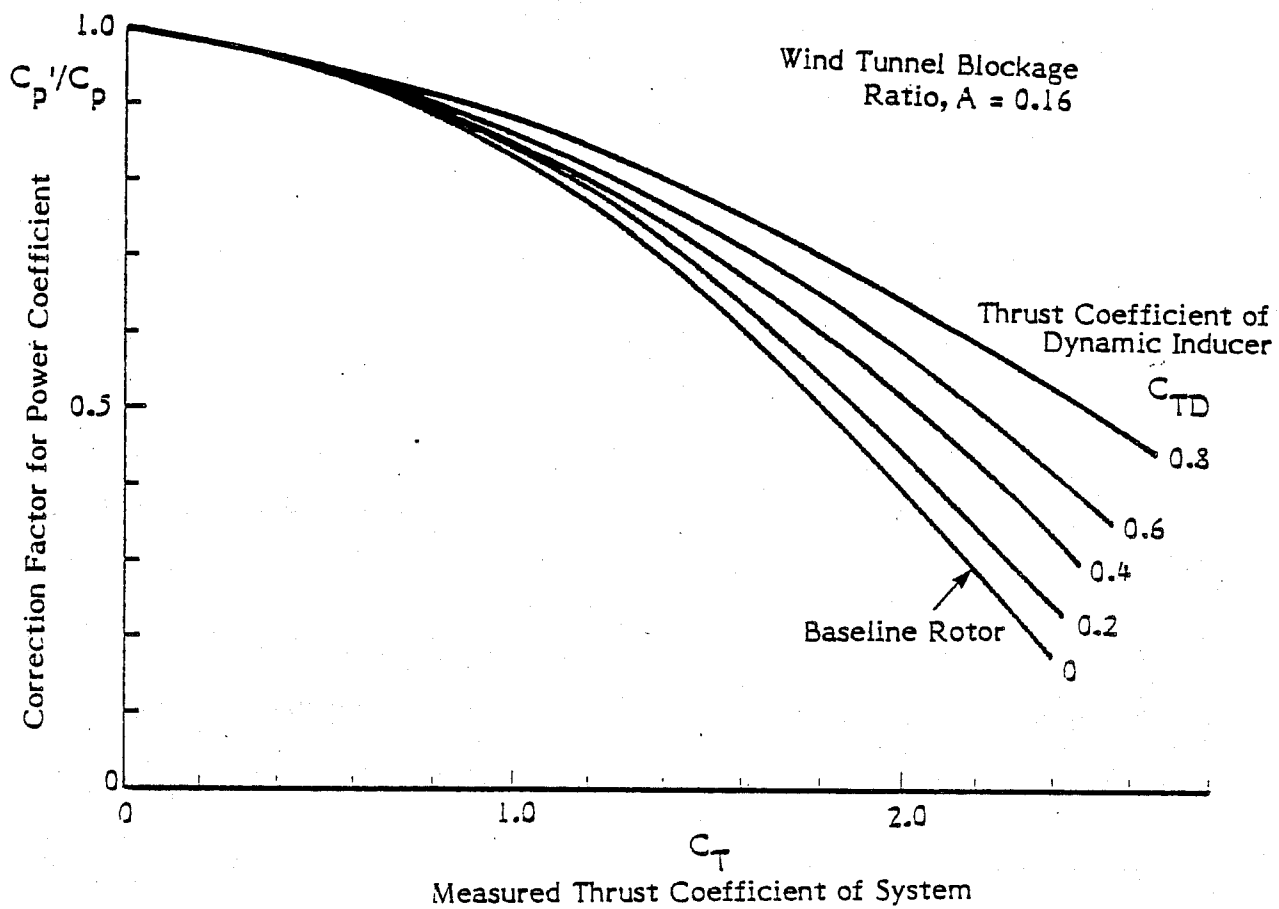
Figure 3-4. WIND TUNNEL CORRECTION FACTORS FOR DYNAMIC INDUCER

SECTION 4.0

ANALYSIS OF WIND TUNNEL MEASUREMENTS

4.1   PERFORMANCE MEASUREMENTS

Figure 4-1 shows the power coefficients measured in the wind tunnel using the one-third scale model. The maximum power coefficients are 0.47 for the rotor alone, and 0.78 for the dynamic inducer configuration. This corresponds to an augmentation ratio of 1.66. The maximum power coefficients occurs at a tip speed ratio of 4.

Figure 4-2 shows the corrected power coefficients using the wind tunnel correction factors discussed earlier. The maximum power coefficients are 0.37 for the rotor alone and 0.62 for the dynamic inducer configuration. This corresponds to an augmentation ratio of 1.68. The maximum power coefficient occurs near a tip speed ratio of 4.

The power coefficients of the dynamic inducer, normalized by the maximum power coefficient of the rotor alone, are plotted against X' in Figure 4-3, using the theoretical predictions and observed and corrected wind tunnel measurements shown earlier. The results indicate that the dynamic inducer increases the maximum power coefficient of the rotor on the order of 70%, and reduces the tip speed ratio range of the system somewhat from 2 to 8 to 2 to 5. Comparison of the wind tunnel measurements with the theoretical predictions shows similar trends. However, the theoretical model predicts lower augmentations occurring at higher tip speed ratios. This is believed to stem from simplifications in the model. Additional work is warranted in this area.

4.2   FLOW VISUALIZATION

In addition to performance measurements, flow visualization was conducted of the dynamic inducer system using tufts mounted on the model and liquid nitrogen as a flow tracer. Figure 4-4 shows the flow field obtained from composite photographs of liquid nitrogen/water vapor jets introduced upstream of the actuator disk. The near wake flow includes the trailing vortices from the two tips of the tip vanes and from the tip of the power blade. Within less than one-third of a revolution, the three vortices merge to form a single coherent trailing vortex filament. The filament intersects the following tip vane about 20% span inboard of the downwind tip of the tip vane and passes over the negative pressure (suction) side of the tip vane. Interestingly, the theoretical staggered array model predicts the vortex intersection to occur at the downwind tip of the tip vane for optimum performance.

It is believed that the presence of the blade tip vortex is altering the overall vortex roll-up process and may be responsible for the intersection being further inboard on the tip vane.

47
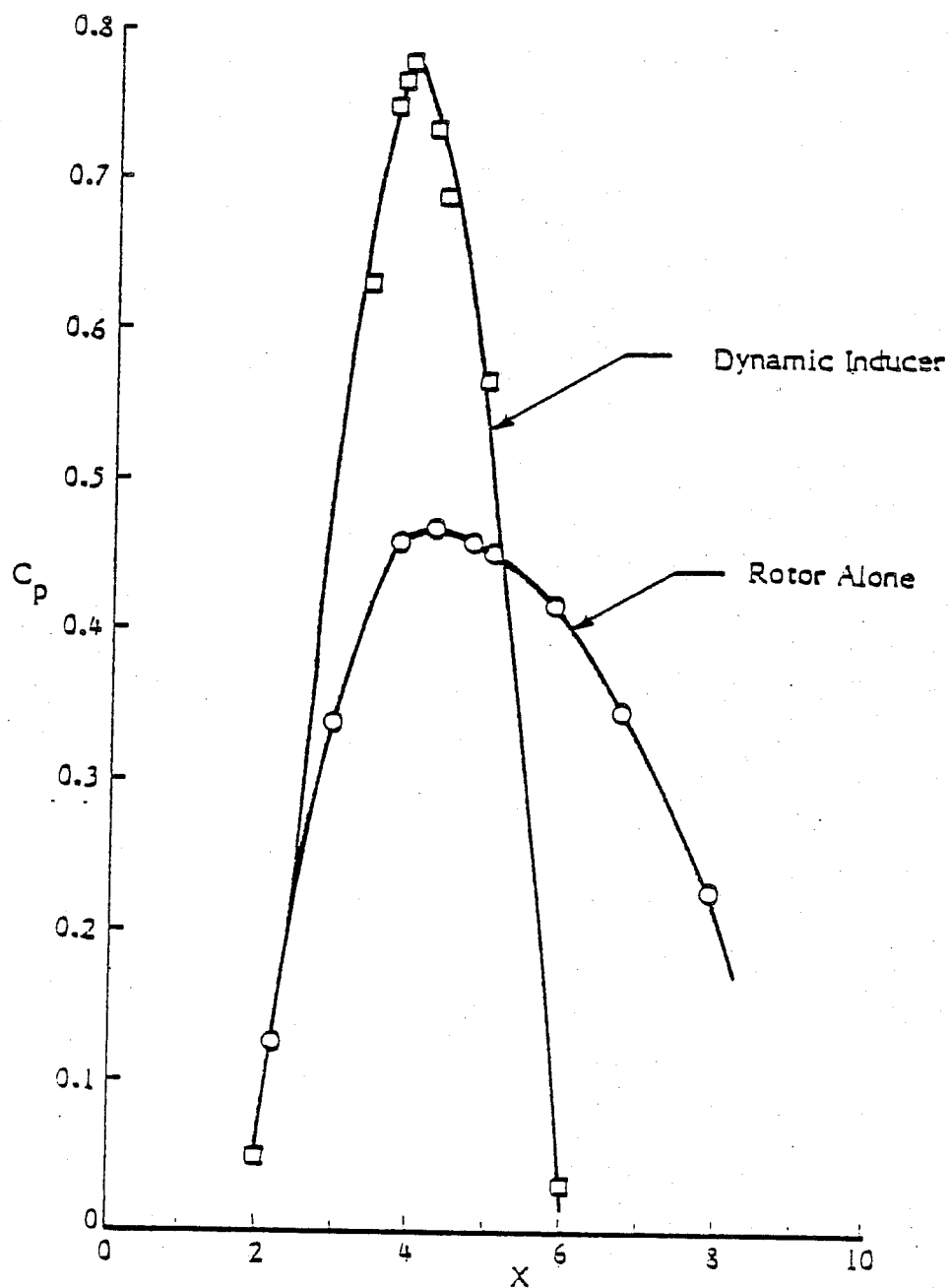
Figure 4-1.   MEASURED POWER COEFFICIENTS VERSUS TIP SPEED
RATIO FOR ROTOR ALONE AND DYNAMIC INDUCER
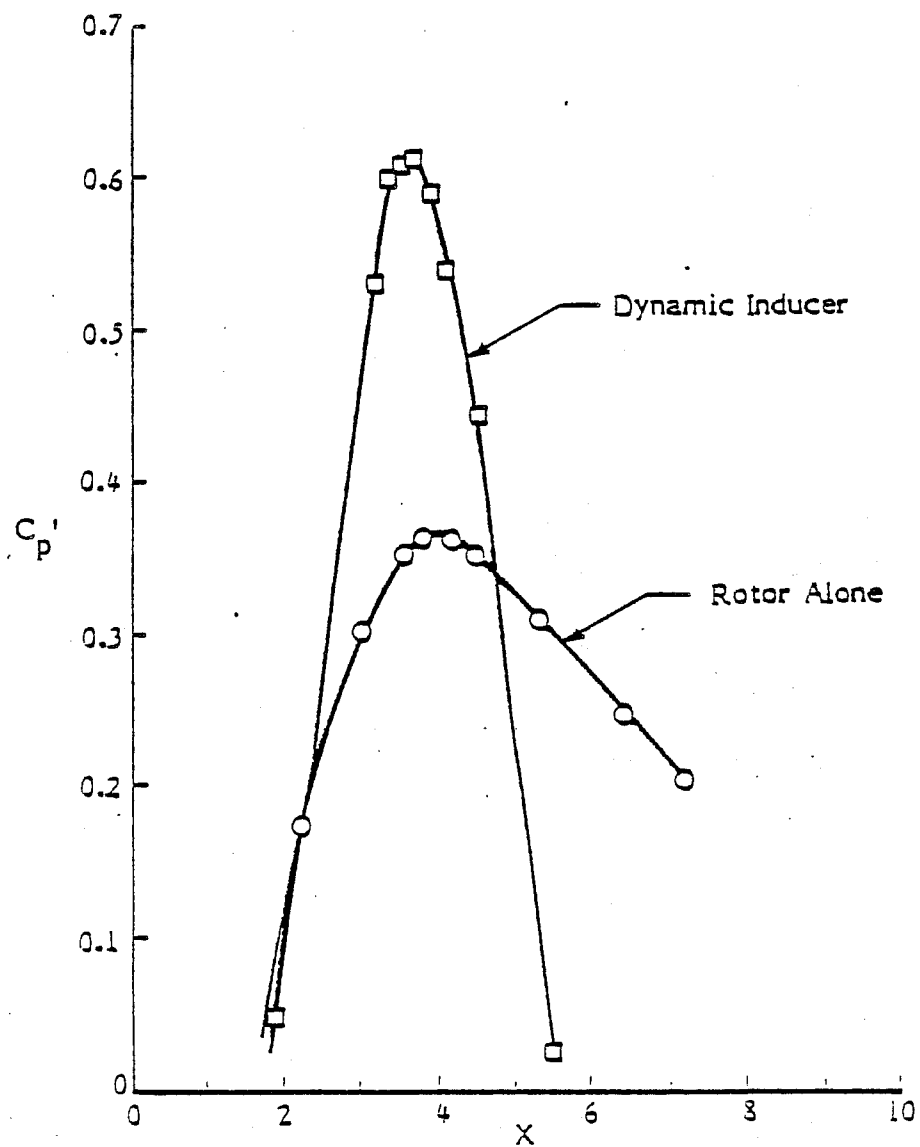
Figure 4-2.   CORRECTED POWER COEFFICIENTS VERSUS TIP SPEED
RATIO FOR ROTOR ALONE AND DYNAMIC INDUCER
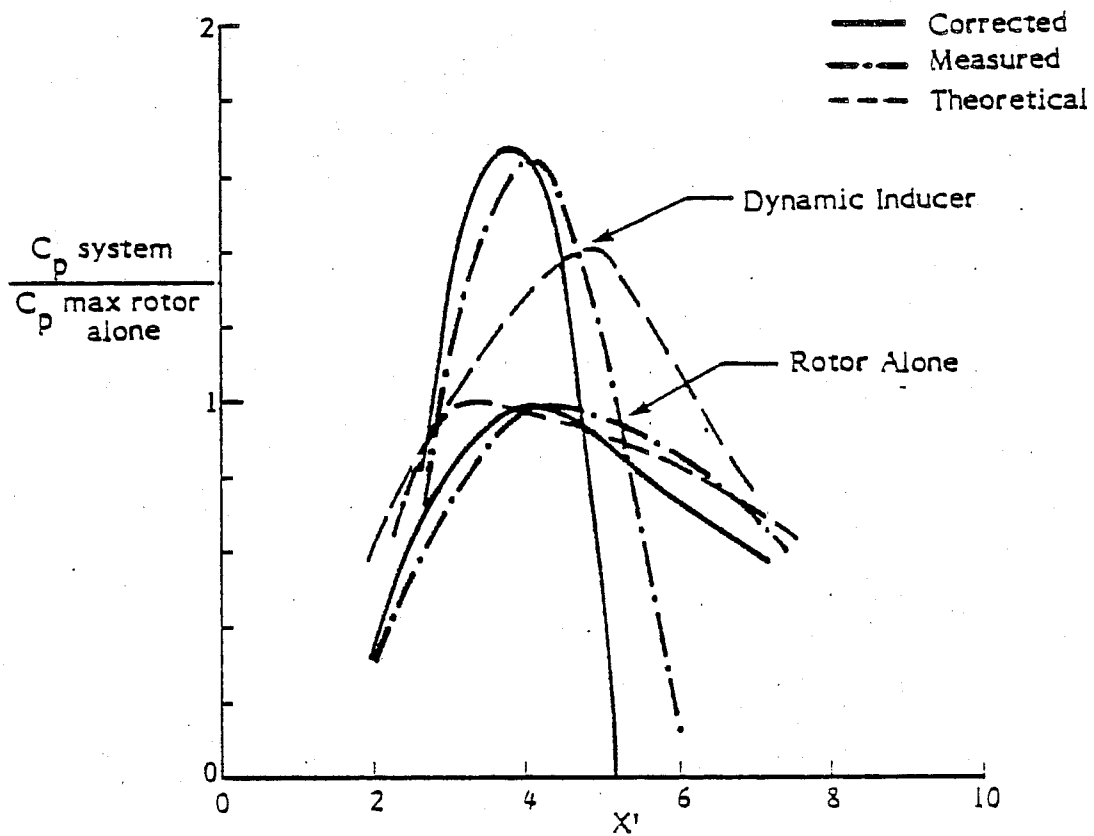
Figure 4-3. NORMALIZED POWER COEFFICIENTS VERSUS TIP SPEED RATIO FOR ROTOR ALONE AND DYNAMIC INDUCER

Tip Vortex, Upwind Tip

Power Blade Tip Vortex

Tip Vortex, Downwind Tip

Freestream Velocity
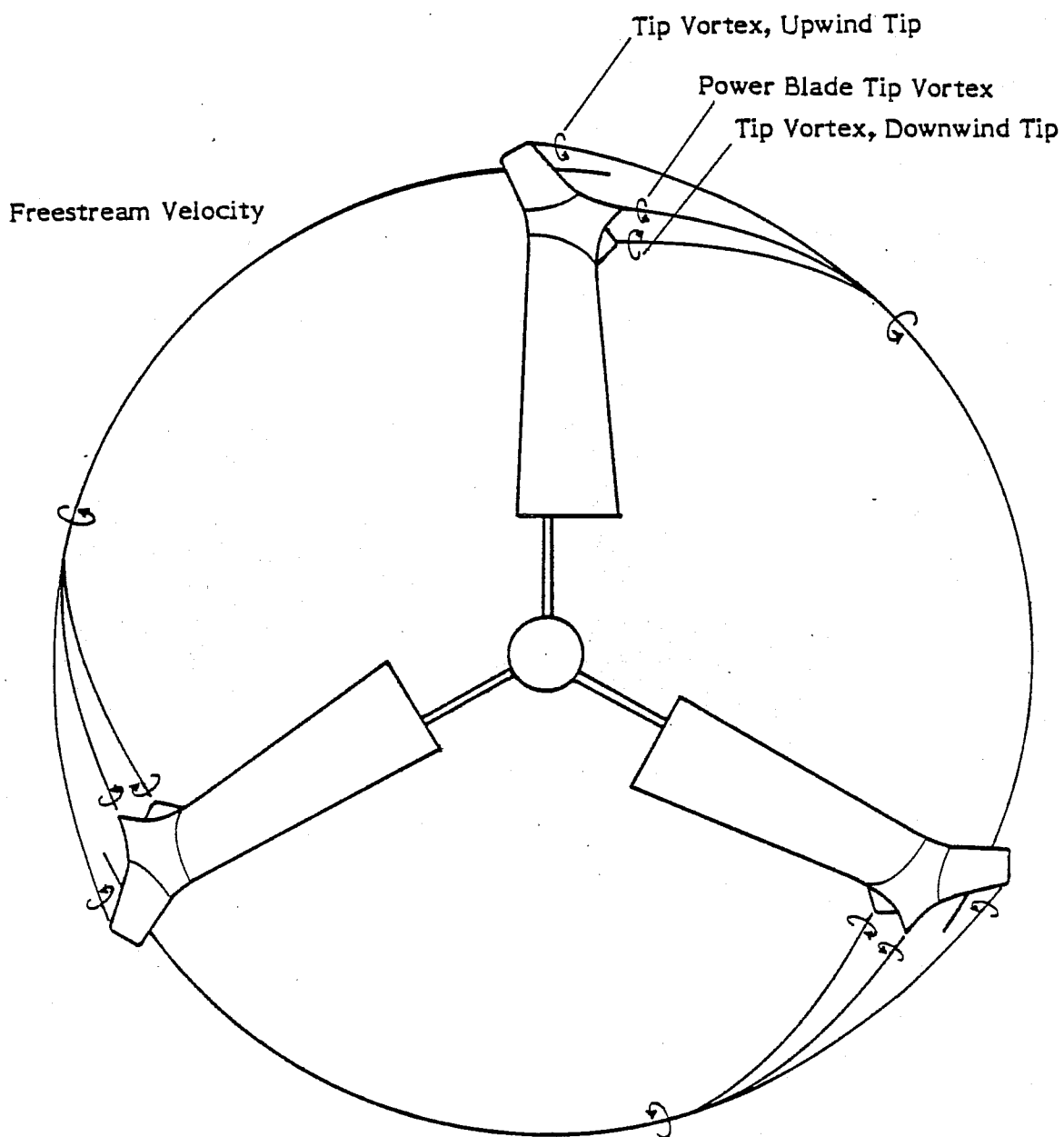
Figure 4-4.   VORTEX PATTERN AT OPTIMUM TIP SPEED RATIO

51

SECTION 5.0

FIELD TEST PROGRAM

5.1   OBJECTIVE OF TEST

A field test was conducted to measure the power output of a full-scale dynamic inducer system. The objective of the tow-test was to demonstrate the operation of the dynamic inducer system under realistic conditions.

5.2   DESCRIPTION OF MODEL

The model consisted of the 3.6-m diameter commercially available three-bladed Kedco wind turbine fitted with tip vanes approximately 1 m in span and 0.25 m in chord, as illustrated earlier in Figure 2-2. Figure 5-1 is a photograph of the model mounted on a trailer. Figure 5-2 shows a close-up of the tip vanes.

5.3   DESCRIPTION OF INSTRUMENTATION

A trailer-mounted tower equipped with an electronic system for varying the electrical load on the Kedco wind turbine was utilized for the field tests. The wind speed was measured by a Gill anemometer mounted on a 5-m boom ahead and above the vehicle. The instrumentation system is described in more detail in an earlier report (Lissaman and Walker, 1978).

For these field tests, the electrical and mechanical efficiency of the Kedco turbine was calibrated using the same dynamometer system which was discussed earlier in Section 3.3. As shown in Figure 5-3, the electromechanical efficiency of the Kedco turbine ranged from 14% to 55%. The field resistance of the alternator was varied from 0 to 14 ohms using a variable resistance, constant voltage load to control the torque and rpm characteristics of the system over the tip speed ratio range of the rotor.

The output of the reference anemometer was calibrated prior to the field tests using a synchronous 1800 rpm motor.

5.4   OPERATING PROCEDURE

The testing of the full-scale turbine involved towing the trailer at a fixed air speed (6 to 8 m/sec) with the rotor positioned about 7 m above ground. Once the rotor reached a selected operating rpm, the output from the turbine including the rpm, field resistance, output voltage, wind speed, and output current was recorded on a five-channel strip chart recorder. Typically, a 10- to 20-second record was obtained at each blade pitch setting. The runs at each setting were repeated several times and no significant drift, intermittency or scatter was noted.

The tip vane system was tested on the baseline rotor at a fixed yaw, tilt, and angle of attack. Efforts were not made to optimize the orientation of the tip vanes due to budget and time constraints.
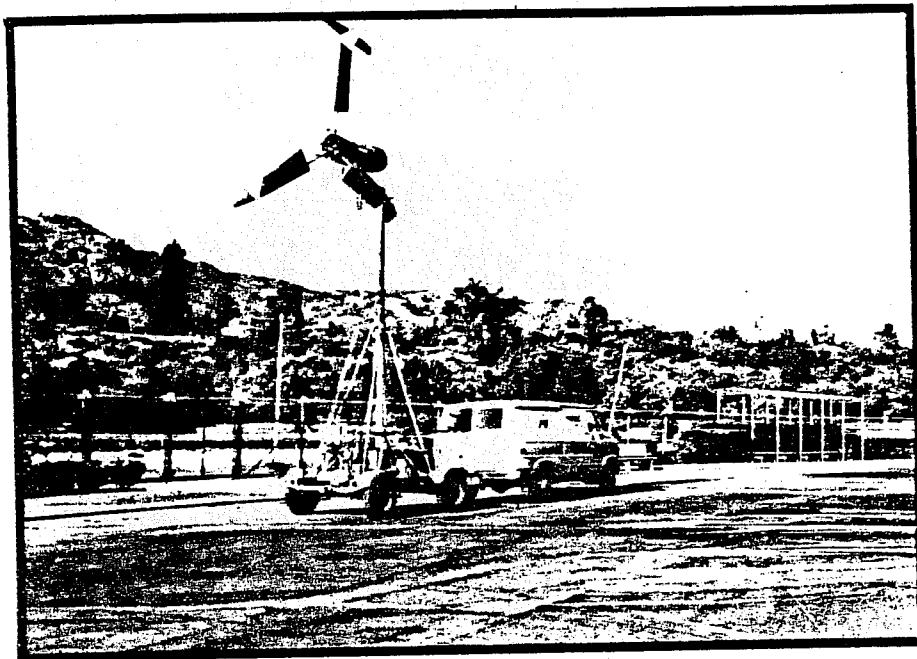
Figure 5-1.   PHOTOGRAPH OF FULL SCALE DYNAMIC INDUCER
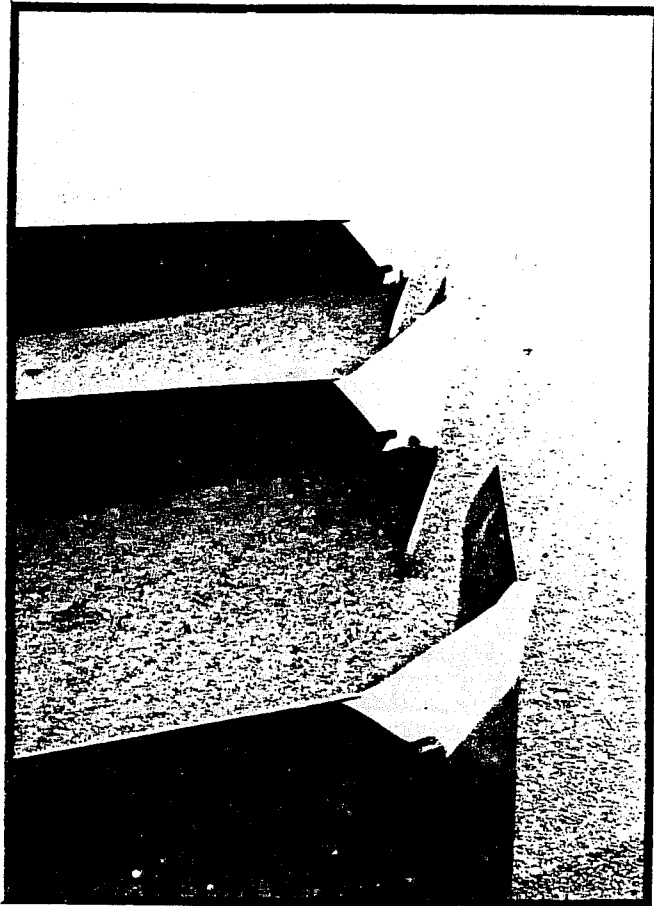
Figure 5-2. PHOTOGRAPH OF FULL SCALE TIP VANES
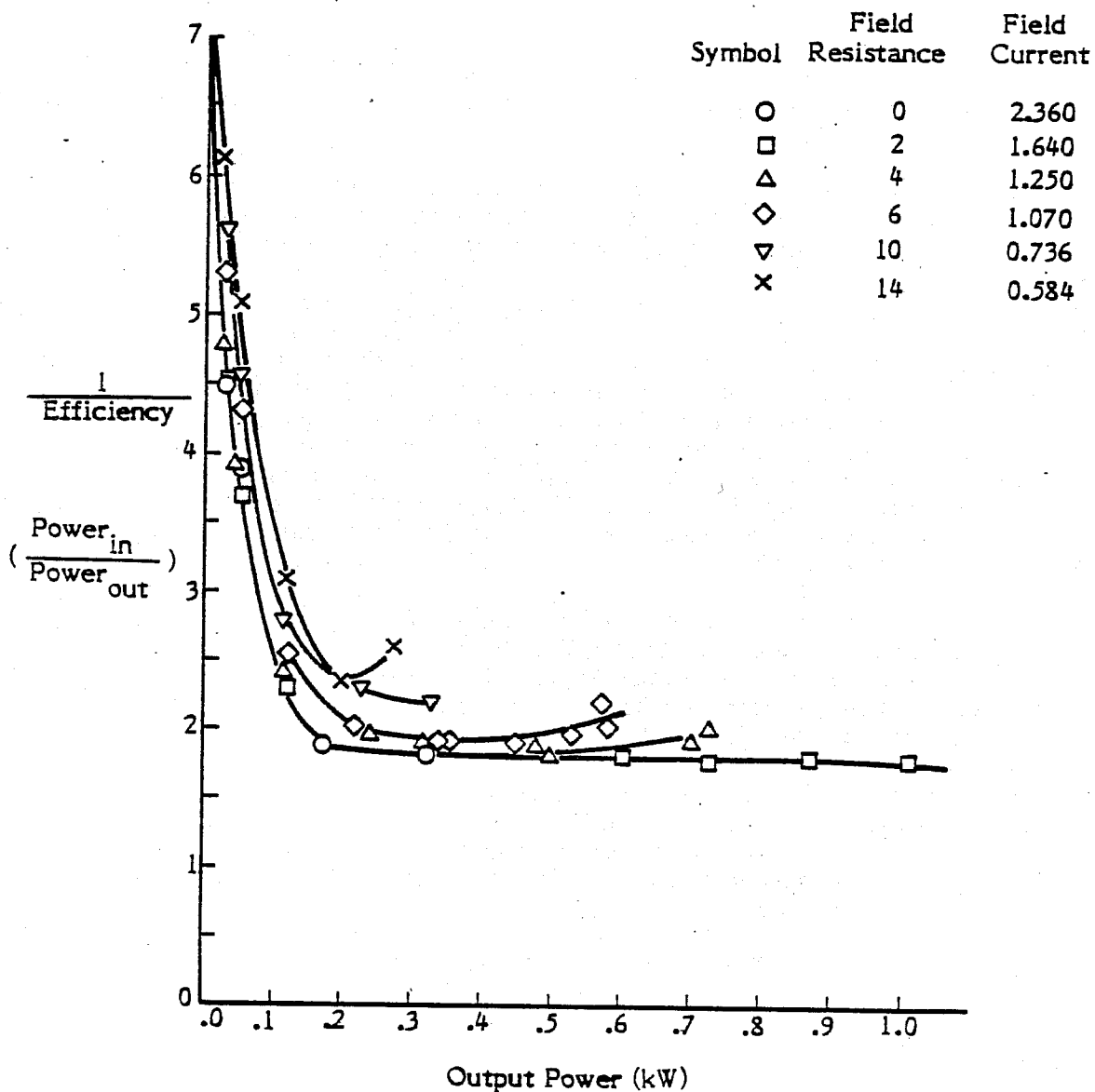
Figure 5-3.   ELECTROMECHANICAL EFFICIENCY OF KEDCO TURBINE SYSTEM

SECTION 6.0

ANALYSIS OF FIELD TEST MEASUREMENTS

6.1   PERFORMANCE OF BASELINE TURBINE

Figure 6-1 shows the power coefficient versus tip speed ratio for the baseline turbine obtained from the tow-tests for the design feather angle, $\beta = 9^\circ$, as well as for off-design conditions, $\beta = 13^\circ$. The results indicate a maximim power coefficient of 0.52 occurring at a tip speed ratio of 4.5.

Figure 6-2 shows the comparison of the measurements obtained from the full-scale tow tests with theory and the results from the earlier wind tunnel tests. The results show a 42% higher maximum power coefficient for the full-scale rotor than for the one-third scale wind-tunnel model. Moreover, the design tip speed ratio is 12% higher for the full-scale rotor than for the wind tunnel model. While a slightly higher performance is anticipated for the full-scale rotor due to the higher Reynolds numbers, such a large increase in performance is suspicious. The reason for the mismatch in power coefficient is not clear. A possible explanation may be an inaccuracy in the measurement of the wind speed. The 42% increase in the maximum power coefficient can result from a 12% increase in the freestream velocity. Improper positioning of the reference anemometer in the accelerated flow field of the van used to pull the trailer can account for a 12% increase in velocity. Significantly, a 12% adjustment of the freestream velocity would also lower the design tip speed ratio for the full-scale rotor and match the results obtained in the wind tunnel.

Comparison was made of the results from the present tow-tests with results published earlier (Lissaman and Walker, 1968). The electrical power output of the turbine was identical. However, in the earlier report the power coefficient of the turbine was calculated based on generated electrical power and included all electrical and mechanical losses in the system. In this report, the power coefficient was based on mechanical power measured at the rotor shaft (no mechanical or electrical losses were included) since it was desired to compare the measurements obtained from the field test and wind tunnel test on a common basis. Thus, higher values of power coefficient are predicted than in the earlier report. The observed power coefficient of 0.52 for the baseline turbine is consistent with the earlier measurements when the proper corrections for density and dynamic pressure are used.

6.2   PERFORMANCE OF DYNAMIC INDUCER

Figure 6-3 shows the power coefficient versus tip speed ratio for the full-scale dynamic inducer. A maximum power coefficient of 0.675 was achieved at a tip speed ratio of 4.0 for a feather angle of $\beta = 10^\circ$. The repeatability of the measurements is within about 10%, as shown by the scatter in the data points.

Figure 6-4 shows a comparison of the performance of the full-scale dynamic inducer with wind tunnel tests and theoretical predictions. The results indicate that the maximum power coefficient of the dynamic inducer is 11% higher for the field tests than for the wind tunnel tests. Comparing the performance of full-scale dynamic inducer (Figure 6-4) with the full-scale rotor (Figure 6-2), a 30% increase in power coefficient is observed.

56
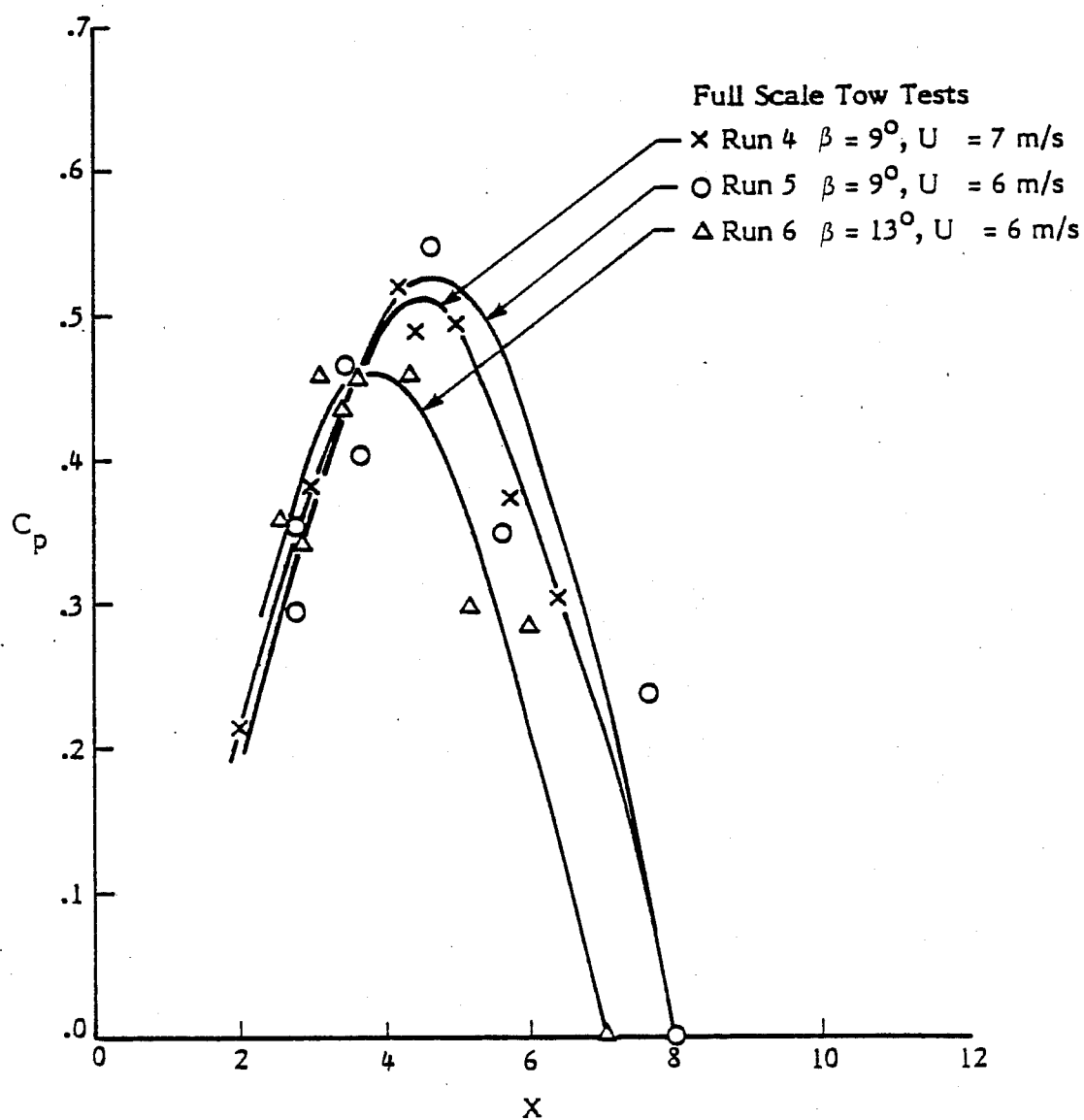
Figure 6-1. POWER COEFFICIENT VERSUS TIP SPEED RATIO FOR FULL-SCALE
BASELINE TURBINE
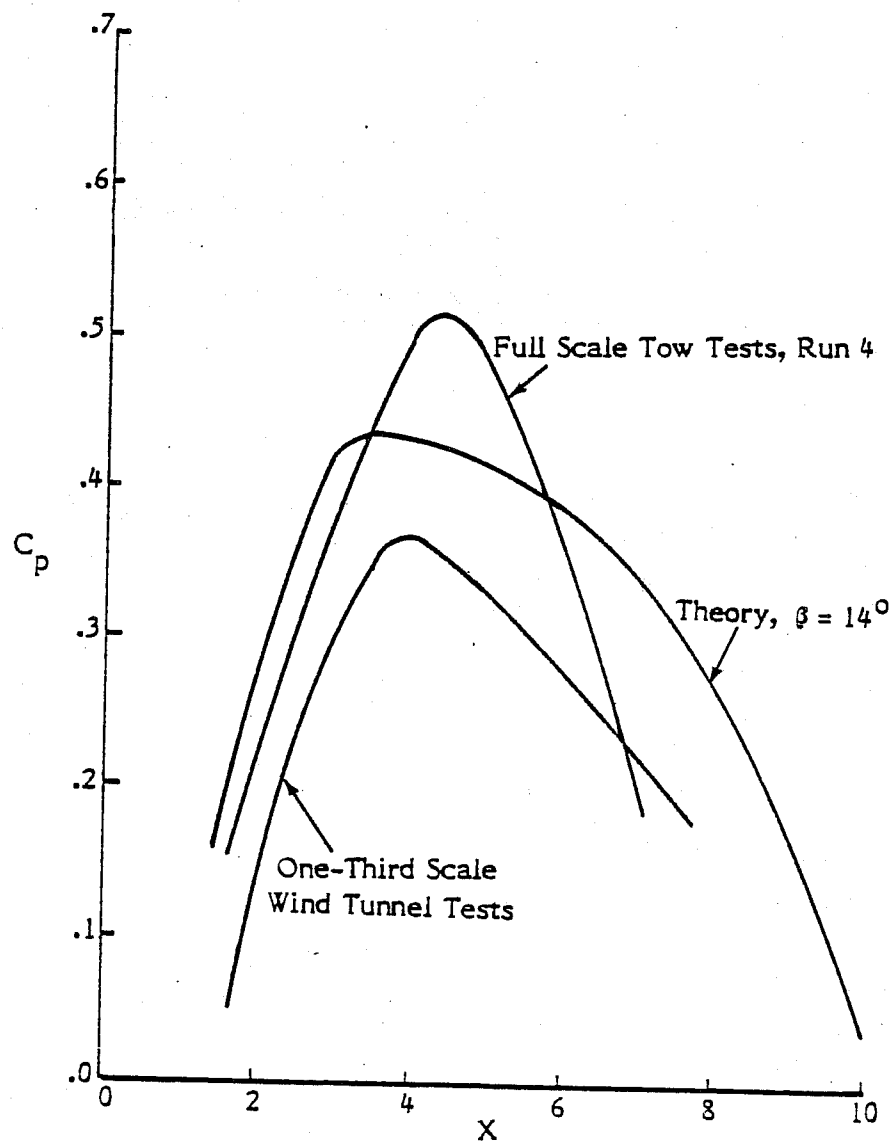
Figure 6-2.   COMPARISON OF POWER COEFFICIENT VERSUS TIP SPEED RATIO
OF BASELINE ROTOR OBSERVED DURING TOW TESTS WITH THEORETICAL
PREDICTIONS AND WIND TUNNEL MEASUREMENTS
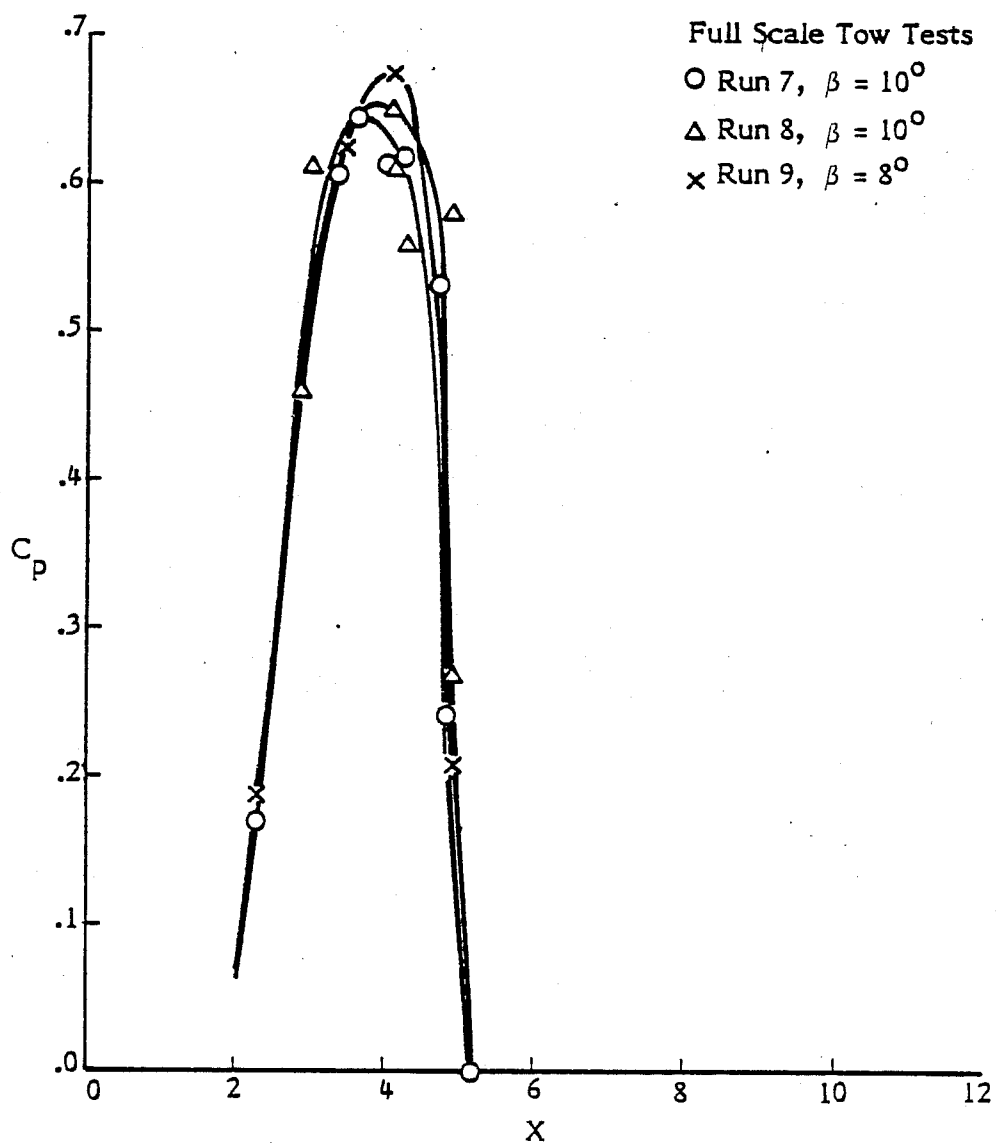
Figure 6-3. POWER COEFFICIENT VERSUS TIP SPEED RATIO FOR FULL-SCALE DYNAMIC INDUCER
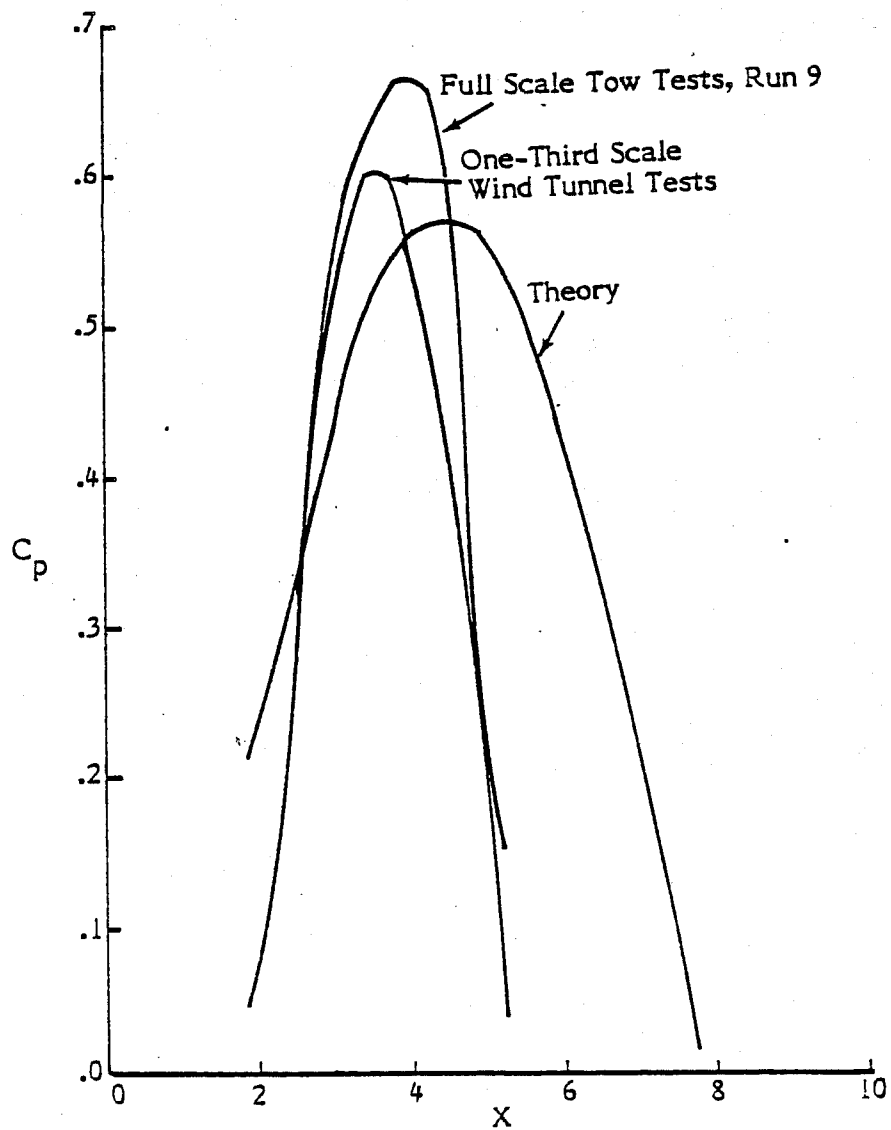
Figure 6-4. COMPARISON OF DYNAMIC INDUCER POWER COEFFICIENT OBSERVED DURING TOW TESTS WITH THEORETICAL PREDICTIONS AND WIND TUNNEL MEASUREMENTS

Comparison of the results of the field tests with the wind tunnel tests is good qualitatively, but has differences in magnitude of power coefficient. It is believed these differences are attributable to scale effect, calibration, geometrical infidelities between model and actual turbine and various random factors associated with field testing. The field tests demonstrated tip vane effectiveness. More extensive testing with a better optimized tip vane will result in further improvements. It is noted that optimization of a tip speed ratio 1.33 times higher will permit a 33% reduction in tip vane span.

It is recognized that the power coefficients observed during the tow tests of the basic Kedco turbine, $C_p \sim 0.5$, are higher than corresponding measurements published by Rocky Flats. The reason for this disagreement is not clear. However, the absolute value of the power coefficient for the baseline rotor is of secondary importance. The purpose of the tow tests was to compare the incremental performance of the baseline rotor compared to the dynamic inducer. The tests demonstrated that the dynamic inducer significantly improves the performance of the rotor. The differences observed between the existing tow test measurements and the Rocky Flats measurements should be addressed in a separate program.

SECTION 7.0

CONCLUSIONS AND RECOMMENDATIONS

The conclusions of this study are:

- the dynamic inducer system can substantially increase the power output of a conventional rotor system,

- wind tunnel corrections are very important for augmented turbine systems, and

- the performance benefits of the dynamic inducer system are likely to be higher for optimized configurations.

The favorable results obtained in this program suggest that the dynamic inducer system can play a major role in future WECS technology.

To demonstrate the technical and economic advantages of the dynamic inducer system, work is recommended in the following areas:

- development of an optimized dynamic inducer system suitable for commercial applications such as a two-bladed high tip speed ratio low solidity WECS,

- evaluation of the potential economic performance of the optimized commercial system, and

- validation of the economic and performance benefits of prototype full-scale dynamic inducer under actual operating conditions.

To develop and refine techniques for testing and evaluating wind turbines, work is recommended in the following areas:

- validation of the wind tunnel correction factors developed for wind turbines by means of a series of controlled wind tunnel tests;

- validation of the tow-test procedures for evaluation of turbine performance by conducting tow tests on the same model at different facilities under controlled conditions.

SECTION 8.0

BIBLIOGRAPHY

de Vries, O. Fluid Dynamic Aspects of Wind Energy Conversion. AGARDograph No. 243; July 1979.

Glauert, H. The Analysis of Experimental Results in the Windmill Brake and Vortex ring States of an Airscrew. Reports and Memoranda No. 1026, AE 222; February 1926.

Glauert, H. and W.F. Durand, eds. Aerodynamic Theory, Airplane Propellers. Vol. IV Division I, Chapter VII, Section 4, pp. 169-360, Julius Springer, Berlin; 1935.

Hibbs, B., and R.L. Radkey Small Wind Energy Conversion Systems (SWECS) Rotor Performance Model Comparison. AeroVironment Inc. Report, AV-R-80/561, UC-60; September 1980.

Lissaman, P.B.S. General Performance Theory for Crosswind Axis Turbines. Proceedings of the International Symposium on Wind Energy Systems, British Hydro Mechanics Research Association, England; September 1976a.

Lissaman, P.B.S. Increased Windmill Performance with Tip Vanes. AeroVironment Inc. Report, AV-TP-80/636; April 1976.

Lissaman, P.B.S. and S. Walker Dynamic Inducer Research Program. DOE Report RLO-1021-77/1; June 1978.

Lissaman, P.B.S., R.L. Radkey, W.J. Mouton, and D.F. Thompson Evaluation of Hydroelastic and Dynamic Behavior of Key Components of the Ocean Turbine System. DOE Report DOE/ET/20518-1 and 2; May 1980.

vanBussel, G.J.W. Analysis of Mutual Interference of Wings in a Plane, Staggered Formation. Delft Institute of Technology, Department of Aerospace Engineering, Memorandum M-315; 1978.

van Holten, T. Performance Analysis of a Windmill with Increased Power Output Due to Tipvane Induced Diffusion of the Airstream. Delft University of Technology, Dept. of Aerospace Engineering, Memorandum M-224; 1974.

van Holten, T. Windmills with Diffusor Effect Induced by Small Tipvanes. Proceedings of the International Symposium on Wind Energy Systems, British Hydro Mechanics Research Association, England; September 1976.

van Holten, T. Work Done by the Tip Vane Group of the Delft University of Technology for the National Research Program Wind Energy Period January 1980 until July 1980. Delft University of Technology, Department of Aerospace Engineering, Memorandum M-375; 1980.

Wilson, R.E., P.B.S. Lissaman, and S. Walker Aerodynamic Performance of Wind Turbines. Final Report under NSF RANN Grant No. AER 74-04014 A03, Oregon State University; June 1976.

APPENDIX A

Predicted Performance of Baseline Rotor Configuration

APPENDIX A

PREDICTED PERFORMANCE OF BASELINE ROTOR CONFIGURATION

The performance of the baseline rotor configuration was calculated from the PROP program using the specified rotor geometry and the lift and drag characteristics of the airfoil. Figure A-1 shows the input airfoil lift and drag characteristics. Table A-1 lists the output from the program. The printout lists the computational features selected in the PROP code and the geometry of the rotor, including the radius, chord, and twist distribution for ten blade element stations. The output consists of the tabulation of the feather angle (FEATHER), tip speed ratio ($X = \Omega R/V_o$), thrust coefficient ($TC = T/1/2\,\rho\,V_o^2\,\pi\,R^2$), power coefficient ($PC = P/1/2\rho V_o^3\,\pi\,R^2$), torque coefficient ($QC = Q/1/2\,\rho\,V_o^2\,\pi\,R^3$), advance ratio ($J = V/nD$), coefficient of thrust ($CT = T/\pi\,n^2 D^4$), coefficient of power ($CP = P/\rho\,n^3 D^5$), coefficient of torque ($CQ = Q/\rho\,n^2 D^4$), and propeller efficiency ($ETA = |P_c/T_c|$ min) where Ω, R, V_o, ρ, n, and D are the rotation rate (rad/sec), rotor radius, freestream velocity, air density, rotation rate (cycles/sec), and rotor diameter, respectively. A more detailed description of the PROP code output is given by Hibbs and Radkey (1980).
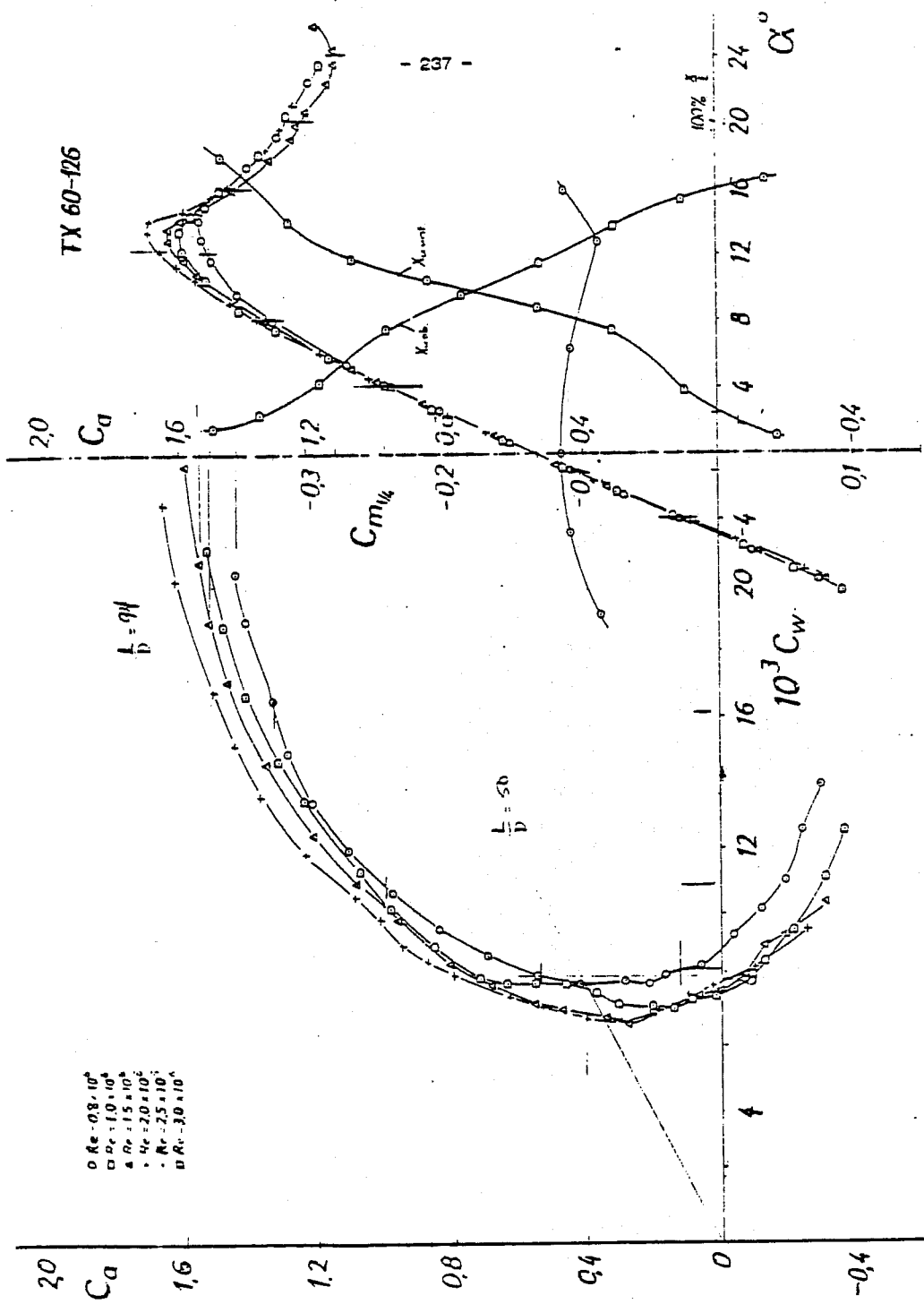
Figure A-1. INPUT AIRFOIL LIFT AND DRAG CHARACTERISTICS

Table A-1.   OUTPUT FROM PROP PROGRAM

```
AIRSCREW GEOMETRY

NUMBER OF BLADES:  3.
CONE ANGLE:  0.00  HUB RADIUS:  .333

LOSS MODELS
0: NONE
1: PRANDTL

TIP LOSS MODEL:  1  HUB LOSS MODEL:  1
ADVANCED BRAKE STATE MODEL USED
AIRSCREW ANALIZED AS WINDTURBINE
WIND EXPONENT: 0.000  HUB HEIGHT/RADIUS: 1.000 NUMBER OF CIRCUMFERENTIAL STATIONS:  1

BLADE ELEMENT DATA
ELEMENT  RADIUS  CHORD  TWIST
     1     .050  0.000.  0.000
     2     .150  0.000   0.000
     3     .250  0.000   0.000
     4     .350   .232   0.000
     5     .450   .221  -1.400
     6     .550   .211  -2.800
     7     .650   .200  -4.200
     8     .750   .189  -5.600
     9     .850   .178  -7.000
    10     .950   .167  -8.400

AIRFOIL SECTION DATA FOR SECTION  1
  ALPHA     CL        ALPHA     CD
 -90.000   0.000     -90.000  1.200
  -5.000   -.500      -6.000   .016
   7.000   1.200      -4.000   .009
   9.500   1.330       4.000   .009
  17.000   1.330       7.000   .010
  90.000   0.000      12.000   .016
  90.000   0.000      90.000  1.200

AIRFOIL SECTION DATA FOR SECTION  2
  ALPHA     CL        ALPHA     CD
 -90.000   0.000     -90.000  1.200
  -8.000   -.500      -6.000   .016
   7.000   1.200      -4.000   .009
   9.500   1.330       4.000   .009
  17.000   1.330       7.000   .010
  90.000   0.000      12.000   .016
  90.000   0.000      90.000  1.200

AIRFOIL SECTION DATA FOR SECTION  3
  ALPHA     CL        ALPHA     CD
 -90.000   0.000     -90.000  1.200
  -8.000   -.500      -6.000   .016
   7.000   1.200      -4.000   .009
   9.500   1.330       4.000   .009
  17.000   1.330       7.000   .010
  90.000   0.000      12.000   .016
  90.000   0.000      90.000  1.200

AIRFOIL SECTION DATA FOR SECTION  4
  ALPHA     CL        ALPHA     CD
```

```
-90.000    0.000      -90.000   1.200
 -8.000    -.500       -6.000    .016
  7.000   1.200        -4.000    .009
  9.500   1.330         4.000    .009
 17.000   1.330         7.000    .010
 90.000    0.000       12.000    .016
 90.000    0.000       90.000   1.200
```

```
AIRFOIL SECTION DATA FOR SECTION  5
 ALPHA     CL          ALPHA     CD
-90.000    0.000      -90.000   1.200
 -8.000    -.500       -6.000    .016
  7.000   1.200        -6.000    .009
  9.500   1.330         4.000    .009
 17.000   1.330         7.000    .010
 90.000    0.000       12.000    .016
 90.000    0.000       90.000   1.200
```

```
AIRFOIL SECTION DATA FOR SECTION  6
 ALPHA     CL          ALPHA     CD
-90.000    0.000      -90.000   1.200
 -8.000    -.500       -6.000    .016
  7.000   1.200        -4.000    .009
  9.500   1.330         4.000    .009
 17.000   1.330         7.000    .010
 90.000    0.000       12.000    .016
 90.000    0.000       90.000   1.200
```

```
AIRFOIL SECTION DATA FOR SECTION  7
 ALPHA     CL          ALPHA     CD
-90.000    0.000      -90.000   1.200
 -8.000    -.500       -6.000    .016
  7.000   1.200        -4.000    .009
  9.500   1.330         4.000    .009
 17.000   1.330         7.000    .010
 90.000    0.000       12.000    .016
 90.000    0.000       90.000   1.200
```

```
AIRFOIL SECTION DATA FOR SECTION  8
 ALPHA     CL          ALPHA     CD
-90.000    0.000      -90.000   1.200
 -8.000    -.500       -6.000    .016
  7.000   1.200        -4.000    .009
  9.500   1.330         4.000    .009
 17.000   1.330         7.000    .010
 90.000    0.000       12.000    .016
 90.000    0.000       90.000   1.200
```

```
AIRFOIL SECTION DATA FOR SECTION  9
 ALPHA     CL          ALPHA     CD
-90.000    0.000      -90.000   1.200
 -8.000    -.500       -6.000    .016
  7.000   1.200        -4.000    .009
  9.500   1.330         4.000    .009
 17.000   1.330         7.000    .010
 90.000    0.000       12.000    .016
 90.000    0.000       90.000   1.200
```

```
AIRFOIL SECTION DATA FOR SECTION 10
 ALPHA     CL          ALPHA     CD
```

Table A-1 (continued).

```
-90.000   0.000      -90.000   1.200
 -8.000   -.500       -5.000    .018
  7.000   1.200       -4.000    .009
  9.500   1.330        4.000    .009
 17.000   1.330        7.000    .010
 90.000   0.000       12.000    .013
 90.000   0.000       90.000   1.200
```

SECTIONS 4 TO 10 INCLUDED IN ANALYSIS

FEATHER	X	TC	PC	QC	J	CT	CP	CQ	ETA
6.0	.4	.152	.002	.004	7.654	3.208	.301	.0480	.012
6.0	.6	.137	.005	.009	5.238	1.471	.295	.0469	.033
6.0	.8	.149	.012	.015	3.727	.899	.270	.0461	.082
6.0	1.0	.168	.023	.023	3.142	.652	.282	.0447	.138
6.0	1.2	.196	.039	.032	2.618	.528	.273	.0434	.197
6.0	1.4	.232	.059	.042	2.244	.460	.262	.0418	.255
6.0	1.6	.277	.085	.053	1.963	.417	.252	.0401	.306
6.0	1.8	.331	.116	.064	1.745	.395	.241	.0384	.350
6.0	2.0	.373	.152	.076	1.571	.381	.231	.0367	.386
6.0	2.2	.465	.192	.087	1.428	.372	.220	.0350	.414
6.0	2.4	.543	.236	.099	1.309	.366	.208	.0331	.435
6.0	2.6	.629	.283	.109	1.208	.361	.196	.0312	.450
6.0	2.8	.719	.323	.116	1.122	.355	.181	.0288	.454
6.0	3.0	.806	.332	.117	1.047	.347	.159	.0253	.457
6.0	3.2	.888	.337	.112	.982	.336	.133	.0211	.402
6.0	3.4	.959	.348	.102	.924	.321	.108	.0168	.365
6.0	3.6	1.015	.353	.092	.873	.304	.087	.0138	.301
6.0	3.8	1.060	.319	.084	.827	.285	.071	.0113	.291
6.0	4.0	1.096	.308	.077	.783	.265	.057	.0073	.281
6.0	4.2	1.129	.377	.071	.748	.248	.049	.0078	.263
6.0	4.4	1.162	.333	.065	.714	.233	.041	.0063	.248
6.0	4.6	1.194	.272	.057	.683	.217	.034	.0054	.226
6.0	4.8	1.226	.258	.054	.654	.206	.026	.0043	.211
6.0	5.0	1.257	.242	.048	.628	.195	.024	.0037	.172
6.0	5.2	1.288	.224	.043	.604	.185	.017	.0031	.174
6.0	5.4	1.318	.204	.038	.582	.175	.016	.0025	.155
6.0	5.6	1.347	.152	.032	.561	.166	.013	.0020	.155
6.0	5.8	1.375	.153	.027	.542	.158	.010	.0016	.115
6.0	6.0	1.403	.134	.022	.524	.151	.008	.0012	.073
6.0	6.2	1.430	.103	.017	.507	.144	.006	.0007	.075
6.0	6.4	1.458	.081	.013	.471	.136	.004	.0006	.055
6.0	6.6	1.486	.052	.008	.476	.132	.002	.0004	.035
6.0	6.8	1.514	.023	.003	.462	.127	.001	.0001	.015
6.0	7.0	1.541	-.008	-.001	.447	.122	-.000	-.0000	.005
6.0	7.2	1.569	-.040	-.006	.436	.117	-.001	-.0002	.028
6.0	7.4	1.574	-.075	-.010	.425	.113	-.002	-.0004	.047
6.0	7.6	1.620	-.111	-.015	.413	.107	-.003	-.0005	.068
6.0	7.8	1.644	-.146	-.019	.403	.103	-.004	-.0006	.070
6.0	8.0	1.668	-.187	-.023	.373	.101	-.004	-.0007	.112
6.0	8.2	1.692	-.227	-.028	.383	.078	-.005	-.0008	.134
6.0	8.4	1.715	-.267	-.032	.374	.074	-.006	-.0007	.157
6.0	8.6	1.738	-.313	-.036	.365	.071	-.006	-.0009	.179
6.0	8.8	1.761	-.356	-.040	.357	.068	-.006	-.0010	.202
6.0	9.0	1.785	-.401	-.045	.347	.065	-.007	-.0011	.223
6.0	9.2	1.808	-.448	-.049	.341	.063	-.007	-.0011	.246
6.0	9.4	1.831	-.496	-.053	.334	.060	-.007	-.0012	.271
6.0	9.6	1.854	-.546	-.057	.327	.078	-.008	-.0012	.293
6.0	9.8	1.877	-.597	-.061	.321	.075	-.008	-.0012	.315
6.0	10.0	1.901	-.650	-.065	.314	.074	-.008	-.0013	.342

FEATHER	X	TC	FC	GC	J	CT	CP	CG	ETA
8.0	.4	.130	.003	.006	7.854	3.140	.802	.0737	.024
8.0	.6	.135	.008	.013	5.236	1.446	.449	.0714	.057
8.0	.8	.147	.016	.020	3.927	.892	.369	.0620	.111
8.0	1.0	.168	.029	.029	3.142	.651	.355	.0565	.174
8.0	1.2	.197	.047	.039	2.618	.550	.331	.0527	.238
8.0	1.4	.234	.070	.050	2.244	.484	.311	.0495	.297
8.0	1.6	.281	.099	.062	1.963	.425	.294	.0468	.355
8.0	1.8	.336	.133	.074	1.745	.402	.279	.0443	.378
8.0	2.0	.400	.174	.087	1.571	.388	.264	.0421	.434
8.0	2.2	.472	.218	.099	1.428	.378	.250	.0397	.462
8.0	2.4	.551	.267	.111	1.309	.371	.235	.0374	.464
8.0	2.6	.635	.315	.121	1.208	.364	.218	.0348	.473
8.0	2.8	.721	.354	.127	1.122	.356	.176	.0313	.471
8.0	3.0	.798	.380	.127	1.047	.344	.171	.0273	.476
8.0	3.2	.864	.378	.118	.982	.327	.140	.0223	.437
8.0	3.4	.915	.369	.109	.924	.307	.114	.0182	.403
8.0	3.6	.952	.358	.099	.873	.285	.093	.0149	.376
8.0	3.8	.979	.350	.092	.827	.263	.078	.0123	.357
8.0	4.0	1.003	.342	.086	.785	.243	.065	.0104	.341
8.0	4.2	1.027	.335	.080	.748	.226	.055	.0088	.326
8.0	4.4	1.050	.327	.074	.714	.210	.047	.0074	.312
8.0	4.6	1.073	.318	.069	.683	.196	.040	.0063	.276
8.0	4.8	1.095	.308	.064	.654	.184	.034	.0054	.231
8.0	5.0	1.118	.297	.059	.628	.173	.029	.0046	.236
8.0	5.2	1.140	.285	.055	.604	.163	.025	.0037	.250
8.0	5.4	1.162	.273	.050	.582	.154	.021	.0034	.255
8.0	5.6	1.183	.259	.046	.561	.146	.018	.0029	.117
8.0	5.8	1.204	.244	.042	.542	.139	.015	.0024	.203
8.0	6.0	1.224	.229	.038	.524	.132	.013	.0021	.187
8.0	6.2	1.243	.212	.034	.507	.125	.011	.0017	.171
8.0	6.4	1.262	.194	.030	.491	.119	.009	.0014	.154
8.0	6.6	1.281	.175	.027	.476	.114	.007	.0012	.137
8.0	6.8	1.298	.155	.023	.462	.109	.006	.0010	.120
8.0	7.0	1.315	.134	.019	.449	.104	.005	.0008	.102
8.0	7.2	1.333	.112	.016	.436	.100	.004	.0006	.084
8.0	7.4	1.349	.090	.012	.425	.096	.003	.0004	.066
8.0	7.6	1.366	.066	.009	.413	.092	.002	.0003	.048
8.0	7.8	1.383	.041	.005	.403	.088	.001	.0002	.030
8.0	8.0	1.399	.016	.002	.393	.085	.000	.0001	.011
8.0	8.2	1.416	-.011	-.001	.383	.082	-.000	-.0000	.008
8.0	8.4	1.433	-.038	-.005	.374	.079	-.001	-.0001	.027
8.0	8.6	1.449	-.067	-.008	.365	.076	-.001	-.0002	.046
8.0	8.8	1.465	-.096	-.011	.357	.073	-.002	-.0003	.066
8.0	9.0	1.481	-.127	-.014	.349	.071	-.002	-.0003	.086
8.0	9.2	1.497	-.159	-.017	.341	.069	-.002	-.0004	.106
8.0	9.4	1.513	-.192	-.020	.334	.066	-.003	-.0004	.127
8.0	9.6	1.528	-.226	-.024	.327	.064	-.003	-.0005	.148
8.0	9.8	1.543	-.261	-.027	.321	.062	-.003	-.0005	.169
8.0	10.0	1.558	-.297	-.030	.314	.060	-.004	-.0006	.191

FEATHER	X	TC	FC	GC	J	CT	CP	CG	ETA
10.0	.4	.127	.005	.012	7.854	3.072	.704	.1459	.037
10.0	.6	.132	.011	.013	5.236	1.426	.603	.0760	.061
10.0	.8	.146	.021	.026	3.927	.884	.489	.0777	.141
10.0	1.0	.168	.035	.035	3.142	.650	.429	.0682	.210
10.0	1.2	.198	.055	.046	2.618	.552	.389	.0617	.279
10.0	1.4	.237	.081	.058	2.244	.488	.360	.0572	.343
10.0	1.6	.284	.113	.071	1.963	.450	.338	.0535	.378

FEATHER	X	TC	PC	QC	J	CT	CP	CQ	ETA
10.0	1.8	.341	.151	.084	1.745	.408	.316	.0502	.443
10.0	2.0	.407	.195	.098	1.571	.394	.297	.0473	.480
10.0	2.2	.478	.243	.111	1.428	.383	.278	.0443	.509
10.0	2.4	.556	.294	.123	1.307	.374	.259	.0413	.529
10.0	2.6	.638	.339	.131	1.208	.366	.233	.0374	.532
10.0	2.8	.712	.378	.135	1.122	.352	.209	.0335	.530
10.0	3.0	.783	.399	.133	1.047	.337	.180	.0286	.509
10.0	3.2	.833	.400	.125	.982	.315	.149	.0236	.480
10.0	3.4	.868	.392	.113	.924	.291	.122	.0193	.452
10.0	3.6	.890	.385	.107	.873	.266	.101	.0160	.433
10.0	3.8	.907	.380	.100	.827	.243	.084	.0134	.417
10.0	4.0	.922	.375	.094	.785	.223	.071	.0113	.406
10.0	4.2	.937	.369	.088	.748	.206	.061	.0097	.374
10.0	4.4	.952	.363	.083	.714	.171	.052	.0083	.381
10.0	4.6	.966	.357	.078	.683	.177	.045	.0071	.367
10.0	4.8	.980	.350	.073	.654	.165	.038	.0061	.356
10.0	5.0	.994	.342	.068	.628	.154	.033	.0053	.344
10.0	5.2	1.007	.334	.064	.604	.144	.029	.0046	.331
10.0	5.4	1.020	.325	.060	.582	.136	.025	.0040	.319
10.0	5.6	1.033	.316	.056	.561	.128	.022	.0035	.306
10.0	5.8	1.045	.306	.053	.542	.120	.019	.0030	.293
10.0	6.0	1.057	.296	.049	.524	.114	.017	.0027	.280
10.0	6.2	1.069	.285	.046	.507	.108	.015	.0023	.267
10.0	6.4	1.080	.273	.043	.491	.102	.013	.0020	.253
10.0	6.6	1.090	.261	.040	.476	.097	.011	.0018	.239
10.0	6.8	1.101	.248	.037	.462	.092	.010	.0015	.225
10.0	7.0	1.111	.234	.033	.449	.088	.008	.0013	.211
10.0	7.2	1.120	.220	.031	.436	.084	.007	.0011	.196
10.0	7.4	1.129	.204	.028	.425	.080	.006	.0010	.181
10.0	7.6	1.138	.188	.025	.413	.076	.005	.0008	.165
10.0	7.8	1.147	.171	.022	.403	.073	.004	.0007	.147
10.0	8.0	1.154	.153	.019	.393	.070	.004	.0006	.133
10.0	8.2	1.162	.135	.016	.383	.067	.003	.0005	.115
10.0	8.4	1.169	.115	.014	.374	.064	.002	.0004	.099
10.0	8.6	1.177	.095	.011	.365	.062	.002	.0003	.081
10.0	8.8	1.183	.074	.008	.357	.059	.001	.0002	.062
10.0	9.0	1.190	.052	.006	.349	.057	.001	.0001	.043
10.0	9.2	1.196	.029	.003	.341	.055	.000	.0001	.024
10.0	9.4	1.202	.005	.001	.334	.053	.000	.0000	.004
10.0	9.6	1.208	-.020	-.002	.327	.051	-.000	-.0000	.013
10.0	9.8	1.214	-.046	-.005	.321	.049	-.001	-.0001	.035
10.0	10.0	1.220	-.072	-.007	.314	.047	-.001	-.0001	.059

FEATHER	X	TC	PC	QC	J	CT	CP	CQ	ETA
12.0	.4	.124	.006	.016	7.854	3.006	1.206	.1920	.051
12.0	.6	.150	.013	.022	5.236	1.405	.758	.1206	.105
12.0	.8	.145	.025	.031	3.927	.877	.589	.0938	.171
12.0	1.0	.168	.041	.041	3.142	.649	.502	.0799	.246
12.0	1.2	.199	.063	.053	2.618	.535	.447	.0712	.319
12.0	1.4	.239	.092	.066	2.244	.472	.408	.0650	.385
12.0	1.6	.288	.127	.079	1.963	.436	.378	.0601	.441
12.0	1.8	.347	.169	.094	1.745	.415	.353	.0561	.487
12.0	2.0	.411	.216	.108	1.571	.399	.328	.0522	.524
12.0	2.2	.483	.267	.121	1.428	.387	.306	.0486	.554
12.0	2.4	.559	.315	.131	1.307	.376	.277	.0441	.565
12.0	2.6	.630	.339	.138	1.208	.361	.249	.0396	.570
12.0	2.8	.698	.372	.140	1.122	.345	.217	.0346	.561
12.0	3.0	.753	.410	.137	1.047	.324	.185	.0294	.545
12.0	3.2	.795	.416	.150	.932	.301	.154	.0246	.523
12.0	3.4	.818	.415	.122	.724	.274	.129	.0205	.507

		TC	PC	GC	J	CT	CP	CG	ETA
12.0	3.6	.834	.413	.115	.673	.249	.108	.0172	.496
12.0	3.8	.843	.411	.108	.827	.227	.091	.0145	.486
12.0	4.0	.854	.407	.102	.785	.207	.077	.0123	.477
12.0	4.2	.863	.403	.096	.748	.190	.066	.0106	.467
12.0	4.4	.871	.399	.091	.714	.174	.057	.0091	.458
12.0	4.6	.878	.374	.086	.683	.161	.049	.0078	.448
12.0	4.8	.885	.389	.081	.654	.149	.043	.0068	.439
12.0	5.0	.892	.383	.077	.628	.138	.037	.0059	.429
12.0	5.2	.878	.377	.072	.604	.129	.033	.0052	.420
12.0	5.4	.704	.371	.069	.582	.120	.029	.0046	.410
12.0	5.6	.709	.364	.065	.561	.112	.025	.0040	.400
12.0	5.8	.914	.357	.061	.542	.105	.022	.0035	.370
12.0	6.0	.918	.349	.058	.524	.099	.020	.0031	.380
12.0	6.2	.722	.341	.055	.507	.093	.017	.0028	.370
12.0	6.4	.925	.332	.052	.491	.088	.015	.0025	.357
12.0	6.6	.929	.323	.049	.476	.083	.014	.0022	.347
12.0	6.8	.932	.313	.046	.462	.078	.012	.0019	.336
12.0	7.0	.935	.303	.043	.449	.074	.011	.0017	.324
12.0	7.2	.937	.292	.041	.436	.070	.010	.0015	.311
12.0	7.4	.939	.280	.038	.425	.066	.008	.0013	.298
12.0	7.6	.941	.268	.035	.413	.063	.007	.0012	.284
12.0	7.8	.942	.254	.033	.403	.060	.007	.0010	.270
12.0	8.0	.944	.241	.030	.373	.057	.006	.0009	.255
12.0	8.2	.945	.226	.028	.383	.054	.005	.0008	.237
12.0	8.4	.945	.211	.025	.374	.052	.004	.0007	.223
12.0	8.6	.946	.195	.023	.365	.050	.004	.0006	.206
12.0	8.8	.946	.178	.020	.357	.047	.003	.0005	.188
12.0	9.0	.946	.160	.018	.349	.045	.003	.0004	.169
12.0	9.2	.945	.141	.015	.341	.043	.002	.0004	.149
12.0	7.4	.945	.121	.013	.334	.041	.002	.0003	.128
12.0	7.6	.744	.101	.010	.327	.040	.001	.0002	.107
12.0	7.8	.742	.079	.008	.321	.038	.001	.0002	.084
12.0	10.0	.941	.056	.006	.314	.036	.001	.0001	.060

FEATHER X		TC	PC	GC	J	CT	CP	CG	ETA
14.0	.4	.121	.008	.020	7.854	2.742	1.509	.2402	.065
14.0	.6	.129	.016	.027	5.236	1.334	.913	.1453	.126
14.0	.8	.144	.029	.036	3.927	.871	.889	.1097	.202
14.0	1.0	.167	.047	.047	3.142	.649	.575	.0916	.132
14.0	1.2	.200	.072	.060	2.618	.538	.505	.0604	.359
14.0	1.4	.241	.103	.073	2.244	.477	.456	.0726	.427
14.0	1.6	.272	.141	.088	1.963	.442	.419	.0647	.483
14.0	1.8	.350	.185	.103	1.745	.419	.387	.0618	.527
14.0	2.0	.416	.236	.118	1.571	.403	.358	.0571	.587
14.0	2.2	.486	.285	.129	1.428	.387	.326	.0518	.586
14.0	2.4	.552	.331	.138	1.309	.372	.292	.0465	.600
14.0	2.6	.618	.370	.142	1.208	.354	.257	.0408	.599
14.0	2.8	.671	.397	.142	1.122	.332	.220	.0351	.591
14.0	3.0	.714	.413	.138	1.047	.307	.186	.0296	.579
14.0	3.2	.742	.420	.131	.982	.281	.156	.0248	.566
14.0	3.4	.758	.424	.125	.924	.254	.131	.0209	.560
14.0	3.6	.769	.427	.119	.873	.230	.111	.0177	.555
14.0	3.8	.777	.428	.113	.827	.209	.093	.0151	.551
14.0	4.0	.785	.429	.107	.785	.170	.082	.0130	.546
14.0	4.2	.771	.428	.102	.748	.174	.070	.0112	.541
14.0	4.4	.776	.427	.097	.714	.159	.061	.0097	.536
14.0	4.6	.800	.425	.092	.683	.147	.053	.0085	.531
14.0	4.8	.803	.422	.088	.654	.135	.046	.0074	.525
14.0	5.0	.806	.419	.084	.628	.123	.041	.0065	.520
14.0	5.2	.807	.415	.080	.604	.116	.036	.0057	.514

Table A-1 (continued).

14.0	5.4	.808	.410	.076	.582	.107	.032	.0052	.505
14.0	5.6	.808	.405	.072	.561	.100	.028	.0048	.501
14.0	5.8	.808	.399	.069	.542	.093	.025	.0043	.474
14.0	6.0	.806	.392	.065	.524	.087	.022	.0038	.487
14.0	6.2	.804	.385	.062	.507	.081	.020	.0034	.479
14.0	6.4	.802	.377	.059	.491	.076	.018	.0028	.470
14.0	6.6	.799	.368	.056	.476	.071	.016	.0025	.461
14.0	6.8	.796	.359	.053	.462	.067	.014	.0022	.451
14.0	7.0	.792	.348	.050	.449	.063	.012	.0020	.440
14.0	7.2	.787	.337	.047	.436	.059	.011	.0017	.428
14.0	7.4	.782	.325	.044	.425	.055	.010	.0016	.418
14.0	7.6	.777	.312	.041	.413	.052	.009	.0014	.401
14.0	7.8	.771	.297	.038	.403	.047	.008	.0012	.386
14.0	8.0	.764	.282	.035	.393	.046	.007	.0011	.367
14.0	8.2	.757	.266	.032	.383	.044	.006	.0009	.351
14.0	8.4	.750	.249	.030	.374	.041	.005	.0008	.332
14.0	8.6	.742	.230	.027	.365	.039	.004	.0007	.310
14.0	8.8	.734	.211	.024	.357	.037	.004	.0006	.287
14.0	9.0	.725	.190	.021	.349	.035	.003	.0005	.262
14.0	9.2	.715	.168	.018	.341	.033	.003	.0004	.233
14.0	9.4	.705	.145	.015	.334	.031	.002	.0003	.205
14.0	9.6	.695	.120	.013	.327	.029	.002	.0003	.173
14.0	9.8	.684	.094	.010	.321	.028	.001	.0002	.137
14.0	10.0	.673	.066	.007	.314	.026	.001	.0001	.079

APPENDIX B

Derivation of Equation 3-4

APPENDIX B

Derivation of Equation 3-4

From Equation 3-3

$$AV_a = A_w V_w \qquad\qquad\qquad \text{(B-1)}$$

Solving for V_a

$$V_a = A_w \frac{V_w}{A} \qquad\qquad\qquad \text{(B-2)}$$

From Equation 3-1

$$1 = M_w + M_o \qquad\qquad\qquad \text{(B-3)}$$

Substituting $M_w = A_w V_w$, $M_o = (1 - A_w) V_o$ into the above expression

$$1 = A_w V_w + (1 - A_w) V_o \qquad\qquad\qquad \text{(B-4)}$$

Solving for A_w

$$A_w = \frac{1 - V_o}{V_w - V_o} \qquad\qquad\qquad \text{(B-5)}$$

Substituting Equation B-5 into B-2

$$V_a = \frac{V_w (V_o - 1)}{(V_o - V_w) A} \qquad\qquad\qquad \text{(B-6)}$$

The above expression is correct dimensionally since the parameters A, V_w, V_o are non-dimensional being normalized to the tunnel reference area and upstream velocity.